

THESIS

EVALUATION OF OCO-2 SMALL-SCALE X_{CO_2} VARIABILITY USING LIDAR RETRIEVALS
FROM THE ACT-AMERICA FLIGHT CAMPAIGN

Submitted by

Emily Bell

Department of Atmospheric Science

In partial fulfillment of the requirements

For the Degree of Master of Science

Colorado State University

Fort Collins, Colorado

Summer 2018

Master's Committee:

Advisor: Christian Kummerow
Co-Advisor: Christopher O'Dell

Scott Denning
Daniel Cooley

Copyright by Emily Bell 2018

All Rights Reserved

ABSTRACT

EVALUATION OF OCO-2 SMALL-SCALE X_{CO_2} VARIABILITY USING LIDAR RETRIEVALS FROM THE ACT-AMERICA FLIGHT CAMPAIGN

With eight 1.25 x 3 kilometer footprints across its swath and nearly 1 million observations of column-mean carbon dioxide concentration (X_{CO_2}) per day, the Orbiting Carbon Observatory (OCO-2) presents exciting possibilities for monitoring the global carbon cycle, including the detection of small-scale column CO_2 variations. While the global OCO-2 dataset has been shown to be quite robust, and case studies have shown successful observation of CO_2 plumes from power plants and cities, the validation of X_{CO_2} gradients on small spatial scales remains challenging: ground-based measurements, while extremely precise, are sparsely scattered and often geographically stationary. In this work, we investigate the use of an integrated path differential absorption (IPDA) lidar as a source for OCO-2 small-scale validation. As part of NASA’s ACT-America project, several campaigns over North America have included a number of direct underflights of OCO-2 tracks with the Multi-Functional Fiber Laser Lidar (MFLL), as well as a set of in situ instruments, to provide a precisely collocated, high-resolution validation dataset. We explore the challenges involved in comparing the MFLL and OCO-2 datasets, from instrument principles to retrieval differences, and develop a method of correcting for some of these differences. After nine underflights, a combination of lidar data and a novel in situ-derived CO_2 “curtain” have helped us to identify systematic spurious small-scale features in the OCO-2 dataset due to both surface and cloud effects. We show that though real X_{CO_2} features on scales of tens of kilometers

remain challenging to observe and validate, the lidar and OCO-2 generally have comparable spatial gradients on synoptic scales.

ACKNOWLEDGEMENTS

This work has been possible only with the help and contributions of a whole host of people. I would like to first thank my advisor Chris O’Dell, who has been instrumental to the development and planning of the project, for his strong guidance and collaboration. Thanks to Ken Davis, Sandip Pal, and the ACT-America team at Pennsylvania State University for their tireless work in the field in pursuit of our science goals, and for pushing out new datasets in a timely fashion. The MFL data processing team at Langley Research Center, headed by Ed Browell and Bing Lin, has also contributed hugely to the progress of this work. Thanks to Joel Campbell, Susan Kooi, and Alice Fan for their work on the lidar optical depth and X_{CO_2} products. Thank you to the MFL instrument team at Harris, especially Jeremy Dobler and Wayne Erxleben, for keeping us abreast of instrument calibration and operation. Additional thanks to Iouli Gordon and Roman Kochanov at the Harvard-Smithsonian Center for Astrophysics for providing updated spectroscopy tables, and to Brad Weir at NASA’s Global Modeling and Assimilation Office for his assimilation work. My gratification extends duly to my thesis committee members, who have taken my scheduling and re-scheduling in stride. This work was supported financially by the NASA ACT-America project, via NASA grant number NNX15A15AI97G.

TABLE OF CONTENTS

ABSTRACT	II
ACKNOWLEDGEMENTS	IV
CHAPTER 1. INTRODUCTION.....	1
CHAPTER 2. INSTRUMENTS AND DATASETS	16
2.1. OCO-2	16
2.2. IN SITU	19
2.3. MFLL	21
2.4. CO ₂ MODELS.....	27
2.4.1. CAMS	27
2.4.2. CARBONTRACKER.....	27
2.5. IN SITU “CURTAIN”	28
2.6. METEOROLOGICAL MODELS.....	32
2.7. SPECTROSCOPIC LOOKUP TABLES	33
CHAPTER 3. X _{CO₂} RETRIEVALS.....	34
3.1. MFLL RETRIEVAL OVERVIEW	34
3.2. MFLL RETRIEVAL INPUT SENSITIVITIES.....	37
3.2.1. METEOROLOGY	38
3.2.2. SPECTROSCOPY	40
3.2.3. WAVELENGTH.....	41
CHAPTER 4. MFLL RETRIEVAL VERTICAL SENSITIVITY CORRECTIONS	44

CHAPTER 5. RESULTS.....	54
5.1. JULY 27, 2016.....	57
5.2. AUGUST 5, 2016.....	60
5.3. AUGUST 27, 2016.....	63
5.4. FEBRUARY 13, 2017.....	65
5.5. FEBRUARY 15, 2017.....	70
5.6. MARCH 8, 2017.....	72
5.7. OCTOBER 22, 2017	75
5.8. OCTOBER 27, 2017	78
5.9. NOVEMBER 9, 2017	84
CHAPTER 6. COMPARISONS AND DISCUSSION	90
CHAPTER 7. CONCLUSIONS AND FUTURE WORK	101
REFERENCES	108

INTRODUCTION

Earth's climate is warming significantly, and as it continues within the next few centuries, it will bring about extreme economic, social, and ecological change. Greenhouse gases are the key to this warming. Earth's most influential greenhouse gas, carbon dioxide (CO_2), has risen by over 100 parts per million in atmospheric concentration since the start of the Industrial Revolution, when the burning of fossil fuels began - and while it seems straightforward to assume a correlation between anthropogenic emissions and atmospheric concentrations, the relationship between the two is extremely complex. There are many mechanisms through

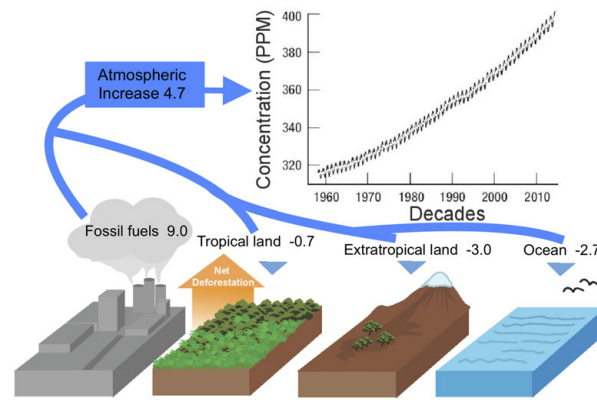


Figure 1.1. Human activity releases CO_2 into Earth's atmosphere, but carbon cycle feedbacks proceed to remove approximately 50% of it for storage in other reservoirs; the net atmospheric result is an increase of over 60 ppm since the 1960s. Figure courtesy of David Schimel.

which carbon in all its forms is exchanged between land, atmosphere, and ocean, including geophysical processes which constantly add and remove anthropogenic CO_2 emissions from Earth's atmosphere. In fact, an estimated 50% of CO_2 from anthropogenic sources is removed from the atmosphere via carbon sinks. Increased understanding of those feedbacks improves their characterization in Earth system models and thus improves scientists' ability to predict

future atmospheric CO₂ concentrations, but remains a demanding scientific challenge. The first step to understanding the complexity of these interactions is thorough observation, which can help characterize the locations and magnitudes of potential carbon sources and sinks. With a robust dataset of CO₂ measurements in space and time, carbon cycle scientists can calculate CO₂ fluxes (the amount of CO₂ moving through a given space at a given rate) and attempt to figure out where atmospheric CO₂ comes from, and where it goes.

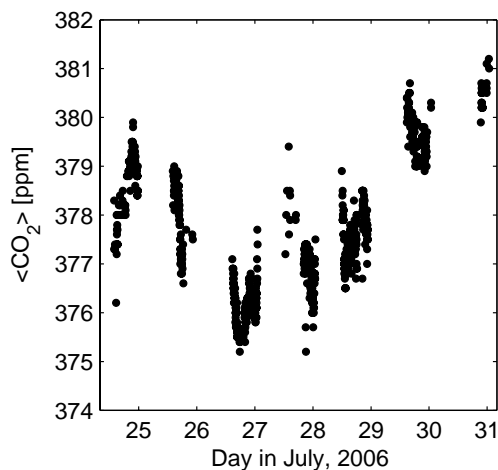


Figure 1.2. From Keppel-Aleks et al. (2011) - Daily X_{CO_2} (written here as $\langle \text{CO}_2 \rangle$) shown for one week in July 2006. Daily spread is consistently between 1 and 2 ppm.

There are two primary methods of calculating CO₂ fluxes. The first is via a “bottom-up” approach: from estimates of the amount of carbon stored, released, and taken up by the terrestrial biosphere and the oceans in a small area, scientists scale up to larger areas to calculate how much CO₂ is added and removed from the atmosphere. Unfortunately, such local data networks lack thorough spatial coverage, as measuring sites are scattered at individual locations across the planet. Local samples may not, in fact, be representative of the larger areas to which they are applied.

The second method of flux calculations is via a “top-down” approach, where atmospheric CO₂ concentrations are measured, and then models are used to determine the transport

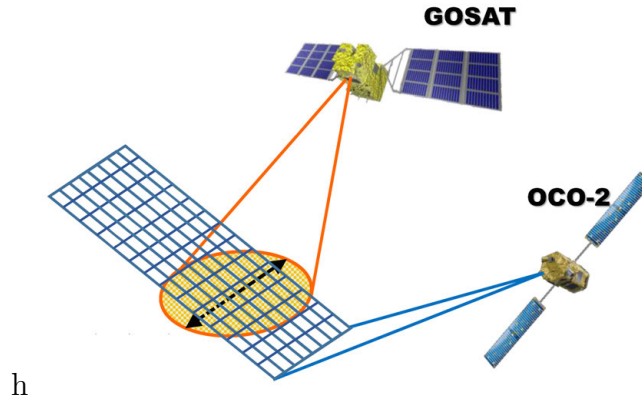


Figure 1.3. Visual comparison of GOSAT and OCO-2 footprint sizes. GOSAT footprint diameter (yellow circle) is 10.5 kilometers, and each OCO-2 footprint (small blue rectangles) is 1.29 x 2.25 kilometers.

and source/sink strengths required to match observations in space and time. Perhaps the seminal “top-down” study was made by Tans, Fung, and Takahashi in their seminal 1990 paper, “Observational Constraints on the Global Atmospheric CO₂ budget”. Ground-based atmospheric CO₂ observing networks had grown significantly since the start of the Mauna Loa record in 1958, and were numerous enough with long enough records by 1991 to make larger-scale, longer-term calculations. Driven primarily by uncertainty in the terrestrial carbon cycle, Tans, Fung, and Takahashi used atmospheric CO₂ measurements from 21 sites, as well as a thorough ocean observation dataset and several model forward runs, to identify the most likely sources of the observed CO₂ concentrations. They found a north-south hemispheric gradient far shallower than expected - concentrations in the northern hemisphere were much lower than modern atmospheric models driven by fossil fuel inventory records had predicted. Due to their inclusion of comprehensive ocean data, their simple conclusion was that the northern hemisphere terrestrial biosphere must be acting as a strong sink, unaccounted for within flux models at the time, and contradicting a study only one year previously (1989) by Heimann and Keeling.

This represented a shift in carbon cycle science, but these hemispheric conclusions were only one step forward from the broadest possible spatial resolution (global). While ground-based observation sites resolve a number of small regions, with high precision (a few tenths of a ppm), their sparseness does not provide a very thorough dataset in space. Only within the past decade has remote sensing of CO₂ developed the potential to fill in those spatial gaps: both the Greenhouse Gases Observing Satellite (GOSAT, launched in 2009) and the Orbiting Carbon Observatory 2 (OCO-2, launched in 2014) have produced CO₂ column-averaged dry air mole fraction (X_{CO₂}) datasets with global coverage and spatial resolution significantly superior to that of any ground-based dataset - GOSAT has a footprint size of 10 by 10 kilometers, and OCO-2 averages a footprint size of 1.25 by 3 kilometers. A visualization of their footprint sizes is shown in Figure 1.3. Such improvement in spatial resolution is revolutionary for flux inversions: if spatial resolutions continue to improve, satellite datasets could help top-down estimates to locate, say, CO₂ fluxes from individual cities and power plants.

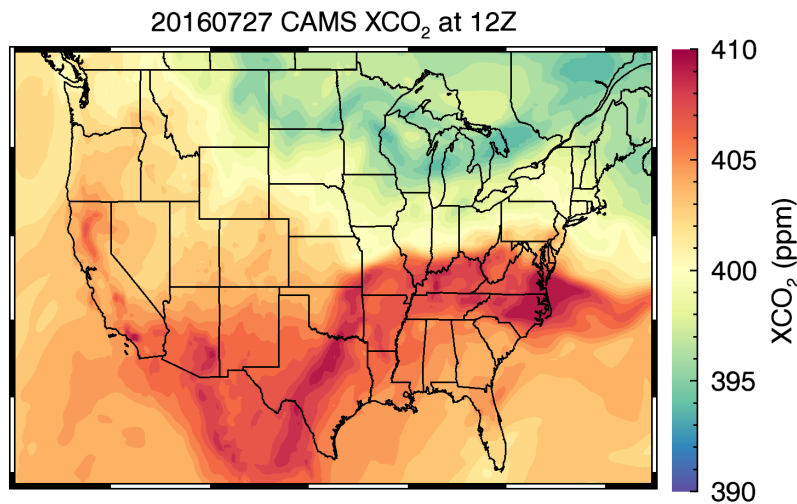


Figure 1.4. CO₂ dry air mole fraction across the United States at 12Z on July 27, 2016 as simulated by the ECMWF CAMS model.

Per in situ data, typical column-integrated values vary globally from around 380 to 420 parts per million (ppm), as illustrated in Figure 1.4, which shows a CO₂ analysis from the European CAMS model (Massart et al., 2016) for July 27, 2018. On local scales, column-integrated variations can reach up to 2 ppm over the course of a single day. Figure 1.2 illustrates this daily variability. In order to capture realistic CO₂ gradients, remote sensing instruments must thus have a measurement uncertainty smaller than these daily fluctuations. It is with such precision in mind that the OCO-2 instrument was designed. Its footprint is an average size of 1.25 by 3 kilometers, and it achieves global coverage (between about 60N and 60S) every 16 days. Two and a half years of OCO-2 data (discussed further in Section 2.1) have now successfully been shown to achieve this level of precision, 0.2-0.5%, or about 0.4-2 ppm error per individual sounding (Eldering et al., 2017). The global dataset has thus been proven quite robust.

While these 0.4-2 ppm errors are large compared to those of ground-based in situ measurements (which are on the order of 0.1 ppm), the increase in data density makes up for this. One of the most promising studies of the OCO-2 era thus far, in terms of identifying carbon sources and sinks, was published in *Science* in 2017. GOSAT and OCO-2 data were assimilated into the NASA Carbon Monitoring System Flux inversion system for both 2011, a La Niña year, and 2015-2016, a strong El Niño event, in an attempt to observe variability in tropical carbon fluxes, which are notoriously difficult to quantify. Using the assimilated satellite data, flux differences between the two events were broken into various components in three key regions (see Figure 1.5). While the sources of these signals require further investigation, it is a promising result of the satellites' continental coverage, and a step forward from both hemispheric estimates and ground-based observations.

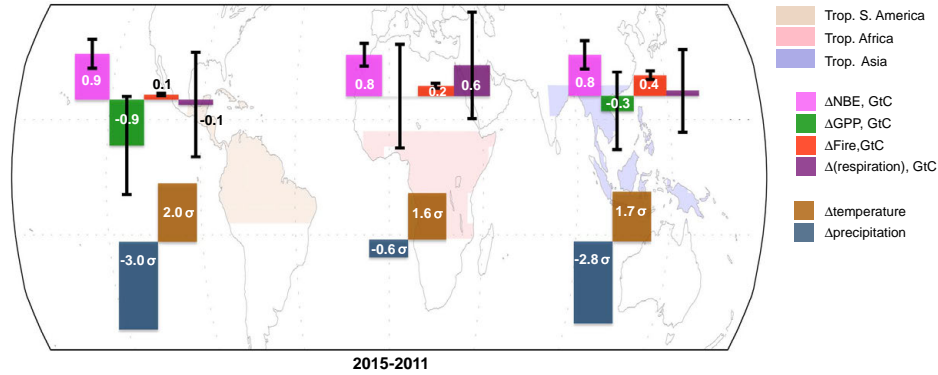


Figure 1.5. From Liu et al. (2017) - 2015 El Niño carbon flux components differenced from 2011 La Niña components. Also shown are temperature and precipitation differences between 2015 and 2011. Upward bars indicate higher values in 2015 than in 2011; σ in the temperature and precipitation values is the 30-year standard deviation from 1981-2010.

With even large-scale X_{CO_2} results still hotly contested, the validity of X_{CO_2} gradients on smaller spatial scales is hardly established. A comparison study by Wunch et al. (2017) between OCO-2 and the Total Column Carbon Observing Network (TCCON) shows that after bias correction (against TCCON) and filtering, the OCO-2 X_{CO_2} version 7 target-mode data can still have residual biases of up to 1.5ppm in RMS difference from their collocated TCCON sites. Comparisons between the target mode and coincident TCCON data can be seen in Figure 1.6 on page 7. (A map of the target mode locations and TCCON sites can be found on page 19, and an explanation of OCO-2's observation modes is also found in the next chapter.) In addition, sources of variability on relatively small scales ($100 \times 10.5 \text{ km}^2$) were evaluated in Worden et al. (2017), using comparisons of observed and predicted noise. The study concluded that some uncertainty in small-scale gradients remains unaccounted for, and that some spurious soundings may be due to variations in surface properties or solar zenith angle. Though both studies indicate small-scale errors in the bias-corrected data, neither attempts to validate the observed gradients in space. These gradients, which are typically on the order of the OCO-2 single-sounding measurement precision, should be

observable with an ensemble of soundings, and can significantly improve local flux estimates if measured accurately.

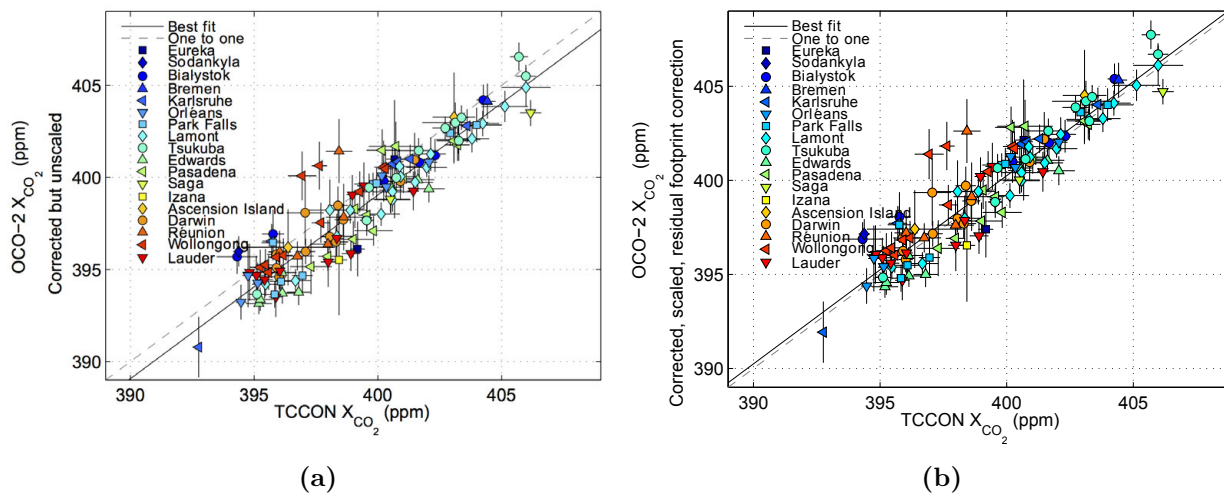


Figure 1.6. From Wunch et al. (2017) - Median X_{CO_2} values of OCO-2 target mode data against median values of coincident TCCON data. Plot (a) shows OCO-2 data with bias correction but without a scaling correction; right plot (b) includes a scaling correction. Note the closeness in slopes of the one-to-one line (solid) and the best fit line (dash), even though some spread remains in the OCO-2 data.

A vertically-integrated mixing ratio, X_{CO_2} variability is influenced by a number of factors which are difficult to parse and which introduce inherent complications to the measurements. (Further detail on the calculation of X_{CO_2} can be found in Chapter 3.) Vertical mixing within the column, surface sources and sinks, and large-scale dynamics all have an affect on the column-integrated value. Traditional in-situ boundary layer CO_2 measurements, taken at or near the surface, are most sensitive to local surface fluxes, but Keppel-Aleks et al. (2011) use correlation studies between X_{CO_2} , potential temperature, and eddy covariance data to show that regional variations in X_{CO_2} at two TCCON sites were more highly correlated with large-scale flux patterns than with local flux sources. Observed diurnal variations in X_{CO_2} only showed correlation with eddy covariance fluxes when averaged over the course of several synoptic cycles. This finding highlights the intrinsic difference between variability in full-column measurements and measurements made within the boundary layer. Figure 1.8

illustrates this difference, showing both TCCON X_{CO_2} and flask CO_2 data from Park Falls, one of the two sites studied in Keppel-Aleks et al. (2011). Over the course of 18 hours on August 27, 2010, the boundary layer data (triangles) clearly show the morning convection of high CO_2 to the level of the tower (396 meters) and the subsequent decrease in CO_2 over the course of the day due to further vertical mixing and photosynthesis, but the column data (+) shows little evidence of any of this variation.

Spatial gradients on regional scales arise from a number of mechanisms. Geographical differences in surface type result in varying magnitudes of carbon sources and sinks; regions of strong sources have elevated CO_2 concentrations, and regions of strong sinks have depressed concentrations. The terrestrial biosphere switches diurnally between source and sink - plants take up CO_2 during the day to perform photosynthesis, and release it at night via respiration. This can lead to spatial patterns that vary throughout the day based on surface types. Anthropogenic sources such as cities and power plants emit CO_2 , elevating concentrations locally, which is often observable in the full column. (Anthropogenic emissions were understood to be the major reason for the north-south hemispheric gradient found in the Tans, Fung, and Takahashi study, with most human activity in the northern hemisphere.) Topography can also cause local CO_2 buildup, leading to areas of elevated X_{CO_2} in valleys, for example, where transport may be minimal and vertical mixing is often suppressed. Existing spatial gradients can be either enhanced or diffused by transport as well, from mesoscale to synoptic scales.

OCO-2 data has already proven successful at observing some of these local features despite the complexity of the X_{CO_2} measurement. A study by Nassar et al. (2017) diagnosed emissions estimates from individual power plants in the U.S., India, and South Africa using

OCO-2 overpass data. In one U.S. case over a power plant in Kansas, X_{CO_2} enhancements in the plume up to 60 km distant were a mere 1 ppm, and yet OCO-2 was able to observe a distinct enhancement. Figure 1.7 shows the OCO-2 overpass as well as visualization of the plume. A simple Gaussian plume model was used to solve for instantaneous plant emissions using OCO-2 observations. The model estimated a value of 31.2 ± 3.7 kt CO_2/day , in remarkable agreement with the bottom-up estimate of 26.7 kt CO_2/day . Six overpasses of different plants yielded similar results, proving that OCO-2 clearly has some success in evaluating small-scale X_{CO_2} patterns within its target precision range. However, validation at these spatial scales is key to our interpretation and understanding of plumes and other surface emission features, and with as little validation as has yet been done, spurious features in the data may yet obscure our observations. The difficulty of this level of validation is demonstrated by the Nassar et al. dataset: in two years of data, only six clear-sky scenes were collocated with strong point sources suitable for case studies. This dearth of clear-sky overpasses stems primarily from the extremely narrow swath of OCO-2, which is only 5-10

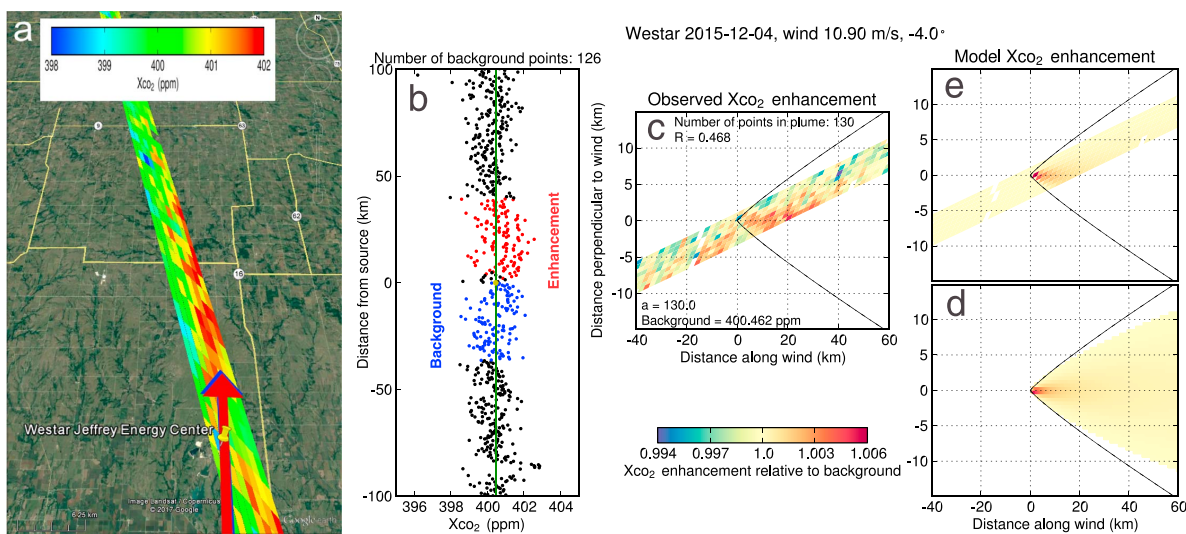


Figure 1.7. From Nassar et al. (2017) - An overpass of the Westar power plant in Kansas. From left to right, visualizations of the observed X_{CO_2} , and the enhancement within the plume compared to the perceived “background.” The enhancement is elevated by up to 1.006ppm from the “background” value and observed up to 60km from the source.

kilometers wide and in three years has only covered about 2% of Earth’s surface, with gaps of approximately 150 kilometers and 16 days between local swaths.

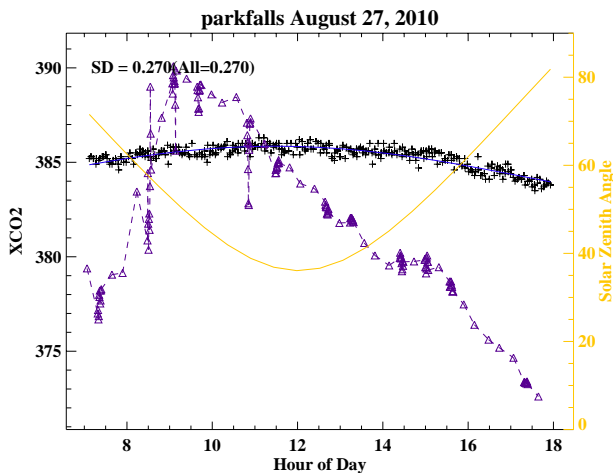


Figure 1.8. TCCON X_{CO_2} data at the Park falls WLEF tall tower (+) over the course of 18 hours on August 27, 2010. Also shown are flask CO_2 measurements taken at 396 meters (triangles), and the solar zenith angle in yellow. Note the lack of correlation between the column data and boundary layer measurements, despite the strong variations at the level of the tower.

Spurious features in the OCO-2 dataset may arise from a few different sources. In particular, the OCO-2 instrument is passive, meaning it relies on reflected sunlight: it “sees” all photons within its viewing angle, including those dramatically scattered by clouds and aerosols, and it cannot differentiate those severely scattered photons from others. This can lead to modified optical path lengths, effectively changing the extent of the measured column, and producing anomalous X_{CO_2} values. In addition, the OCO-2 version 7 data revealed some sensitivity to surface features such as topography and albedo, though the version 8 data shows improvement.

NASA has funded the Atmospheric Carbon and Transport (ACT) - America mission in part to deploy an active instrument which might shed light upon these types of biases in the OCO-2 overpass-level dataset. The ACT-America mission goals are threefold: to quantify and reduce atmospheric transport uncertainties; to improve regional-scale, seasonal

prior estimates of CO_2 and CH_4 fluxes; and to evaluate the sensitivity of OCO-2 column measurements to regional variability in tropospheric CO_2 (Davis et al., 2017). The first two goals can be achieved with in situ sensors, with which both mission aircraft (Langley C-130 and B-200) are equipped and which are utilized in both fair-weather conditions and near frontal boundaries, to help assess both surface fluxes and transport of CO_2 due to mesoscale and synoptic transport mechanisms. In pursuit of the third goal, the C-130 aircraft flies the Multi-Functional Fiber Laser Lidar (MFL), developed by the NASA Langley Research Center (LaRC) and Harris, along OCO-2 orbital tracks at (nearly) concurrent times of day at an altitude typically between 8 and 9 kilometers. The MFL measures tropospheric X_{CO_2} at a frequency of 10 Hz along-track, or 8-10 km spatial resolution when data is averaged

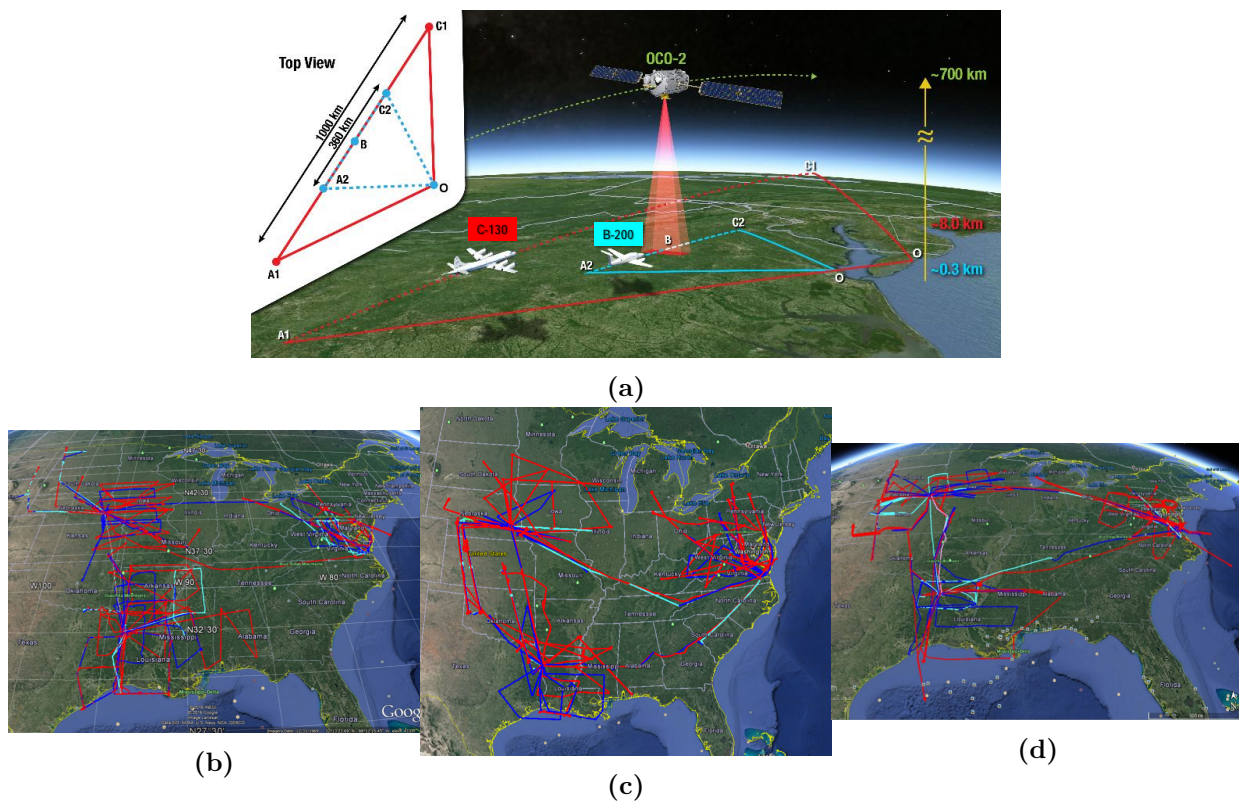


Figure 1.9. (a) ACT-America OCO-2 underflight diagram, and flight tracks from the (b) Summer 2016, (c) Fall 2017, and (d) Winter 2017 campaigns, provided by Davis et al. (2017).

into 60-second bins. A diagram of an OCO-2 underflight plan is shown in Figure 1.9a, and the coverage of the first three flight campaigns - summer, winter, and fall - are shown in the bottom row from left to right. A total of nine OCO-2 underflights were completed during these three campaigns, three in each season.

An active instrument like the MFLL, carrying its own power source, has the potential to observe small-scale X_{CO_2} patterns without the filtering inefficiencies of the OCO-2 instrument. Retrievals near cloud and aerosol features may in principle improve significantly, since active instruments detect the same signal that they emit. Detectors monitor the returned signal for irregularities, such as a premature return time, which would indicate the presence of a scatterer in the column. Signals representing significantly altered path lengths can thus be easily filtered out, eliminating any spurious measurements from clouds and scattering features. Variations due to albedo or topography can also be more easily identified by carefully monitoring variations in the emitted signal and comparing to those in the returned signal; signal range and surface elevation can be calculated from the data to within 3 meters' accuracy and precision (Dobler et al., 2013, Lin et al., 2013). Section 2.3 discusses MFLL instrument performance in further detail.

The MFLL has been developed as part of the Active Sensing of Carbon over Nights, Days, and Seasons (ASCENDS) mission, which seeks to improve upon the global carbon monitoring of passive sensors by deploying an active space-based instrument. Including its range-resolving ability, the MFLL as employed in the ACT-America campaign takes measurements at a higher spatial resolution than OCO-2 (in this study, the relative density of MFLL to OCO-2 measurements in space is at least 20 to 3), providing a larger ensemble of observations along-track which may better characterize X_{CO_2} features. This volume of

data helps to reduce noise, but there are several other differences between the two datasets which may play a role in validation success. OCO-2 samples at thousands of wavelengths across three CO₂ absorption bands, whereas the MFL samples at only three wavelengths across one CO₂ absorption peak. This significantly lower spectral resolution in the MFL can lead to stronger manifestation of spectroscopy and line shape imperfections in the X_{CO₂} retrievals, an effect which has not been thoroughly studied until this point, but is discussed at some length in Section 3.2.

The varying definition of the physical “column” in X_{CO₂} measurements is an important discrepancy between the two measurements as well - the MFL measures only the tropospheric column up to about 9 km, whereas OCO-2 measures close to the full atmospheric column. Thus, the MFL-retrieved X_{CO₂} in its simplest form can only be used to evaluate the column sensitivity of OCO-2 to CO₂ concentrations in the troposphere, as stated in the ACT-America mission goals. One other key difference between the retrieved X_{CO₂} from MFL and OCO-2 is addressed in this work: the instruments have different weighting functions, meaning that they are most sensitive to different vertical locations within the column. This could bias the results of one higher or lower than the other based on the CO₂ values in the particular part of the column to which the instrument in question is most sensitive. These two factors, the vertical column extent and the weighting function shape, lead to fairly significant differences in the retrieved X_{CO₂}, and our method of evaluating and addressing these differences is detailed in Chapter 4.

This work seeks to assess the agreement between the MFL and OCO-2 datasets for nine ACT-America underflights. Since OCO-2 has a relatively mature X_{CO₂} dataset, but the MFL retrieval is extremely young and yet untested, the first step is developing a relatively

simple MFLL retrieval and assessing its sensitivity to various assumptions. The second step is assessing the differences between the MFLL and OCO-2 retrievals and correcting for those differences. Then we can compare the MFLL and OCO-2 results - and due to the uncertainties involved in our corrections and the MFLL retrieval itself, we explore further 'truth' sources, both model and in situ.

Given these goals, the following questions are useful in framing the process detailed in this paper:

- (1) How well can the MFLL validate OCO-2?
- (2) Is the majority of the OCO-2 observed gradient at scales of hundreds of kilometers primarily real or spurious?
- (3) Is the majority of the OCO-2 observed gradient at scales of tens of kilometers primarily real or spurious?
- (4) Can we identify spurious variability and its causes in the OCO-2 X_{CO_2} data?

The contents of this paper are thus structured as follows. In Chapter 2, all datasets used in comparisons are described in detail, including instrument details in the cases of OCO-2 and the MFLL. Also described are the two in situ "curtains," 2-D vertical fields of CO_2 constructed from ACT-America in situ data. Sources of retrieval meteorology and spectroscopy are also provided. Chapter 3 briefly describes the key differences between OCO-2 and MFLL X_{CO_2} retrieval algorithms, and details MFLL retrieval sensitivities to variable spectroscopic and meteorological inputs as well as instrument wavelength variations. We make two additional corrections to the MFLL retrievals in an attempt to equalize the MFLL and OCO-2 measurements; these corrections are discussed in Chapter 4. A highly detailed summary of the nine OCO-2 underflights is found in Chapter 5, and Chapter 6

provides a more succinct overview and discussion of key comparison results. The final chapter summarizes the findings of this work, reviews implications of the results with regards to the questions laid out above, and considers the potential for future work.

CHAPTER 2

INSTRUMENTS AND DATASETS

2.1. OCO-2

Launched in July 2014, OCO-2 travels a sun-synchronous polar orbit in NASA’s A-Train, and records nearly 1 million soundings per day on eight footprints across its swath, with an average single-footprint area of about 1.25 by 3 kilometers. Around one hundred thousand of these are sufficiently cloud-free and suitable for full-column X_{CO_2} analysis; the X_{CO_2} data typically achieve a precision of 0.3% (1ppm) or better, in line with OCO-2’s mission goals and instrument design (Eldering et al., 2017). Global X_{CO_2} observations are shown in Figure 2.1, as well as a sample track showing observations across all eight footprints in Figure 2.3.

The OCO-2 instrument is a passive sensor, using a high-resolution grating spectrometer to measure, from reflected sunlight, the amount of atmospheric absorption due to CO_2 in two spectral bands: the weak band at 1.6 μm , and the strong band at 2.0 μm . It also measures absorption in the O_2 A-band at 7.26 μm . The instrument measures at high spectral

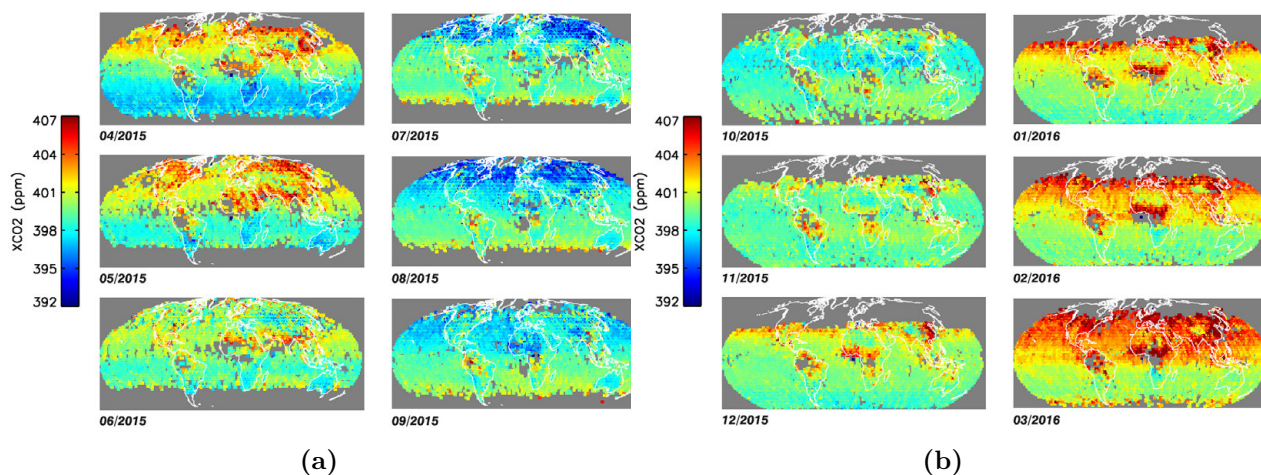


Figure 2.1. From Eldering et al. 2017 - (a) OCO-2 global X_{CO_2} from April to September 2015 and (b) October 2015 to March 2016.

resolution, with 1016 spectral elements in each of the three bands (Eldering et al., 2017). The absorption spectra in the weak CO₂ band and the O₂ A-band can be seen in Figure 2.2.

The satellite operates in three modes, depending on geographic location and science goals: nadir mode, at which time the instrument is pointed perpendicular to the ground; glint mode, in which the instrument is pointed at the solar “glint spot”, where solar reflectance is greatest from Earth’s surface - this is the primary operation mode over ocean; and target mode, in which the instrument remains pointed at one geographic location for a period of 15-20 minutes, and makes repeated measurements over that location.

Cloud-free soundings from the two CO₂ bands are processed through a retrieval algorithm to produce the X_{CO₂} product. The OCO-2 retrieval algorithm employs an optimal estimation scheme, in which, using an a priori estimate and observed values, a cost function is minimized to determine the state vector of atmospheric variables which produce the most probable posterior result, as described in O’Dell et al. (2012). Chapter 3 discusses the basic mathematical principles of the X_{CO₂} retrieval, which are common between OCO-2 and the MFL, but further details of the OCO-2 retrieval are not included in this work.

Though the focus of its mission is the X_{CO₂} product, OCO-2 measures a variety of atmospheric components, including water vapor and surface albedo (Eldering et al., 2017). In this study, we use the ACOS L2 version 8 X_{CO₂} product. Clouds and aerosol effects can result

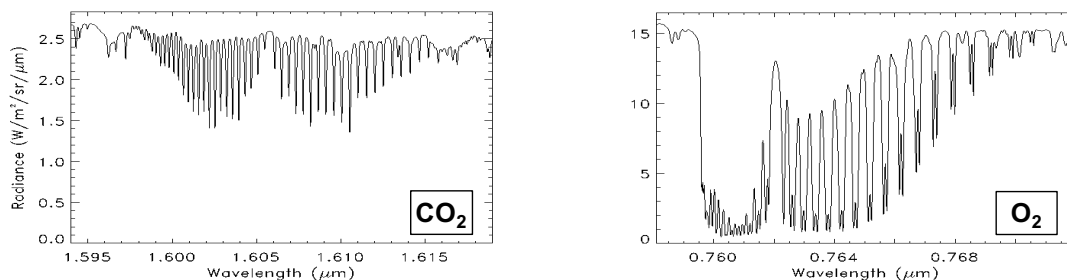


Figure 2.2. Absorption spectra of CO₂ in the weak band (left) and O₂ in the A-band (right).

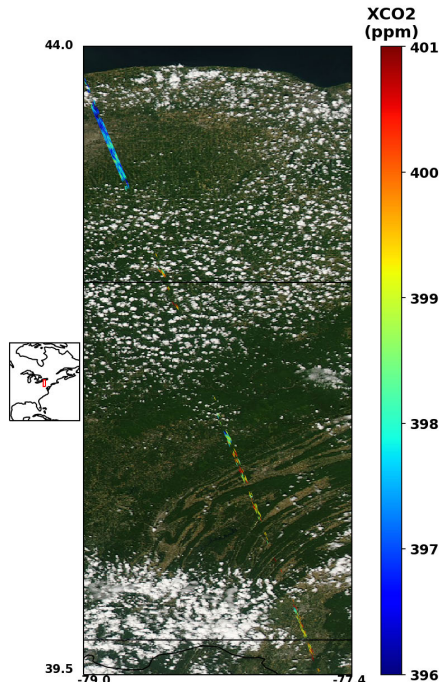


Figure 2.3. OCO-2 X_{CO_2} data from July 27, 2016 over (south to north) Maryland, Pennsylvania, and New York. OCO-2 data is overlaid on MODIS (Moderate Resolution Imaging Spectrometer) visible imagery from the same day, taken merely minutes prior to the OCO-2 overpass. MODIS flies in the A-Train with OCO-2, following nearly the same ground track.

in an altered path length, scattering photons multiple times or prematurely, resulting in a measurement that is not representative of the full vertical column. The data used in this study has thus been cloud- and aerosol-screened using pre- and post-processing algorithms described in Taylor et al. (2015). We further filter the dataset using the quality flag field, which depends on a variety of factors (detailed in Mandrake et al., 2016) including observed surface albedo, surface roughness, aerosol optical depth, and offset from prior model estimates. The data analyzed in this study is bias-corrected per O’Dell et al. (2018, in prep) and Osterman et al. (2017), and has quality flag = 0. As described later in the Results and Discussion sections, some notable cloud features still remain in the data after standard cloud screening procedures, resulting in some spurious features.

Bias correction is performed against the Total Column Carbon Observing Network. TC-CON is a system of global ground-based FTS (Fourier transform spectrometer) instruments



Figure 2.4. All OCO-2 target mode locations, including TCCON sites as shown in Wunch et al. 2017.

which produce X_{CO_2} measurements at precisions high enough - 0.25%, 1ppm or less - to match (and exceed) the measurement goals of OCO-2. In a study by Wunch et al. (2017), 123 sets of B7r OCO-2 target-mode measurements were chosen based on collocation with TCCON sites in both space and time. Bias-corrected soundings were shown to have an R^2 value of 0.86 when compared to TCCON values, and agreed within 1ppm in most cases. A map of OCO-2 target mode locations, including TCCON sites, is shown in Figure 2.4.

For best comparison to MFLL measurements, the OCO-2 data in this study is binned in one of two ways: (1) to spatially coincide with 60-second MFLL bins, to within about 8km of the center of the 60-second MFLL track, yielding the same number of data points between datasets - making correlation calculations simple; and (2) at 0.25 second intervals, in order to sufficiently reduce measurement noise and clearly illustrate the desired spatial features.

2.2. IN SITU

NASA's Airborne Science Program has outfitted the ACT-America science team with both a C-130 and B-200 aircraft. The C-130 carries the MFLL instrument; an in-situ PI-CARRO instrument and several flasks, for the sampling CO_2 and other greenhouse gases; the Cloud Physics Lidar (CPL); a GPS; and a suite of instruments for measuring atmospheric

ACT-America Science Instruments

Instrument (Platform)	Variables Measured	Sampling Frequency	Data Latency (Archiving)	Purpose of Measurement
MFL (C-130)	Column CO ₂ number density, altimetry, surface reflectance	10 Hz	1 day (≤6 months)	Core GHG CO ₂ measurement & ranging capability
CPL (C-130)	ABL height, aerosol distribution	2 Hz, 30m vertical resolution	1 day (≤4 months)	Transport model constraint, OCO-2 validation
PICARRO Air (C-130 & B-200)	CO ₂ , CH ₄ , CO, H ₂ O mole fraction	1 Hz	1 day (≤4 months)	Core GHG measurements, combustion & air mass tracer
2-B Tech. (C-130 & B-200)	O ₃ mole fraction	1 Hz	1 day (≤4 months)	Air mass tracer
Atm. state and nav. (C-130)	GPS lat-lon, wind speed, direction, pressure, temp.	1 Hz or higher	1 day (≤6 months)	Evaluate atmospheric transport models
Atm. state and nav. (B-200)	GPS lat-lon, wind speed, direction, pressure, temp.	1 Hz or higher	1 day (≤6 months)	Evaluate atmospheric transport models
Flasks (C-130 & B-200)	Multiple trace gases	12 flasks / aircraft / flight	1 month (≤6 months)	Core GHG measurements, GHG source tracers
PICARRO Ground	CO ₂ , CH ₄ , H ₂ O mole fraction	1 Hz	1 day (≤6 months)	Core GHG measurements

Figure 2.5. A table of the science instruments involved in the ACT-America campaign, the aircraft on which they are carried, and information on their data availability and functionality, from the mission website at <https://act-america.larc.nasa.gov/>.

variables such as wind, temperature, and pressure. The B-200 also carries a PICARRO, some flasks, and GPS and atmospheric state instruments. In situ data principally used in this work are PICARRO data, along with GPS data for latitude, longitude, and altitude measurements. Figure 2.5, from the mission website at <https://act-america.larc.nasa.gov/>, shows a table of instruments and the aircraft which carry them, as well as their data availability and functionality.

In this study, the PICARRO data is primarily useful for column measurements, in the form of aircraft spirals from cruising altitude to near-surface. PICARRO instruments use a technique called Cavity Ring-Down Spectroscopy (CRDS) to measure CO₂ concentrations with an estimated precision of 0.3ppm and a similar level of accuracy, significantly exceeding the precision goals and capabilities of any remote sensing instrument. Combined with a meteorological model, the vertical resolution of the in situ data gives an accurate representation of the CO₂ profile and the X_{CO₂} value at the spiral location. The data used to construct

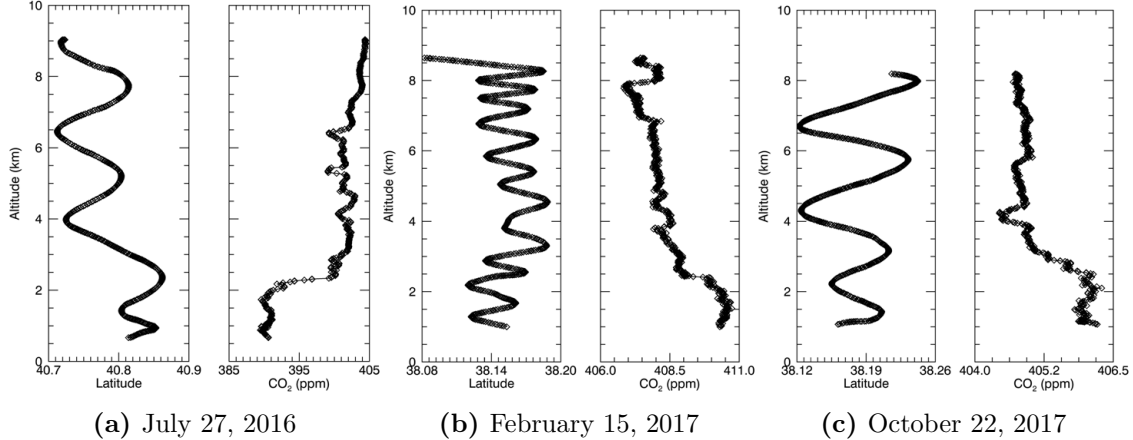


Figure 2.6. Example in situ spiral profiles in latitude (left) and CO₂ space (right) for one flight from each of the three campaigns, flown in three different seasons - summer, winter, and fall. Note the strong boundary layer drawdown in figure (a) in the summer.

the spiral column is most often the 1-second average PICARRO data from the “merge” files generated by the in situ instrument team - occasionally, the raw PICARRO file is used, where temporal resolution may be slightly finer. However, spiral data does not represent the instantaneous column in time, nor is it taken at a single point in space. A typical aircraft spiral spans up to 0.3 degrees in longitude and latitude, and up to 45 minutes in time. Figure 2.6 shows one spiral profile from each of the three campaigns in both latitude and CO₂ space. As a simple means of comparison in this study, we do not attempt to “correct” for either of these factors, because there are already discrepancies between the MFLL and OCO-2 measurements in both time and space anyway.

The PICARRO data is secondarily used in this study to help generate an in situ “curtain”, or a two-dimensional slice of CO₂ concentrations along the OCO-2 ground track. More details on the construction of the curtain dataset are found in Section 2.5.

2.3. MFLL

The Multi-Functional Fiber Laser Lidar (MFLL), developed by NASA’s Langley Research Center (LaRC) and Harris (Dobbs et al. (2008), Dobler et al. (2013)), has been designed

specifically to achieve the goals set by the ASCENDS mission and is the first Intensity-Modulated Continuous-Wave (IM-CW) Laser Absorption Spectrometer (LAS). Figure 2.7 shows the standard setup of sampling wavelengths on the absorption line. Operational since 2005, the MFLC emits at three wavelengths on a single CO₂ absorption line centered at 1571.112nm, which was chosen for MFLC operation due to its relative insensitivity to both relative humidity (RH) and temperature. One emission wavelength is in the center of the line (referred to as the “ON” line), and the other two are placed further out toward the wings (“OFF” lines). For all but one flight (August 5, 2016) in this study, the configuration had the two OFF wavelengths at ± 50 pm to either side of the ON line. We refer to these as the Short (S) and Long (L) lines, at 1571.062 and 1571.162 nm respectively. For the August 5 flight only, the Long line was moved to a position halfway between the ON and Short lines at 1571.087 nm in attempt to reduce sensitivity to contamination by a water vapor absorption feature. The MFLC X_{CO₂} retrieval relies on the Integrated Path Differential Absorption (IPDA) method. The differential absorption ($\Delta\tau$) between two of the three sampling wavelengths - either ON and OFF_S or ON and OFF_L - is calculated by taking ratios of the transmitted and received powers for those two wavelengths. The two retrieval results from the two wavelength pairs can differ by up to about 2 ppm along a given flight track, as will be shown in the Results section. This is presumably due in part to the higher water vapor sensitivity of the OFF_L wavelength. The MFLC retrieval, including its sensitivity to wavelength, spectroscopy, and meteorology, as well as its key differences from the OCO-2 retrieval, is detailed further in Chapter 3.

Early tests of the MFLC instrument demonstrated successful X_{CO₂} measurements in a variety of conditions and over a variety of surface types (Browell et al., 2008, Browell et al.,

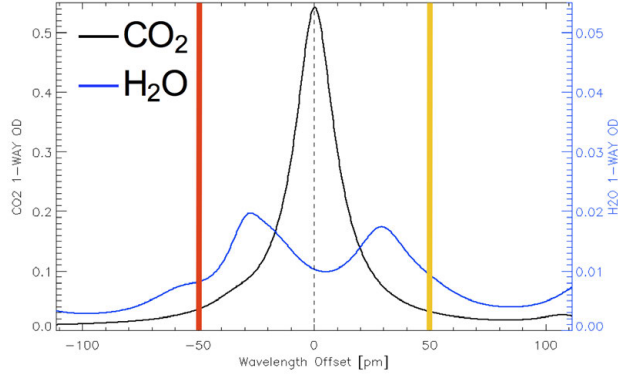


Figure 2.7. Standard MFLLE sampling wavelengths: CO₂ one-way OD is shown in black and H₂O in blue. The ON line is centered at 1571.11nm (dashed), and for all but one flight, the OFF_S (red) and OFF_L (yellow) are positioned 50 pm to either side.

2010, Dobler et al., 2013). The first flight campaigns found signal-to-noise ratios (SNRs) higher than 250 for 1-second averaged data over land, and yielded CO₂ concentrations as precise as 0.6ppm, in line with the ≤ 1 ppm precision of OCO-2 measurements (Browell et al., 2008, Browell et al., 2010). A series of 2010 flights measured SNRs better than 600 over desert, 500 over vegetation, and 150 over ocean for 1-second data; 2011 flights showed X_{CO₂} column agreement to within 0.65 ppm between MFLLE and in situ measurements (Dobler et al., 2013). Figure 2.8 shows MFLLE measured optical depths (ODs) compared to ODs derived from in situ measurements (“model”) for two of these flights; over Central Valley, California, the average difference between measured and modeled ODs was -0.28%, or about 1.1 ppm, and over the Rocky Mountains the average difference was -0.44%, or 1.7 ppm.

A key feature of the MFLLE as an active instrument is the identification of intermediate scatterers in the observed column. This is accomplished via a range-encoded intensity-modulation technique which, using the magnitude and timing of the returned signal, differentiates surface-reflected signals from those reflected off of scatterers in the midst of the column. The timing of the returned signal can be used to calculate the range to the surface, which has been shown to be better than 3 meters in both precision and accuracy (Dobler

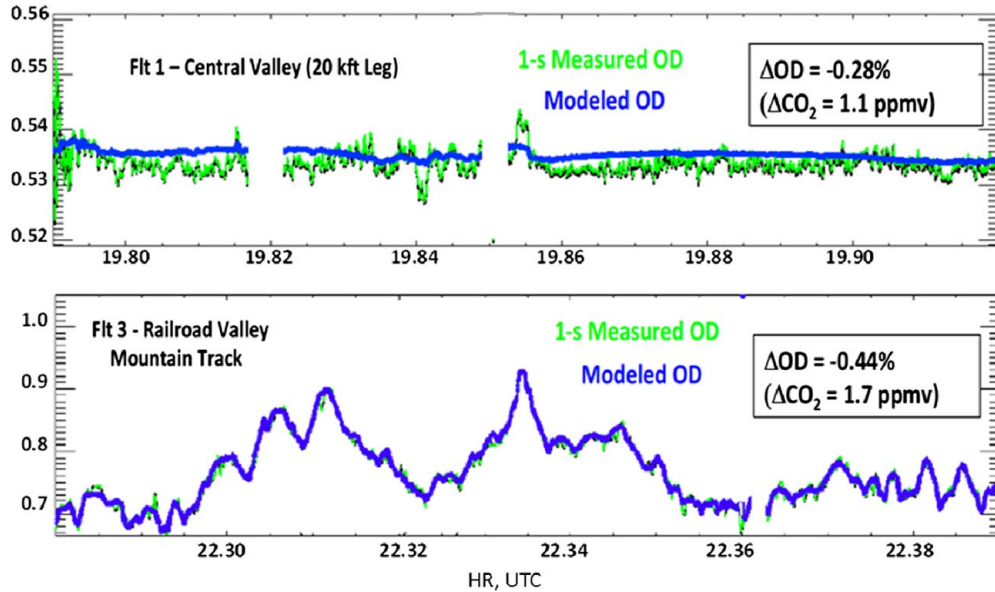


Figure 2.8. From Dobler et al. (2013) - Comparison of measured versus “modeled” optical depths, derived from in situ, for two 2011 flights. The top plot shows an example from over Central Valley, California, over relatively flat landscape; the bottom plot shows a transit flight over the Rocky Mountains. The legend indicates the percent difference between the ODs, and the approximate equivalent difference in measured CO_2 .

et al., 2013, Lin et al., 2013). This level of accuracy was also found in range calculations to cloud and aerosol levels.

The MFLM measurements are provided at 10Hz, and prior to any averaging or retrieval, some preliminary filters are applied. When a maximum returned power is reached, the detector becomes insensitive to any changes in the signal (the signal reaches “saturation”). The data from each of the three detected lidar signals is thus filtered out above a prescribed threshold. The data is then averaged into 1-second bins. The reported pitch angle is adjusted by a reported offset angle - unique to each flight campaign but around -3.4° on average - based on the position of the instrument inside the C-130. Slant ranges less than 100 meters are disposed of in order to filter out open-path calibration measurements, which are made at close range, usually at the start of the flight. In addition, the range is highly sensitive to the view angle, and the view angle is recorded at a lower sampling rate, which can lead

to significant uncertainty in the range calculation when the aircraft is banking or turning quickly. Stability filters are applied to changes in range, slant range, and elevation for this reason.

Figure 2.9 shows a diagram of the mechanism for recording wavelength drift. Small changes in the emitted wavelengths can affect retrieved X_{CO_2} values by up to a few tenths of a part per million (as discussed in Chapter 3) and are monitored via a separate reference laser, which is precisely calibrated, locked to a well-characterized acetylene gas line, and sent through an acetylene gas chamber to a detector. If the detector finds any wavelength drift, the laser is immediately readjusted to return to the center of the acetylene line. Some portion of the signal from this reference laser is also sent to the same wave meter as the three MFLL signals. Expecting the reference wavelength to remain flat due to the constant correction of its position, it is assumed that any drift in the reference signal within the wavemeter must be due to some environmental factor which also affects the three measured MFLL wavelengths. This offset, which is variable in time, is applied to each channel. All three channels of MFLL data are then combined with GPS data into a 1-second averaged product, and are run through the X_{CO_2} retrieval, which is discussed in Chapter 3. (Section 3.2 discusses the potential implications of uncertainties in this system.)

A few campaign-unique issues have affected the MFLL dataset. After the conclusion of the summer 2016 ACT-America campaign, a cross-talk issue was discovered between two of the MFLL channels, causing some additional bias in the data. A correction to this issue was discovered and applied to a new data version; the data shown here includes the cross-talk correction. The effect on retrieved X_{CO_2} values ranged from on the order of 1-2 ppm for ON/OFF_S and around 4-5 ppm for ON/OFF_L, depending on the day. During the

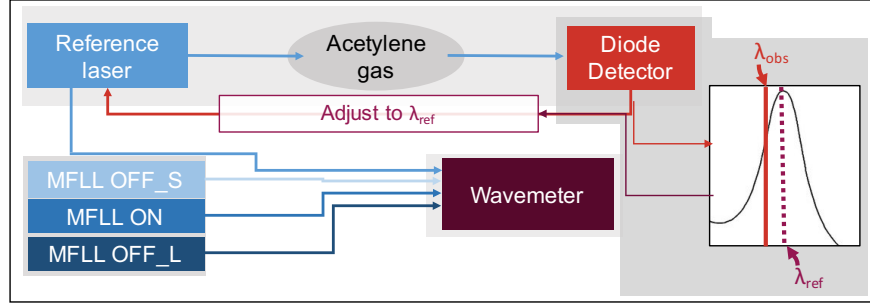


Figure 2.9. The wavemeter measuring emitted MFLW wavelengths is also connected to a reference laser. The reference laser is calibrated to continuously adjust onto the center of a precisely known acetylene absorption line. The measured reference wavelength is thus expected to be constant in time; any drift in time is assumed to stem from environmental factors which also affect emission at the three MFLW channels. This time-dependent offset is applied to each of the MFLW reference wavelengths.

winter 2017 campaign, a coating degradation on the MFLW viewing window on the C-130 was reported after the first test flight, on February 5. The window was unable to be replaced during the campaign, resulting in increased MFLW measurement noise for all three flights. In an attempt to get a reasonable SNR, the C-130 flew lower than usual on the three winter OCO-2 underflight tracks: around five kilometers elevation, as opposed to nine.

The MFLW data also demonstrates some range dependence, which appears to vary slightly from flight to flight. In percent difference of optical depth (OD) between MFLW and in situ data, the campaign-wide biases from campaigns 1 and 2 show a slope of up to -3 (% difference versus measured OD) and a standard deviation of up to 0.8 (% difference). The cause of this dependence is still under investigation, but a bias correction has been released for the summer 2016 campaign data by the Langley team, and is applied in this study. The Langley team continues to work on bias corrections for the second and third campaign data.

The level 1 data product (available only for summer 2016), which reports optical depths for the ON/OFF_S measurements only, includes a campaign-wide bias correction which was developed by adjusting MFLW optical depths to those calculated from in situ spirals at the spiral locations. The level 1 product also includes its own set of cloud and data quality flags,

which have been used in this study to filter the data. Results shown for the three summer flights include only cloud-free observations (`cloud_ground_flag = 0`) and observations with `data_quality_flag = 0`, in which signal strength is above some minimum threshold and both the pitch and roll angles are under five degrees.

2.4. CO₂ MODELS

In this study, model CO₂ data is used primarily for the generation of two MFL retrieval correction factors. The first correction accounts for differences in X_{CO_2} when identical model profiles are weighted using the OCO-2 and MFL weighting functions. The second correction uses model partial column X_{CO_2} above the plane to correct for this portion of the column, which is absent in MFL observations. Straight pressure-weighted X_{CO_2} from models is also used as a comparison for magnitude and latitudinal gradients.

2.4.1. CAMS. The European Centre for Medium-Range Weather Forecasts (ECMWF) produces a forecast model of atmospheric components via the Copernicus Atmosphere Modeling Service (CAMS). The CO₂ forecasts assimilate the GOSAT BESD X_{CO_2} product (Heymann et al., 2015); data are provided to the CSU team at six-hourly time steps on a 0.25° latitude by 0.25° longitude grid, with 137 vertical levels from surface to top of atmosphere (TOA).

2.4.2. CARBONTRACKER. CarbonTracker, a post-inversion product from NOAA ESRL in Boulder, Colorado, provides near-real-time analyses which include ground-based flask measurements Peters et al. (2007). Model CO₂ fields are provided at 3 by 2 degree spatial resolution and 3-hourly time resolution. It includes 26 vertical levels between surface and TOA. Comparisons between CAMS, CarbonTracker, and in situ data have revealed a

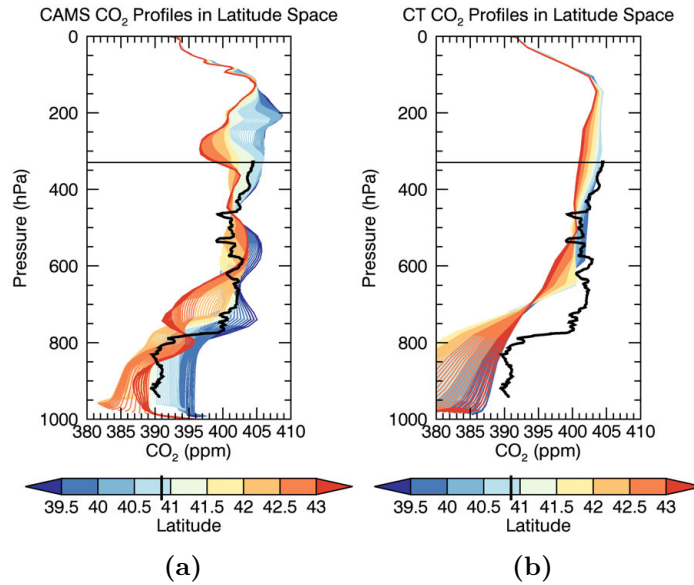
slight high bias in CAMS in winter, shown in Figure 2.10, presumably due to flask measurements making CarbonTracker more sensitive to subtle near-surface drawdown in wintertime. For this reason, CarbonTracker is used for the upper column MFLL correction in winter 2017 flights. CarbonTracker data was unavailable for the fall 2017 underflight dates, but is expected to be similarly preferable to CAMS for those flights. Data can be found at <http://carbontracker.noaa.gov>.

2.5. IN SITU “CURTAIN”

Because of the relative immaturity of the MFLL X_{CO_2} retrieval, the desire arises for additional datasets with which to validate OCO-2 and the MFLL. Therefore, as another potential validation source, in situ data has been used to construct two “curtains”, or two-dimensional CO_2 fields across the latitude range of the underflight track. The ACT-America team at the Pennsylvania State University (PSU) has generated a simple version of the “curtain” using the PICARRO data from both the C-130 and the B-200 aircraft, which, combined, usually fly nearly the full latitudinal range of the OCO-2 overpass at at least three different altitudes. With a nearest-neighbor approximation, vertical and horizontal gaps in the flight track are filled in using the in situ measurements at a relatively fine horizontal resolution (about 1,000 points along a few degrees latitude) and relatively coarse vertical resolution (20 points over 10 kilometers in altitude). Figure 2.11 shows the raw in situ data and the result after nearest-neighbor interpolation. The resulting curtain yields thousands of CO_2 profiles derived from PICARRO data, which can be sampled as desired to make X_{CO_2} estimates along the full OCO-2 underflight track.

The PSU curtain data delivered to CSU only reaches up to the height of the C-130, around 9 kilometers. In order to achieve a more robust comparison to OCO-2, model CO_2 data is

July 27, 2016



February 15, 2017

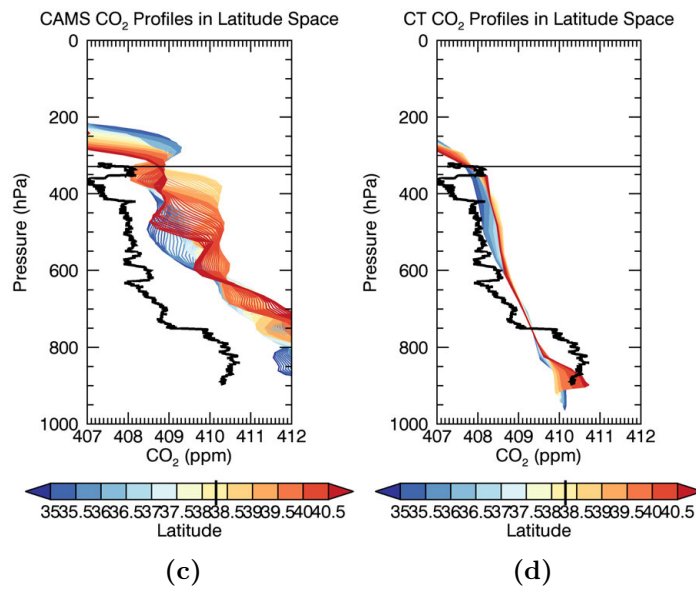


Figure 2.10. Model profiles, colored in latitude, compared to in situ profiles (black), from one summer flight (top panels) and one winter flight (bottom panels). The latitude of the in situ profile is marked by a tick on the color bar. Note that in panel (c) the CAMS profiles appear consistently high compared to the in situ, whereas the CarbonTracker profiles in panel (d) are more comparable in magnitude. This is a consistent trend in the winter data, but is absent from the summer data (panels (a) and (b)), in which CAMS agrees better with in situ than does CarbonTracker.

used in a very simple manner to create a full column. Model data is interpolated to the precise location and time of each curtain profile, and then layers above the highest point of the curtain profile are added to the top of the curtain profile.

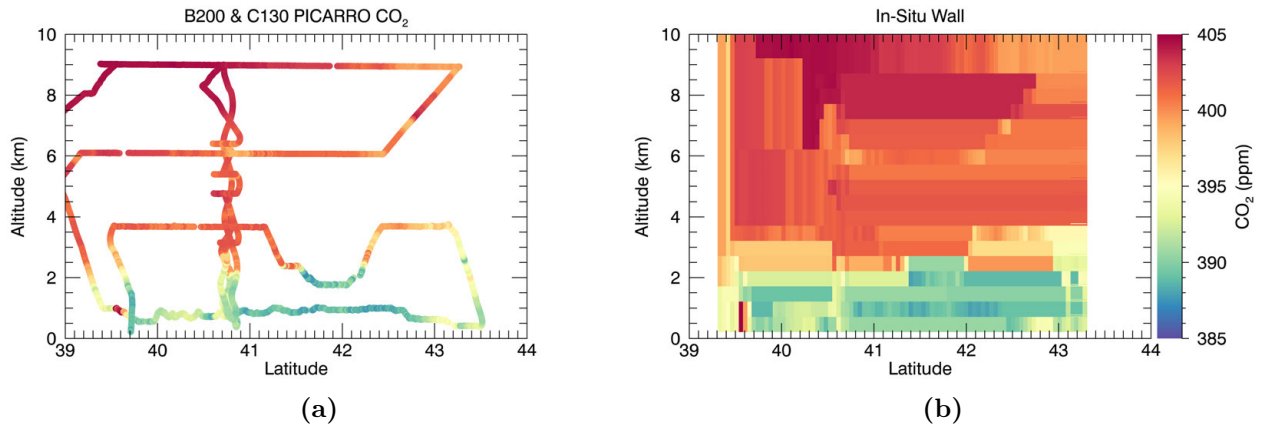


Figure 2.11. Figure (a) shows the PICARRO data from both the B-200 and C-130 flight tracks on July 27, 2016. Figure (b) shows the resulting “curtain” (alternatively, “wall”) after using nearest-neighbor approximation to fill in vertical and horizontal gaps. A total of 1,045 profiles are created along the flight track between 39 and 44N. Curtain data courtesy of Sandip Pal, PSU.

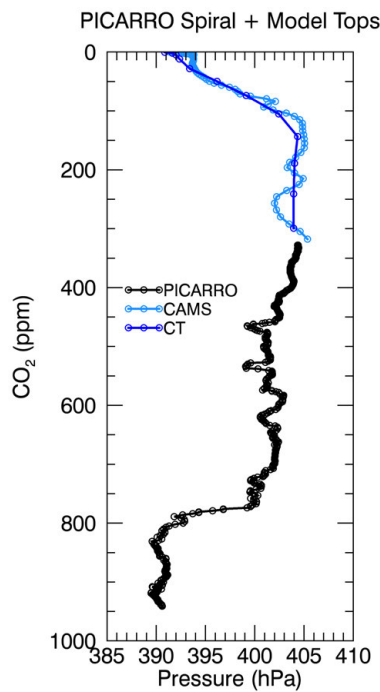


Figure 2.12. In situ profile from July 27, 2016, black, shown with two different model datasets used for the upper column. The ECMWF CAMS model is in light blue, and the CarbonTracker near-real-time model is in dark blue.

The two-part full profile is used to make the X_{CO_2} calculation used for comparison to OCO-2 and the MFLL. An example of the constructed full column, using the spiral in situ profile, can be seen in Figure 2.12. Note that the two models shown in Figure 2.12 differ in varying

amounts vertically throughout the upper column, and by up to 3 ppm in places. The reliance on uncertain model data above the plane - a partial column which consistently represents about one third of the total column dry air mass - introduces some uncertainty to the curtain data as well, and can shift curtain X_{CO_2} values slightly toward the X_{CO_2} values of model data. (Typical observed model biases are discussed in the next section.)

The PSU curtain used in this study does not take into account the time variability of the flight path, but rather treats the full flight track as an instantaneous snapshot of the CO_2 field at the median time of flight. Future improvements in methodology will attempt to account for time dependence using model data to estimate how significantly CO_2 concentrations varied over the duration of the flight. In addition, future versions will attempt to use boundary layer data from both models and instruments (namely the Cloud Physics Lidar, or CPL, also onboard the C-130) to adjust the height of the boundary layer in the spatial gaps of the in situ data, and according to any strong time dependence.

Another version of the in situ “curtain” is also shown in this work, constructed by Brad Weir at NASA’s Global Modeling and Assimilation Office (GMAO). Using the same in situ data as the PSU curtain, the GMAO curtain uses a more sophisticated vertical and horizontal interpolation to nudge CO_2 model output toward the observations. The model also provides temporal information, and decorrelation lengths are prescribed along the flight track to incorporate predicted variability over the duration of the flight. Both the PSU and GMAO curtains have been constructed for only the summer 2016 underflights.

2.6. METEOROLOGICAL MODELS

Various meteorological models are used in this work for MFL X_{CO_2} retrievals. MFL retrievals rely on model data for vertical atmospheric state information, such as water vapor mixing ratios, temperature profiles, and pressure profiles, all of which are required to calculate the absorption cross-section of the column as the MFL itself does not provide any vertical profile information. The in situ spiral locations are an exception to this need. Model data fields are interpolated to MFL measurement latitude, longitude, and time. A hypsometric adjustment is also made to model surface pressures. MFL retrieval results vary by a few tenths of a ppm when different meteorological models are used in the retrieval - as discussed in more detail in the Chapter 3. Three different models are used in this work to evaluate MFL retrieval sensitivity.

- (1) MERRA2 reanalysis data from the GMAO at NASA Goddard Space Flight Center (GSFC) (Gelaro et al., 2017) are provided at 0.625 by 0.5 degree spatial resolution, at 3-hourly time steps on 73 vertical pressure levels.
- (2) The GEOS5-FP model data used in this study have also been provided by the GMAO, and are produced in real time and provided at 0.3125 by 0.35 degree spatial resolution at 3-hourly timesteps with 42 vertical pressure levels.
- (3) The NCEP reanalysis product from NOAA ESRL (Kalnay et al., 1996) is provided at 2.5 by 2.5 degree spatial resolution every 6 hours, with only 17 vertical pressure levels.

The Results chapter shows only retrieval results using MERRA2 meteorology, but Chapter 3 discusses the observed differences between the models.

2.7. SPECTROSCOPIC LOOKUP TABLES

This study uses a variety of spectroscopic lookup tables in different combinations to calculate the differential optical depths of CO₂ and water vapor. Of primary use are the ABSCO 4.2, HITRAN 2012, and precursors to the HITRAN 2016 tables. The ACOS/OCO-2 absorption coefficient (ABSCO) tables are developed by the NASA Jet Propulsion Lab (JPL) for use with the OCO-2 retrieval algorithm, and updated versions of the table are released with each major update to the OCO-2 Level 2 product: ABSCO version 4.2 was released in 2013, and version 5.0 in the summer of 2017. Details on version 4.2 can be found in Thompson et al. (2012).

HITRAN linelists are available publicly at <http://hitran.org>, and HITRAN 2012 documentation is provided in Rothman et al. (2013). Pre-HITRAN 2016 tables were provided by Iouli Gordon, and the official 2016 release is documented in Gordon et al. (2017).

X_{CO₂} RETRIEVALS

This chapter includes a high-level review of the MFLX X_{CO₂} retrieval theory, including an examination of the MFLX retrieval sensitivities to various inputs, including spectroscopic lookup tables, meteorological models, and wavelength. These sensitivities have not been studied thoroughly in the past, as the X_{CO₂} retrieval is fairly young, and appear to have non-negligible effects on the X_{CO₂} results.

3.1. MFLX RETRIEVAL OVERVIEW

Remote sensing of any atmospheric component is based on a few of the same physical principles. Some initial signal is emitted into the atmosphere, where it is absorbed and scattered by atmospheric components so that the signal which later escapes the top of the atmosphere is somewhat depleted. In the case of OCO-2, the initial signal comes from the sun, and in the case of MFLX, the initial signal comes from the laser. The basic relation to describe the extinction of the signal is

$$(3.1) \quad P_{rec,\lambda} = C P_{trans,\lambda} e^{-\frac{2\tau}{\mu}}$$

Here $P_{rec,\lambda}$ is the received signal, $P_{trans,\lambda}$ is the initially transmitted signal. The constant C includes factors that are independent of the signal wavelength, such as surface reflectance, and instrument factors such as receiver antenna gain. The exponential term accounts for atmospheric extinction: the $\frac{2}{\mu}$ factor describes the path length, where μ is the cosine of the viewing angle θ , which is equal for the MFLX transmitted and received signals, giving the

factor of 2. This is usually not true for OCO-2, where the transmitted (solar) angle is not the same as the observation angle, so that $\frac{1}{\mu_{out}} + \frac{1}{\mu_{in}}$ is referred to the “airmass” or “airmass factor.”

The optical depth of the atmosphere is represented by τ , a dimensionless value which represents the sum of the optical depths of all major atmospheric components at a given wavelength. In the 1.6 μm band used by both OCO-2 and MFL, the main absorbing gases are CO_2 and water vapor. Other components of extinction include Rayleigh scattering, aerosols, and clouds. Thicker clouds are filtered out of the MFL dataset using the MFL’s intensity-modulation range-gating method; thin clouds remain more difficult to identify. In the MFL retrieval, these intermediate sources of extinction are largely assumed to be wavelength-independent. For example, with Rayleigh scattering, τ scales as λ^4 , which at 1.6 μm would change the optical depth by 0.001. Compared to the one-way differential optical depth of 0.5 for CO_2 and H_2O at the same wavelength, a factor of 0.001 makes very little difference in the retrieved X_{CO_2} . As such, Rayleigh scattering and other sources of intermediate extinction are largely assumed to be wavelength-independent and as such are accounted for within the constant coefficient.

A ratio of Equation 3.1 for two wavelengths (ON and OFF for MFL) yields

$$(3.2) \quad \ln \frac{P_{rec, \lambda_{OFF}}}{P_{rec, \lambda_{ON}}} = \ln \left(\frac{P_{trans, \lambda_{OFF}}}{P_{trans, \lambda_{ON}}} \right) \frac{-2}{\mu} (\Delta\tau_{\text{CO}_2, \lambda} + \Delta\tau_{\text{H}_2\text{O}, \lambda})$$

Where $\Delta\tau = \tau_{\lambda_1} - \tau_{\lambda_2}$, or the differential optical depth (DOD). Equation 3.2 is the basis of all differential absorption lidar (DIAL) measurements, a technique originally pioneered by Edward Browell for water vapor in the 1970s (Browell et al., 1979). In this equation, P_{rec}

and P_{trans} are measured; $\Delta\tau_{H_2O}$ is assumed to be known, either from a model (in the case of MFLL) or observations or both (in the case of OCO-2); and the target variable is $\Delta\tau_{CO_2}$.

The optical depth of any gas at a given wavelength can be calculated as the following:

$$(3.3) \quad \tau(\lambda) = \int_{P_{lower}}^{P_{upper}} \sigma(\lambda, P, T, q) dN_{CO_2}$$

where, in the case of the MFLL, P_{lower} is the pressure at the surface and P_{upper} is the pressure at the cruising altitude of the C-130. The absorption cross-section σ depends on wavelength, temperature, pressure, and humidity. Instruments such as OCO-2 and the MFLL, built particularly to gather data on CO_2 , must rely on model data for estimates of all but wavelength. N_{CO_2} is the moles of CO_2 per square meter of dry air, which also depends on both pressure and humidity, and thus also relies on model data. Spectroscopic tables are used to look up estimates of the corresponding cross-sections once estimates of T, P, and q are obtained.

Finally, X_{CO_2} is calculated by scaling a prior profile according to observed values. Assuming a constant prior profile (as the MFLL retrieval does), $\Delta\tau_{CO_2}$ is proportional to the CO_2 concentration (from Equation 3.3), and thus:

$$(3.4) \quad X_{CO_2} = \frac{\Delta\tau_{CO_2}(observed)}{\Delta\tau_{CO_2}(400)} \times 400$$

The MFLL retrieval results thus relies on three particularly variable inputs: meteorology, spectroscopy, and wavelength. The following section describes our investigation of these

sensitivities. (Preliminary tests also show a mild dependence on the shape of the prior profile, though detailed work has not been done on this front.)

3.2. MFLL RETRIEVAL INPUT SENSITIVITIES

Since the MFLL only measures CO₂ absorption at three wavelengths, its X_{CO₂} retrieval can be particularly sensitive to variability in spectroscopy and meteorological inputs. The level of these sensitivities has been only briefly studied in the past. Zaccheo et al. (2014) used a radiative-transfer-based simulation framework to estimate that X_{CO₂} errors for an MFLL-like instrument can range from 0.2 to 0.8 ppm depending on line positions; Crowell et al. (2015) concluded generally that uncertainty in atmospheric state estimates must be taken into account in the process of instrument design and error analysis. In order to quantitatively test these principles within MFLL retrievals, X_{CO₂} in this study has been calculated using three different meteorological models, combinations of three different spectroscopic databases, and with simple line position shifts. Table 3.1 provides a summary of the findings of these sensitivity studies: in general, we find that the ON/OFF_L retrievals are more sensitive to inputs than ON/OFF_S, with the exception of CO₂ spectroscopy.

TABLE 3.1

MFLL Retrieval Sensitivities Summary			
Variable	$\Delta X_{\text{CO}_2,S}$	$\Delta X_{\text{CO}_2,L}$	Summary
Meteorology	≤ 0.4 ppm	≤ 0.5 ppm	ON/OFF _S slightly less sensitive than ON/OFF _L ; ΔX_{CO_2} smaller than for spectroscopy changes
H ₂ O Spectroscopy	0 to 3 ppm	0 to 6 ppm	ON/OFF _L more sensitive to water vapor; differences larger in summer by a factor of 2 or greater
CO ₂ Spectroscopy	3 to 8 ppm	5 to 8 ppm	ON/OFF _S more sensitive to CO ₂ ; ΔX_{CO_2} largest of variables tested; differences similar in winter and summer but vary by day
ON Wavelength	≤ 0.2 ppm	≤ 1.2 ppm	ON/OFF _L more sensitive to offsets in ON wavelength; observed λ variations indicate little effect on X _{CO₂}

3.2.1. METEOROLOGY. Meteorological models provide vertical profiles of temperature, pressure, and water vapor, which are used in the calculation of absorption coefficients for each model level in the column. These are integrated vertically to get an optical depth per Equation 3.3. With variations in the vertical profiles come variations in the σ values, resulting in differing optical depths and X_{CO_2} results. Surface pressure is of particular importance, as differences in surface pressure are equivalent to differences in surface elevation and thus vertical column extent, or path length. A difference of 1 millibar in surface pressure can lead to a difference in X_{CO_2} of 0.4 ppm.

In this work we use three different meteorological models in our MFLL retrievals to evaluate retrieval sensitivity to atmospheric state parameters. We do not attempt to separate changes due to temperature profiles from changes due to water vapor profiles or surface pressure, though each has its own effect on the retrieval. Figure 3.1 shows the resulting X_{CO_2} differences (ΔX_{CO_2}) for two flights - one summer, one winter - when input meteorology is changed. The black and red datasets are the ΔX_{CO_2} for the ON/OFF_S and ON/OFF_L retrievals, respectively. The July 27th flight is on the left, and the February 15th on the right; all four panels hold spectroscopic inputs constant. The top panels show the difference between retrievals run with the GEOS5-FP and NCEP models, and the bottom panels show the difference between MERRA2 and NCEP. Notice that the patterns and magnitude of both GEOS5-FP and MERRA2 (top and bottom) when differenced with NCEP are similar. MERRA2 and GEOS5-FP are both produced by NASA's GMAO, and are similar products, but GEOS5-FP is an analysis while MERRA2 is a reanalysis. The difference between the two is often smaller than either of their differences from NCEP, which is why the difference from NCEP is shown here.

ΔX_{CO_2} values never exceed a few tenths of a ppm for any of the nine underflights, though the variation in space does slightly change the retrieved X_{CO_2} spatial gradients. This can affect MFLC comparisons to OCO-2, especially when best-fit slopes are used as a proxy for similarity in latitudinal gradients. Note that ΔX_{CO_2} is more variable in magnitude and in space in the summer flight (left) than in the winter flight, and that the OFF_S ΔX_{CO_2} is consistently of slightly lesser magnitude than the OFF_L ΔX_{CO_2} . This is because the OFF_L wavelength is slightly more sensitive to water vapor absorption. On days with higher relative humidity, we can expect differences in the prescribed water vapor profiles to have more of an effect on the X_{CO_2} retrievals.

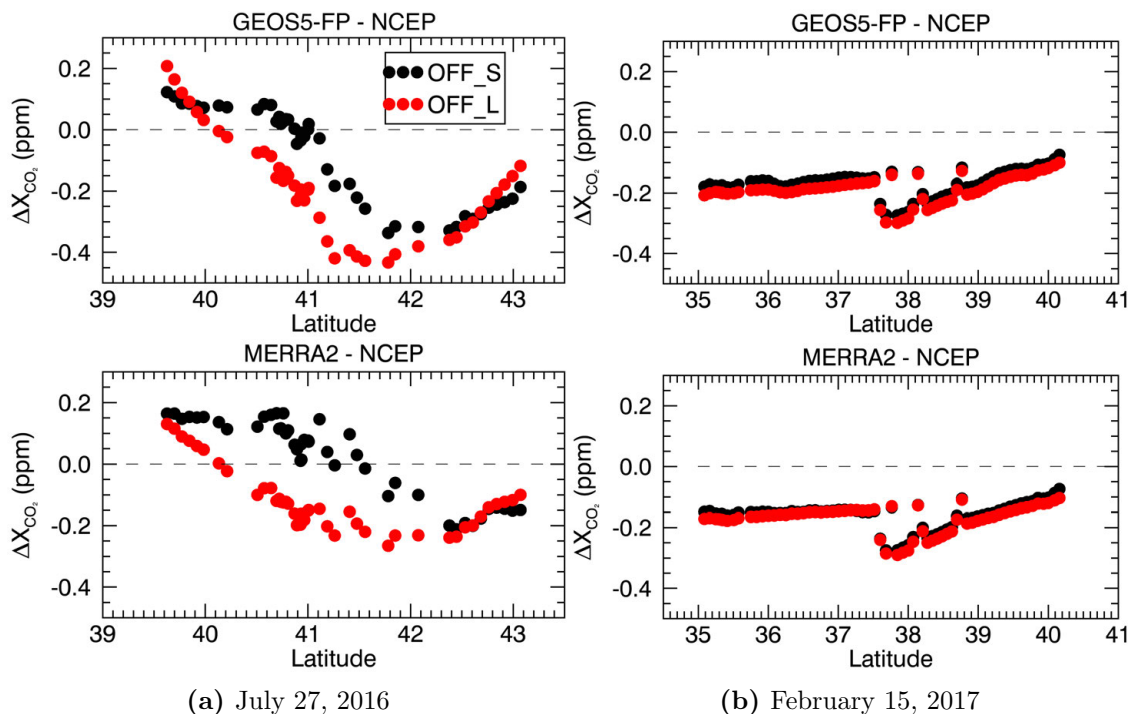


Figure 3.1. Changes in MFLC retrieved X_{CO_2} (ΔX_{CO_2}) due to changing the input meteorology. Black and red are the ON/OFF_S and ON/OFF_L retrievals. The left column shows the July 27th flight and the right shows February 15th. The top panels difference retrievals using GEOS5-FP meteorology from those using NCEP, and the bottom differences MERRA2 retrievals from NCEP. Results are variable in space and from day to day, but particularly from season to season, as the summer months with higher humidity (a) are more sensitive to changes in water vapor inputs. OFF_S ΔX_{CO_2} also tends to be smaller in magnitude, because it is less sensitive to water vapor absorption than the OFF_L wavelength.

3.2.2. SPECTROSCOPY. Spectroscopic lookup tables are used to find the absorption cross-sections of water vapor and CO₂ at a given wavelength, temperature, pressure, and humidity. Lookup tables contain values measured carefully in lab settings, but measurements of σ can vary. In this work we tested several combinations of spectroscopic tables in an attempt to learn what kind of variability σ variations can induce in the MFLL retrievals. Figure 3.2 shows the results for the same two flights as Figure 3.1, but when CO₂ and water vapor spectroscopy are changed. Each column is one flight. In the top panel, ΔX_{CO_2} is the difference between retrieved values using a common meteorology (GEOS5), common CO₂ spectroscopy (ABSCO 4.2), but different water vapor spectroscopy: ABSCO 4.2 minus HITRAN 2012. Notice that variability in the X_{CO_2} results is far greater in the summer case (left) than in the winter cases (right), since relative humidity is lower in the winter months. Some humidity variations between winter flights do exist, but ΔX_{CO_2} values largely remain at 1 ppm or less, whereas summer flights consistently show a multiple-ppm change. Also notice that with higher humidity, the OFF_L retrieval changes more than the OFF_S retrieval, since the OFF_L wavelength is more sensitive to water vapor absorption. In the summer case, ΔX_{CO_2} varies by a little over 2 ppm over the length of the flight track in the OFF_L retrievals, which can significantly change the observed spatial gradient.

The bottom row shows ΔX_{CO_2} when the water vapor spectroscopy is held common (HITRAN 2012), but the CO₂ spectroscopy is variable: ABSCO 4.2 versus pre-HITRAN 2016. There is less variation in space than for H₂O spectroscopy changes, which is no surprise, as water vapor concentrations are far more variable in the atmosphere than CO₂ concentrations. Again, we see changes of several parts per million, this time more consistent in magnitude between the two seasons. Retrieval results differ by at least 4 parts per million

for both OFF_S and OFF_L on each day, though OFF_S changes most - a consistent result throughout the nine flights. A change of similar magnitude - usually around 6 ppm - is found when the HITRAN 2012 CO₂ tables are changed to a more recent pre-HITRAN2016 CO₂ version.

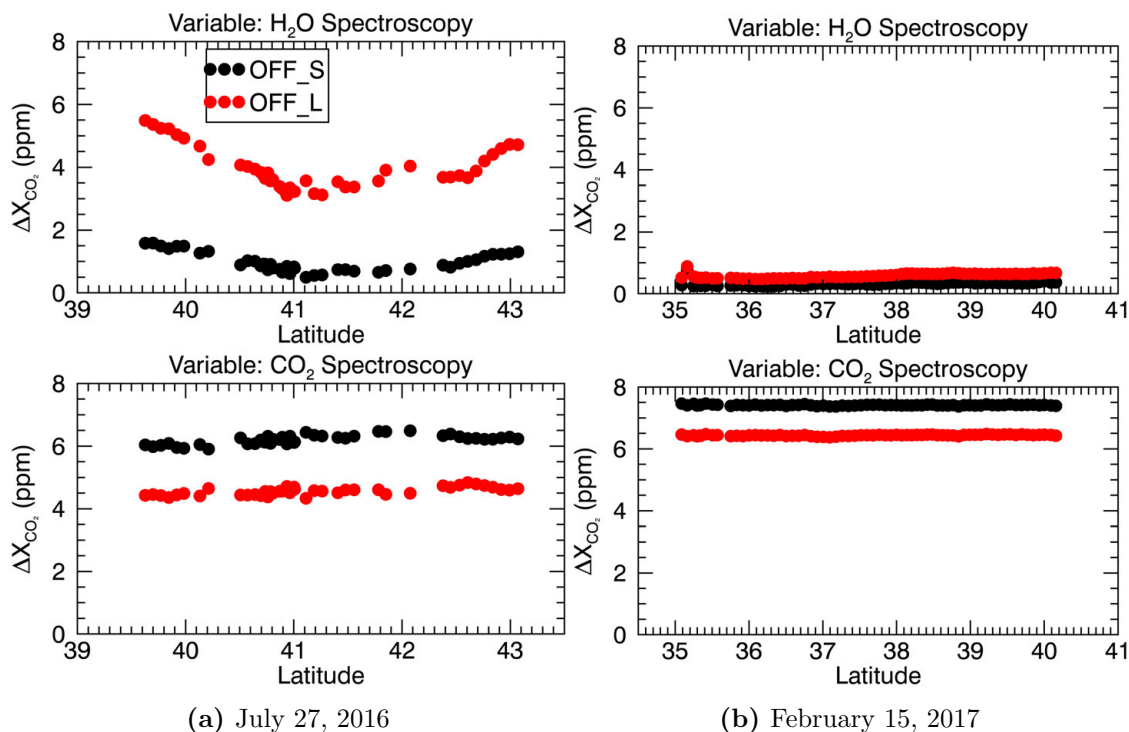


Figure 3.2. Changes in MFL retrieved X_{CO₂} (ΔX_{CO₂}) for two ACT-America OCO-2 underflights (left and right) when using different spectroscopic lookup tables. Black and red are changes in the ON/OFF_S and ON/OFF_L retrievals, respectively. The top two panels keep meteorology and CO₂ spectroscopy the same, but change the H₂O spectroscopy (ABSCO 4.2 - HITRAN 2012). Changes are far greater in the summer (**a**) when the humidity is higher, and OFF_L retrievals change more than OFF_S retrievals because the OFF_L wavelength is more sensitive to water vapor absorption. The bottom two panels keep meteorology and H₂O spectroscopy the same, but change CO₂ spectroscopy (ABSCO 4.2 - pre-HITRAN 2016). ΔX_{CO₂} magnitudes are more consistent in latitude and between the two seasons in this case, because atmospheric CO₂ concentrations vary less in those dimensions than water vapor does. The difference between OFF_S and OFF_L changes are also more consistent - a few ppm - between summer and winter for the same reason.

3.2.3. WAVELENGTH. Finally, we investigate how the precision and accuracy of our wavelength knowledge might change MFL retrieval results. The reference laser used to track

wavelength drift in time due to environmental variables is assumed to be locked at one wavelength at the peak of an acetylene absorption line (see Figure 2.9 on page 26 for a diagram of this setup), and measured with an accuracy of 0.1 pm. The July 27, 2016 retrieval was

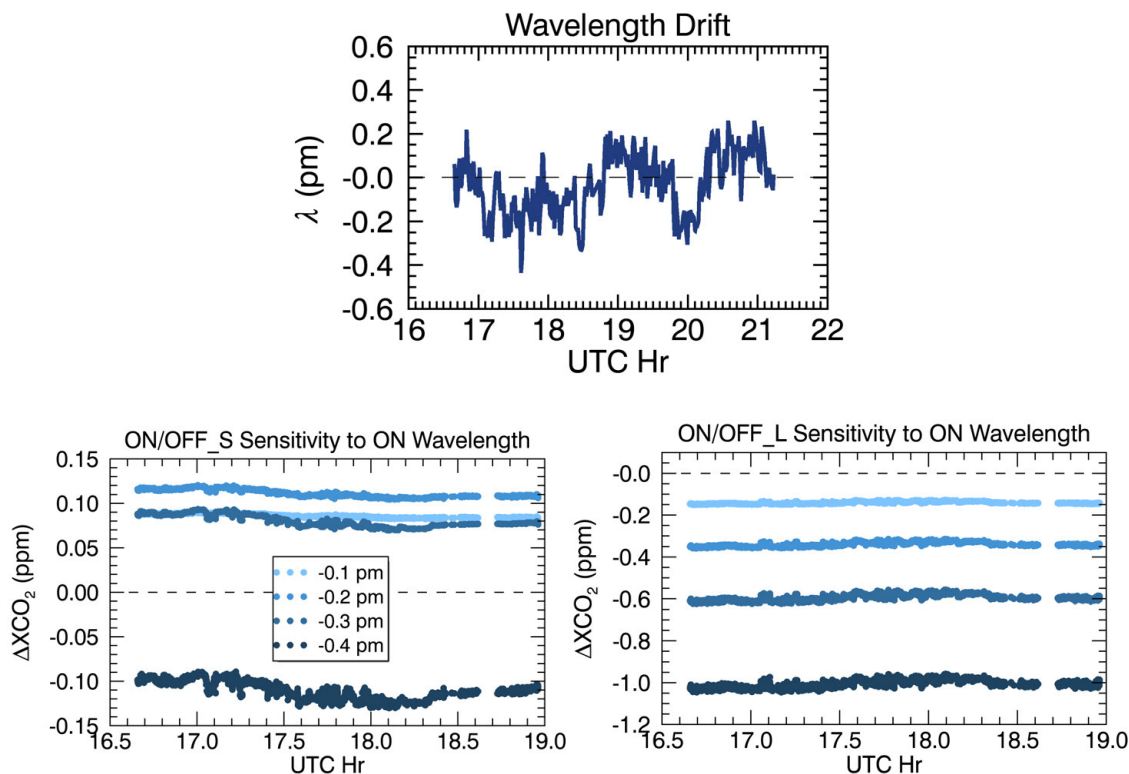


Figure 3.3. The top panel shows wavelength drift due to environmental factors for the July 27, 2016 underflight. Bottom panels show changes in 9-kilometer ON/OFF_S retrieved X_{CO_2} (left) and ON/OFF_L X_{CO_2} (left) when the value of the ON wavelength is adjusted by a constant amount (indicated by the legend in the lefthand panel) for the duration of the flight. Note the different y axis ranges in the bottom plots. Shifts in the ON wavelength have relatively small - but not insignificant - effects on the retrieved ON/OFF_S results; a 0.1 pm shift to the “short” side changes the retrieved X_{CO_2} by nearly a tenth of a ppm. The ON/OFF_L sensitivity is far greater. When the ON wavelength is shifted 0.1 pm to the short side, retrieved X_{CO_2} decreases by almost 0.2 ppm. Shifting the ON wavelength by 0.4 pm can result in a full part per million change.

run using several different ON wavelength offsets in steps of 0.1 pm. Figure 3.3 shows the reference wavelength drift (top) over the course of the flight, in picometers from the reference value. This drift is assumed to be representative of environmental variations which affect the MFLL lasers as well, and is applied as a correction to the reference values for all three

MFLL channels. The magnitude of this drift consistently spans only a few thousandths of a picometer. The bottom panels of Figure 3.3 shows the ΔX_{CO_2} of the OFF_S (left) and OFF_L (right) retrievals when the value of only the ON wavelength is shifted by the values shown in the legend. Results show that if indeed the wavelength is measured to within 0.1 pm, retrieved X_{CO_2} from either wavelength combination should change by no more than a few tenths of a ppm. The OFF_L retrievals are more sensitive to wavelength uncertainty, changing by more than 1 ppm when the ON wavelength is offset by 0.4 pm, but this appears to be near the upper limits of a typical detected in-flight wavelength variation. If for some reason variations of this magnitude were missed, they appear only to impose an offset, but not to change the spatial variability and gradients.

We conclude from these tests that both meteorological and spectroscopic inputs can affect the magnitude and spatial variability of MFLL retrievals in non-negligible ways, but that given the accuracy of the measured reference wavelength, wavelength variations should have very little effect in most cases.

MFLL RETRIEVAL VERTICAL SENSITIVITY CORRECTIONS

The basic physical and mathematical principles outlined in Section 3.1 are common between the MFLL and OCO-2 retrievals, but there are a few significant differences which may affect data comparisons.

- (1) The MFLL, due to its range-gating technique, is not sensitive to atmospheric scattering or surface albedo, whereas OCO-2 is.
- (2) Both the MFLL and OCO-2 X_{CO_2} retrievals rely on assumed profiles of temperature, pressure, and water vapor - but OCO-2 attempts to retrieve some information on these quantities, where the MFLL does not. This may, as detailed in Chapter 3, make the MFLL measurements more sensitive to meteorological errors.
- (3) The MFLL appears to be more sensitive to spectroscopy because it samples only one CO_2 line at three places, whereas OCO-2 samples dozens of lines across two CO_2 absorption bands.
- (4) OCO-2 and the MFLL have different vertical sensitivities, which complicates the comparison of their column-averaged values.

This chapter discusses our attempts to address the final point in this list. Both the MFLL and OCO-2 essentially return weighted averages of the CO_2 profile, but the weights differ in the vertical between the two instruments according to their relative weighting functions, which are shown in Figure 4.1. The OCO-2 averaging kernel, shown in yellow, is near enough to a straight-pressure weighting function (blue) that in this work, they are treated as the same. The MFLL weighting function, however, shown in red, is different enough to change the column average significantly. In this chapter we describe our method of “transforming”

the MFLL retrieval into a full straight-pressure column measurement by using models to inform the vertical shape. Using model data in this process necessarily introduces some error, so we test two models, CAMS and CarbonTracker, and look at their differences to roughly quantify the potential errors imposed.

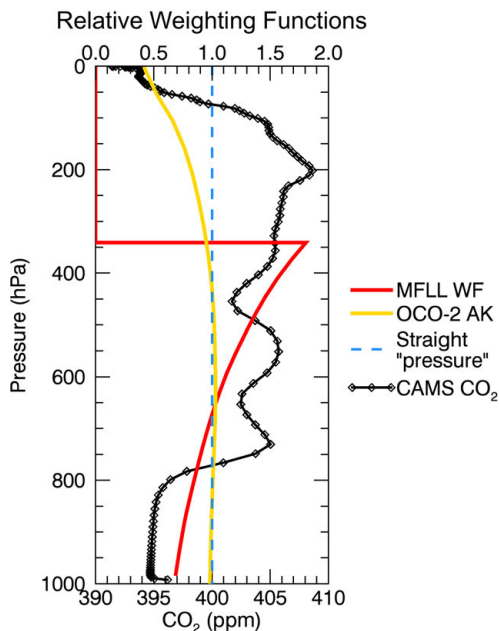


Figure 4.1. MFLL, OCO-2, and straight-pressure “weighting functions” for July 27, 2016, with sample CAMS CO₂ profile in black. Note that the MFLL weighting function goes to zero above the altitude of the airplane. This missing section of the column can cause a bias in the MFLL X_{CO₂} compared to the full column OCO-2 value.

The MFLL, as a surface-pointing an airborne instrument, can only measure the column below the level at which the C-130 is flying (nominally 9 kilometers for OCO-2 underflights); OCO-2, at an altitude of 700 kilometers, effectively measures the full atmospheric column. There is thus a portion of the upper column absent from the native MFLL X_{CO₂} measurement, but which is present in OCO-2 measurements. The concentrations in this part of the column, if substantially different from those throughout the column below the aircraft, can change the X_{CO₂} value noticeably: the air above 9 kilometers (about 350 hPa) accounts for about one-third of the total column.

The shape of the MFLl weighting function below the aircraft is also significantly different from that of OCO-2. The OCO-2 averaging kernel is nearly straight through much of the troposphere, peaking slightly around 600 hPa. The MFLl is most sensitive to atmospheric layers just below the plane, and as it approaches the surface, its sensitivity tapers off to nearly one-third its maximum value.

These idiosyncrasies in the MFLl measurements can lead to X_{CO_2} values which are up to 1.5 ppm different from the OCO-2 X_{CO_2} values, either higher or lower depending on the shape of the profile. Average CO_2 concentrations above 350 hPa are indeed often lower than those in the rest of the column by several parts per million, and MFLl's strong over-weighting of the values just below the aircraft can shift the X_{CO_2} results based on the relative CO_2 values in that portion of the column. This is particularly true in summer, when mid-tropospheric concentrations are often several ppm higher than those in the lower troposphere and boundary layer due to surface drawdown by the biosphere. A sample CO_2 model profile is included in black in Figure 4.1 to illustrate how the shape of the profile might affect the X_{CO_2} value in these ways: mid-tropospheric values in this example are about 5 ppm higher than boundary layer values.

In order to evaluate the general magnitude of these effects on the X_{CO_2} results, for six of the nine flights, we sample the CAMS CO_2 model along the OCO-2 ground track. We then calculate X_{CO_2} along the track three times, using the MFLl pressure weighting function (PWF), OCO-2 averaging kernel, and a straight pressure-weighted average. When using the MFLl PWF, which goes to zero above the C-130, the CO_2 column is cut off above the aircraft altitude for the given flight. Figure 4.2 shows the results of this exercise for two different underflights, one in summer (left) and one in winter (right). The top panel in

each figure are the X_{CO_2} values, and the bottom panels show the difference from straight-pressure weighted X_{CO_2} (blue) when using MFLL and OCO-2 weighting (red and yellow). The OCO-2 averaging kernel consistently yields X_{CO_2} values only slightly lower than the straight pressure values, by a few tenths of a ppm or less, while the MFLL results exhibit two interesting features. First off, the MFLL-weighted X_{CO_2} values are different than both the OCO-2 and straight pressure results by up to a few parts per million. This difference is more pronounced in the winter data due to low CO_2 concentrations in the missing upper column throughout the flight track, shown in Figure 4.3, where CAMS model profiles (left) are colored in latitude and the in situ profiles are overlaid in black. The upper column concentrations (above the horizontal black line, the C-130 cruising altitude) in summer are more similar to those below the plane, so exclusion of the upper column has a less dramatic effect on the column average. This is also true of the CarbonTracker profiles, in the right hand panels of Figure 4.3. The second notable feature of the MFLL-weighted X_{CO_2} is its enhanced spatial variability compared to both OCO-2 and the straight pressure results.

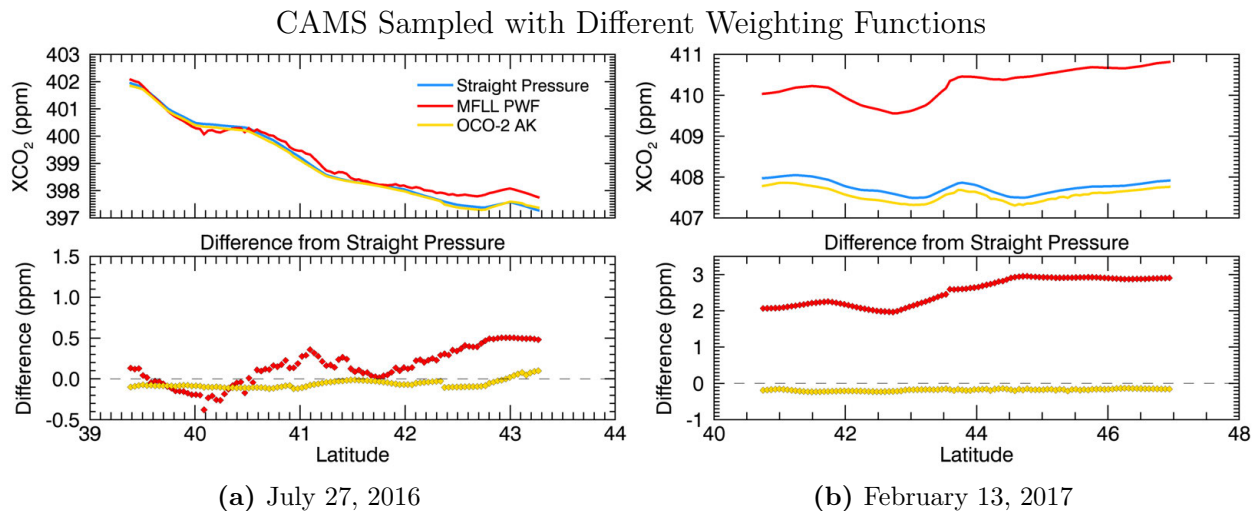


Figure 4.2. X_{CO_2} calculated from CAMS model CO_2 profiles, using three different vertical weighting schemes: the MFLL weighting function, OCO-2 averaging kernel, and a “straight pressure” weighting function. Note that the y-axes vary between plots in both top and bottom windows. Also note that the MFLL results (red) show consistently higher values.

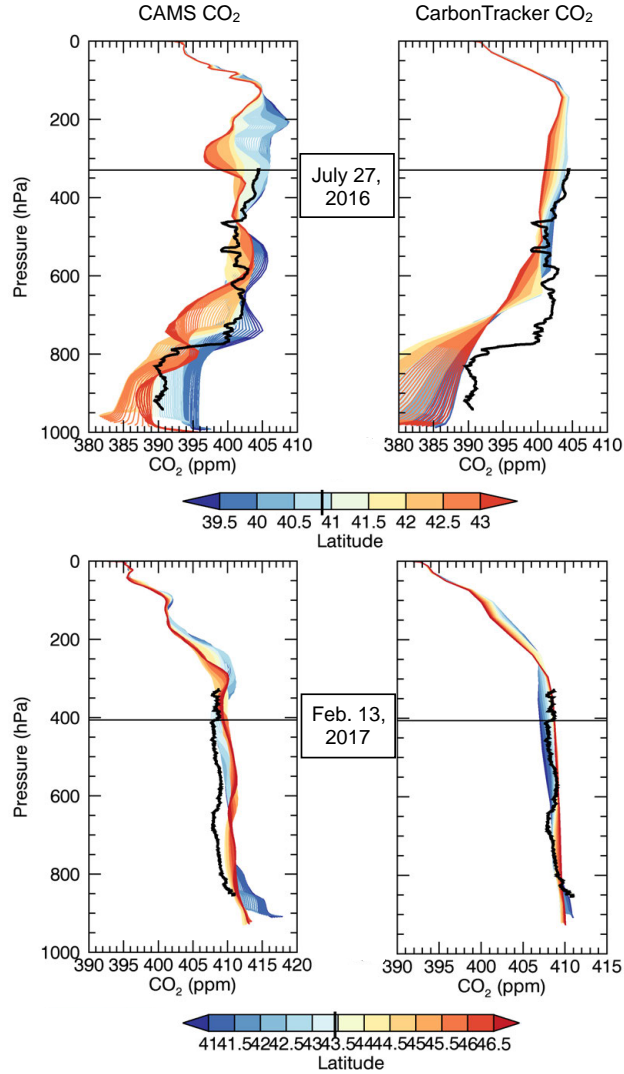


Figure 4.3. CAMS model profiles (left) along the July 27 and February 13 flight tracks, colored by latitude. CarbonTracker profiles are on the right. Overlaid on each plot is the in situ spiral profile, whose latitude is indicated in each case by a tick mark on the color bar. Horizontal black lines indicate the average cruising altitude of the C-130 during the underflight.

If either the missing upper column or the weighting function shape introduces some spatial variability to the MFL X_{CO_2} data, as they appear to do in this exercise, that variability is representative of the lower troposphere and gets averaged out in the OCO-2 data. Parsing out this variability in comparisons between the two may be challenging.

Thus, in order to correct for any such variability, we generate correction factors for the two defining differences: the MFLL weighting function shape and the unobserved upper column. The left panels of Figure 4.4 provide a visualization of these two corrections (dashed lines) in latitude for the July 27 and February 13 flights. The red lines show the difference between the MFLL-weighted CAMS X_{CO_2} and straight pressure-weighted CAMS X_{CO_2} , same as shown

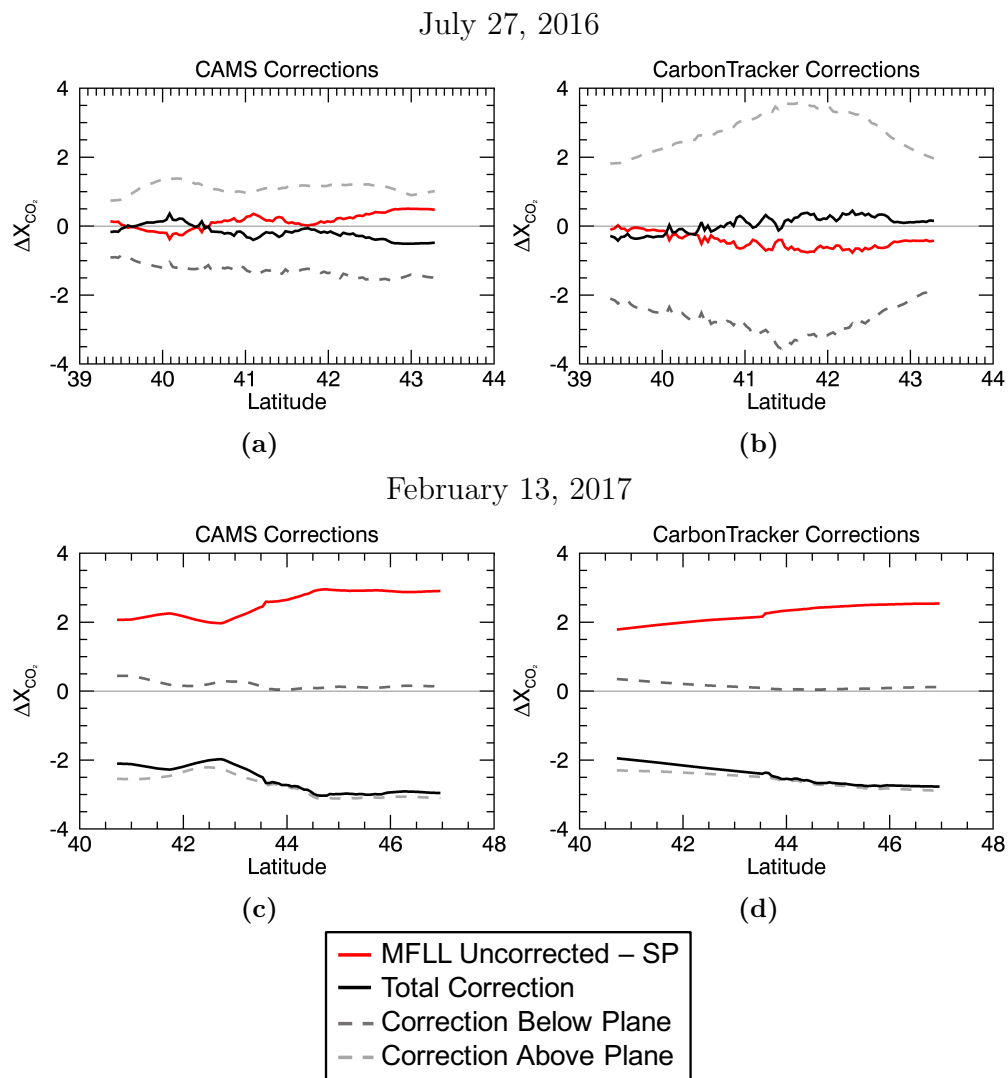


Figure 4.4. Figures (a) and (b) show, in red, the difference between uncorrected MFLL-weighted CAMS X_{CO_2} and straight pressure-weighted CAMS X_{CO_2} , as shown in Figure 4.2. The corrections above and below the aircraft, in dashed lines, sum to produce the total correction factor in black. Note that the black and red lines mirror each other, canceling to replicate a full straight pressure-weighted average. This eliminates variability in the partial column as observed by the MFLL.

in the bottom panels of Figure 4.2. The black line is the total correction we apply, with is the sum of the two dashed lines. Note that the red and black dashed lines cancel to zero, eliminating the variability caused by the MFLl weighting function and successfully replicating the full column straight-pressure average. The right panels of this figure show the same corrections when this exercise is performed using CarbonTracker model profiles.

The MFLl corrections shown in Figure 4.4 are derived as follows. The column below the plane is referred to as B , the column above as A , and the full column as X . We start by comparing the full column average using straight pressure, X , with the MFLl-weighted partial CAMS (or CarbonTracker) column below the aircraft, or B_m . $B_m - X$ is the red line in Figure 4.4. The first correction we apply, Δ_B , the dark gray dashed line, accounts for the shape of the MFLl weighting function: we calculate the partial column below the plane using straight pressure (B), and use the correction

$$(4.1) \quad \Delta_B = B - B_m$$

When applied to the MFLl-weighted value as in equation 4.2, Δ_B gives us a straight pressure-weighted partial column below the plane.

$$(4.2) \quad B_m + \Delta_B = B$$

This equation seems redundant in this model exercise, as we could simply start with B , but when dealing with real observations, B_m is measured by the MFLl from the true CO₂ field. Since the MFLl does not return vertical profile information, we cannot calculate the

corresponding true B and must use the closest model estimate, which varies by day. For example, we use CAMS on July 27th (and for all summer flights) due to its similarity to the in situ spiral in Figure 4.3 (left), and because CarbonTracker (right) clearly underestimates concentrations near the surface. On February 13th, however, we use CarbonTracker, because the CAMS profiles (left) are consistently a few ppm higher than the in situ suggests they should be. The CarbonTracker profiles on the right appear to be roughly the correct magnitude.

The correction above the aircraft, Δ_A , the light gray dashed line, produces a full column value by doing a weighted average of the straight pressure partial column below the plane (B) and the straight pressure partial column above the plane (A). Weights, f_A and f_B , are the fraction of total column dry air molecules in A and B . f_A is typically around 0.3, or 30% of the total column. The fully corrected column-averaged X_{CO_2} is thus

$$(4.3) \quad X = f_A A + f_B B$$

and the correction above the plane has a magnitude of

$$(4.4) \quad \Delta_A = X - B$$

Based on the sum of the two correction factors (black line = $\Delta_A + \Delta_B$) in Figure 4.4, we conclude that each correction has an effect on the total, varying by day and season. There is more small-scale variability in the summer corrections (top row) than in the winter corrections (bottom row) from both models, due to the enhanced variability below the aircraft

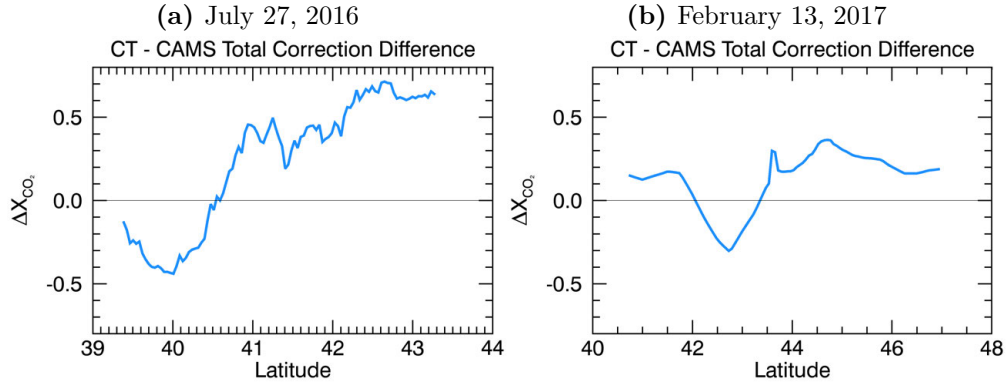


Figure 4.5. CarbonTracker total correction minus CAMS total correction (black lines from Figure 4.4). The corrections are different by up to 0.71 ppm in summer (a) and up to 0.36 ppm in winter (b), and there is difference in the spatial variations between them. These differences highlight the need to choose the model which best represents the true CO₂ field on a given day.

in the summer. In addition, the winter corrections from both models are due primarily to the correction above the plane because the profiles below the plane are relatively flat (see bottom panels of Figure 4.3), so the vertical shape of the MFLC weighting function has less effect on the column average.

Note that Δ_A , like Δ_B , relies on model profiles, since neither the MFLC nor in situ sample above nine kilometers at best. The use of model data thus necessarily introduces error through both corrections. We estimate this error by looking at the difference (Figure 4.5) between the total model corrections (black lines in Figure 4.4). The summer corrections differ most between the two models, by up to 0.71 ppm, and the winter corrections differ by up to 0.36 ppm. In both cases they also show differences in their spatial variability. This indicates that based on the true atmospheric state at the time of the MFLC observations, different models can produce corrected results with differences on the order of a 0.3 to 0.7 ppm, which, in summer, is comparable to the size of the correction itself.

Based on these model exercises, we conclude that both the upper column and weighting function corrections will have non-negligible effects on the MFLC - OCO-2 comparison, and

indeed should improve the comparison. We thus incorporate both of them into our X_{CO_2} results for each set of flight comparisons. Using different models can result in differences of several tenths of a ppm in the corrected results, so we attempt to choose the model best representative of the true CO_2 field sampled by the instruments: CAMS in the summer and CarbonTracker in the winter. CarbonTracker data were not available for fall flights but would presumably show similar agreement to in situ as they do in winter, making them the best source of our corrections.

RESULTS

This chapter details at length each of the nine OCO-2 underflights completed by ACT-America to date. Included and discussed for each flight are maps and cross-sections of the flight track in time, cross-sections of in situ data from both the C-130 and B-200 aircraft, and comparisons of in situ CO_2 profiles to model profiles. Also shown are maps of the OCO-2 X_{CO_2} data, and finally, comparisons of X_{CO_2} datasets. At the end of each comparison is a table of statistical parameters concerning each dataset and their intercomparisons, and at the end of each flight section, a summary of key findings is provided. For a less exhaustive overview of the comparison results, the reader can see Chapter 6, which will reference particularly interesting figures from this chapter.

For each of the nine OCO-2 underflights, MFL data evaluated is isolated to the underflight track. After data and cloud filtering are applied, the MFL data are averaged in 60-second bins to reduce noise. Each bin is filtered by a minimum number of required observations. To evaluate similarities in spatial variability along the flight track, OCO-2 data is collocated in space to each 60-second MFL bin, which usually spans about 7.5 - 8 kilometers in ground area. Any OCO-2 footprint whose center is within this 8-kilometer distance of an MFL bin center is averaged together and taken to be the OCO-2 value at that location; the noise on each bin after this averaging is relatively small, between 0.1 and 0.2 ppm on a typical summer day and closer to 0.3 ppm in winter, for both OCO-2 and the MFL. Figure 5.1 shows a flow chart of the steps taken to prepare the MFL and OCO-2 datasets for comparison. This results in an equal number of measurements along the flight track for both datasets, such that correlation coefficients can be calculated without requiring

any spatial interpolation. The r values shown in the tables for each flight are calculated in this fashion.

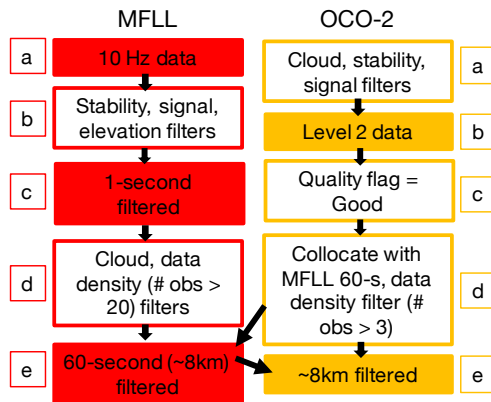


Figure 5.1. Flowchart showing the filtering and averaging process leading to MFL and OCO-2 data comparisons.

There is a table of statistics included for each flight. The correlation coefficient r_{OCO_2} is the correlation with the OCO-2 data, and the r value in parentheses is the correlation with OCO-2 after the latitudinal gradient is removed. This represents the correlation of X_{CO_2} features on scales smaller than the full flight track length. The slope for each dataset in latitude is included, calculated using the best-fit line through the length of underflight track. Also included is the mean difference from OCO-2, and the standard error of the mean, in which the 2σ standard deviation (also shown) is divided by the square root of the number of observations in each 60-second bin.

Typical requirements for minimum number of observations per 60-second bin are different for OCO-2 and the MFL. OCO-2 bins require at least three soundings, and MFL require at least 20, unless otherwise noted. These numbers are chosen to sufficiently reduce noise and reveal spatial gradients; OCO-2 requires less soundings than MFL because it has less observations along the ground track by its nature.

The X_{CO_2} plots in this chapter do not show this collocated, averaged version of the data. Instead, all data available from each dataset along the length of the underflight track is displayed, as large triangles, using an appropriate averaging window for each. This is done to visualize the most data possible - for example, if OCO-2 loses data to clouds, we can still see the MFL data along that portion of the track. The MFL data is averaged at 60 seconds, but the OCO-2 data is averaged at 0.25 seconds, though they are similar spatially, and curtain data (currently only available for July 27) is averaged in space at 0.1-degree latitude intervals. The small yellow triangles in the background of each plot show the un-averaged OCO-2 data that contribute to the large triangles - these data have been cloud-screened and quality-flagged. A green star represents the X_{CO_2} column calculated from the in situ spiral, including a model profile top, using a straight pressure weighting function.

Each X_{CO_2} plot uses MERRA2 meteorology and pre-HITRAN 2016 spectroscopy. The plot title lists the average spatial coverage of the 60-second MFL bins (based on average aircraft speed along the underflight track), and which CO_2 model profiles were used to conduct the column “corrections” above and below the plane. CAMS and CarbonTracker full column X_{CO_2} data are also shown for each flight, except for the fall 2017 campaign, because CarbonTracker data is not yet available for that period.

Note also that the summer campaign dates show retrieval results using the MFL Level 1 data product, which includes bias correction and several data filters different from the proceeding campaigns (these are described in Section 2.3). The Level 1 product only reports an optical depth using the ratio of ON to OFF_S; thus there are no OFF_L results pictured in the summer results. This product has not yet been released for the winter and fall ACT-America campaigns.

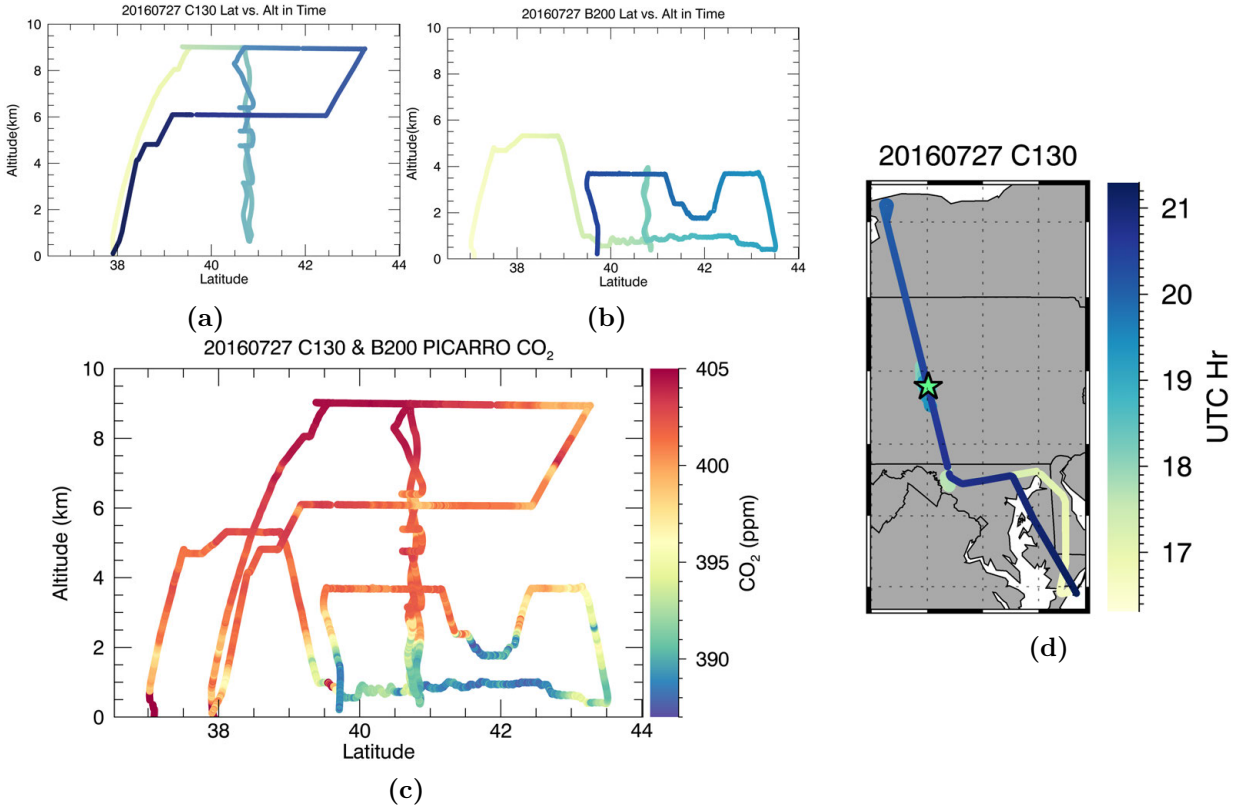


Figure 5.2. Latitude-altitude plots for each individual aircraft on July 27, 2016, and a map of the C-130 flight track, all colored in time. Note that the underflight track, at an altitude of approximately 9 kilometers, spans nearly two hours, whereas an OCO-2 overpass of the same distance takes around 1.5 minutes. Also shown is the combined CO₂ in situ data from both aircraft.

5.1. JULY 27, 2016

The C-130 flew along the OCO-2 underflight track over Pennsylvania at an altitude of around 9 kilometers for a period of nearly 2 hours. One spiral maneuver was completed in the middle of the underflight; its geographic location, near State College, PA, is indicated by the star on the map on the right hand side of Figure 5.2. The OCO-2 data is shown in Figure 5.4, plotted on top of MODIS visible imagery to provide context for cloud cover and surface albedo patterns along the track.

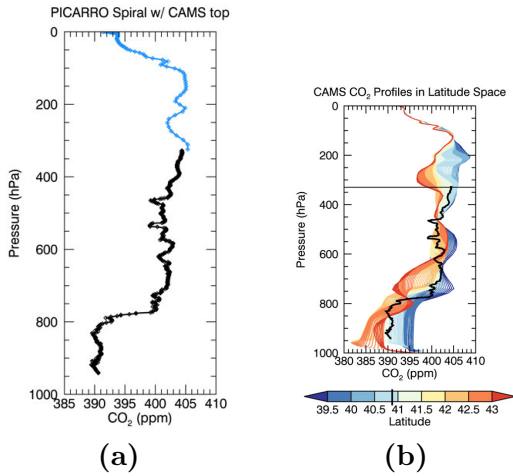


Figure 5.3. (a) July 27 in situ spiral up to the C-130 height (black), with CAMS model profile above (blue), which has been interpolated to location and time. (b) In situ spiral in black, with CAMS model profiles along-track at the median time of the spiral, colored in latitude. The cruising altitude of the plane is marked by the black line around 350 hPa.

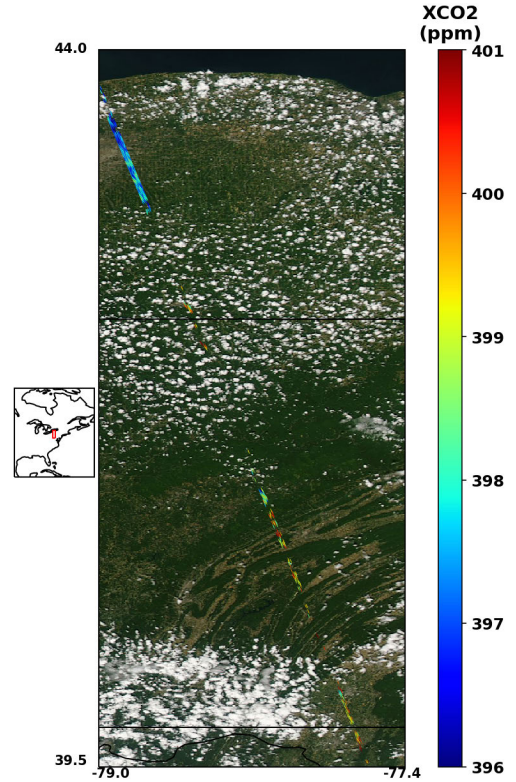


Figure 5.4. OCO-2 X_{CO_2} along the July 27 MFL underflight track, showing all eight footprints atop MODIS visible imagery.

There are a few notable features in Figures 5.2 and 5.4. Firstly, the in situ CO_2 data in 5.2c displays, in both the boundary layer and at 9 kilometers, a strongly decreasing south-to-north gradient in CO_2 . This is also apparent in the OCO-2 data, though the gradient is less steep due to the data being column-averaged. A field of popcorn cumulus clouds obscures the OCO-2 track across roughly 1.5 degrees latitude between 41 and 43N; however, a few soundings do pass the OCO-2 cloud flag in this area, around 42N. Figure 5.5 shows that those values do not appear in line with the larger latitudinal gradient, and hence appear to be spurious.

Figure 5.3 a shows the in situ PICARRO CO_2 spiral in black with the interpolated CAMS profile above, which is used to make the X_{CO_2} adjustment above the plane. The boundary

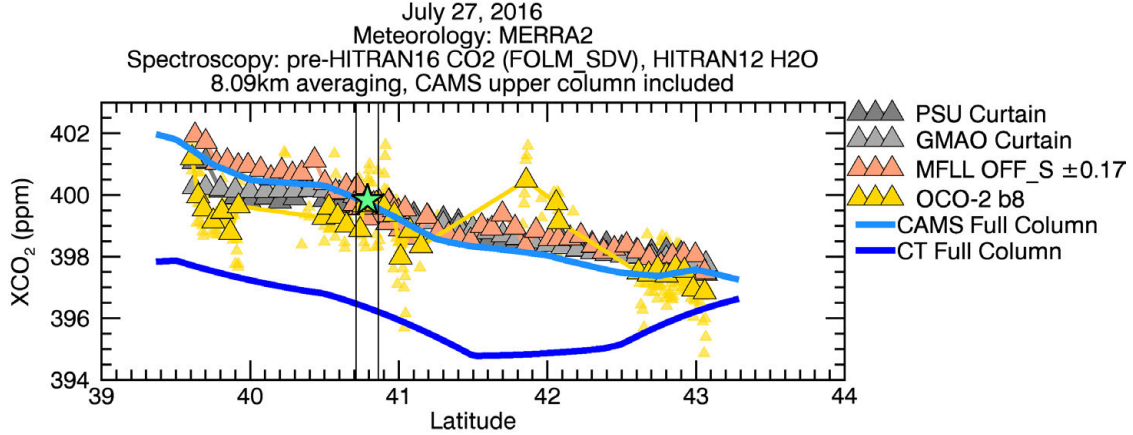


Figure 5.5. Comparing various X_{CO_2} datasets from the July 27 underflight. The in situ spiral column-averaged value, with CAMS model top included, is shown as a green star. The CAMS full column values are calculated using a straight pressure weighting function.

layer below 800 hPa shows strong surface drawdown, characteristic of the summer growing season. Figure 5.3b shows the CAMS profiles colored in latitude, with the PICARRO spiral profile overlaid in black and marked in location by a tick on the color bar. The decreasing value in X_{CO_2} to the north appears clearly in the model, due particularly to decreasing CO_2 concentrations in the lower troposphere between 800 and 600 hPa.

TABLE 5.1. July 27, 2016 Slopes and Correlations with OCO-2

	σ (ppm)	Mean $\Delta X_{\text{CO}_2} \pm \text{Error}$ (ppm)	$r_{\text{OCO-2}}$	Slope (ppm/°)
OCO-2	0.69	0 ± 0.24	-	-0.70
MFLLS	1.10	0.58 ± 0.17	0.67 (-0.29)	-1.06
PSU Curtain	0.10	0.40 ± 0.01	0.72 (-0.05)	-0.81
GMAO Curtain	0.02	0.38 ± 0.002	0.75 (0.07)	-0.84
CAMS	-	0.33	0.71 (-0.30)	-1.22
CarbonTracker	-	-2.64	0.24 (-0.64)	-0.68

Visual evaluation of the X_{CO_2} patterns from the datasets in Figure 5.5 reveals latitudinal gradients of similar magnitude among curtains, OCO-2, CAMS, and MFL. The MFL level 1 retrieval results, however, even with both the upper column and weighting function corrections applied, shows a slightly (up to 1 ppm) lower X_{CO_2} relative to the other datasets. We take the magnitude of the higher datasets to be true based on their agreement with the

in situ column value. Table 5.1 lists the slopes, standard errors, and correlations with OCO-2 for each of the datasets shown, along with their X_{CO_2} differences compared to OCO-2.

OCO-2 and CarbonTracker have the shallowest slopes over the flight track, at -0.70 and -0.68 ppm per degree latitude respectively. However, CarbonTracker disagrees with OCO-2 on both magnitude and sub-degree spatial features, and the two have a correlation coefficient of only 0.24, the lowest for this day: CarbonTracker data are consistently several ppm lower than the other datasets, consistent with discussion in 2. The in situ curtains have the next closest slope to OCO-2 with -0.81 and -0.84 ppm/°. The MFL and CAMS data have steeper slopes of -1.06 and -1.22 ppm/°, starting at slightly higher concentrations at the southern end of the track. All datasets except CarbonTracker show a relatively strong correlation with OCO-2 in latitude space, but the GMAO curtain is strongest with $r = 0.75$. The PSU curtain and MFL level 1 ON/OFF_S retrievals are next, with r values of 0.72 and 0.67. The $r_{\text{OCO-2}}$ values with latitudinal gradients removed are significantly lower, all but one below zero. This indicates that there is little agreement of smaller-scale spatial features.

5.2. AUGUST 5, 2016

The second summer 2016 flight out of Lincoln, Nebraska crossed South and North Dakota, flying up to the Canadian border. The underflight was completed at an altitude of about 9 kilometers, with a secondary leg along the flight track around 5.5 kilometers. The 9 kilometer track was flown over the course of roughly two hours, as shown in Figure 5.6a. The B-200 executed the spiral maneuver around 47 degrees latitude, shown in Figure 5.6b and as a star in Figure 5.6d. The in situ data in Figure 5.6c shows decreasing CO_2 concentrations from south to north, fairly consistently in the vertical anywhere below about 8 kilometers in altitude. Once again, the OCO-2 data (shown in Figure 5.7) appears to confirm some

latitudinal gradient, on the order of about 2 ppm across the full flight track. The northernmost and southernmost ends of the overpass are obscured by clouds, though a few spurious OCO-2 soundings do pass the cloud screening process around 47.5N, visible in Figure 5.9.

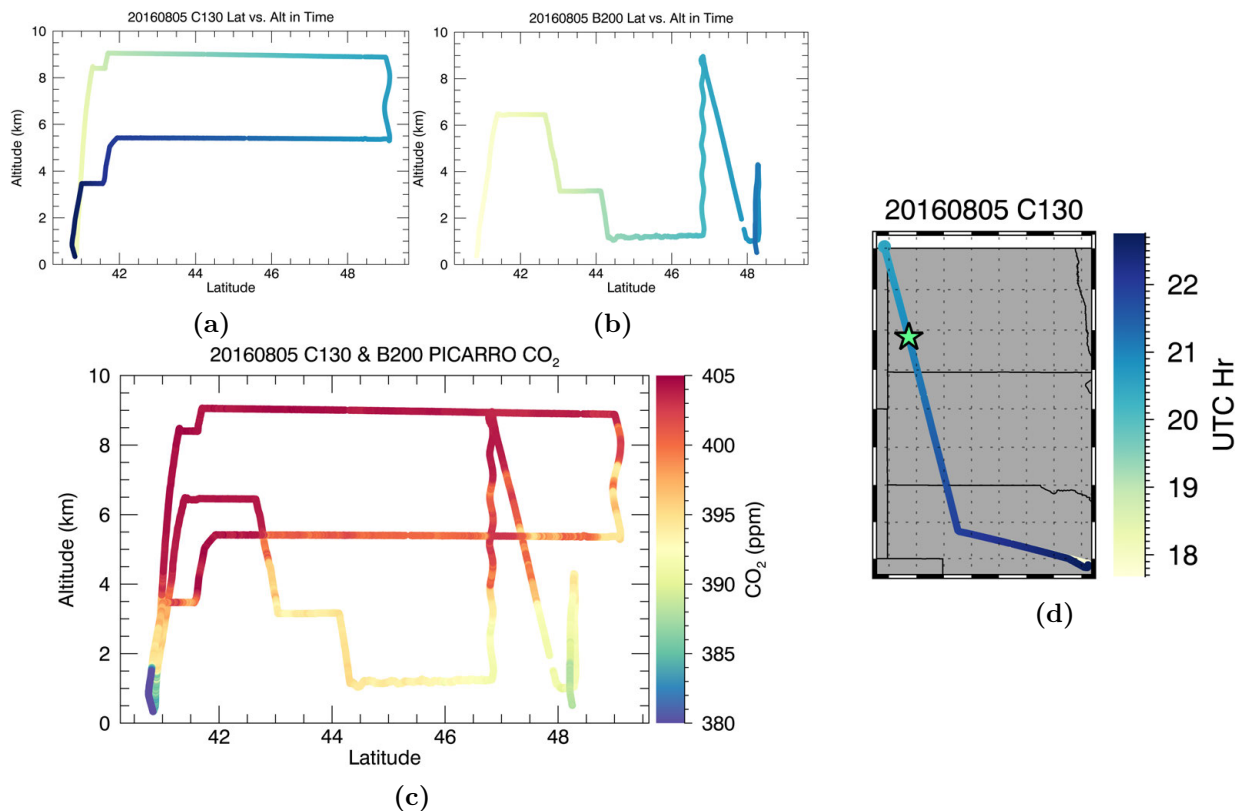


Figure 5.6. Both aircraft in latitude and altitude, colored in time (a, b and d) along with a flight map, and in situ CO₂ data (c) for August 5, 2016.

TABLE 5.2. August 5, 2016 Slopes and Correlations with OCO-2

	σ (ppm)	Mean $\Delta X_{\text{CO}_2} \pm \text{Error}$ (ppm)	$r_{\text{OCO-2}}$	Slope (ppm/°)
OCO-2	0.63	0 ± 0.17	-	-0.43
MFLLS	0.59	0.92 ± 0.08	0.71 (0.18)	-0.36
PSU Curtain	0.01	$2.4 \pm 1\text{E-}3$	0.59 (-0.07)	-0.21
GMAO Curtain	4E-3	$0.76 \pm 5\text{E-}4$	0.69 (0.24)	-0.15
CAMS	-	0.20	0.14 (-0.41)	-0.26
CarbonTracker	-	1.32	0.78 (-0.03)	-0.31

The in situ profile from the B-200 is shown in Figure 5.8 with the CAMS profile, interpolated in space and time, shown beside the full CAMS profiles in latitude in Figure 5.8. Both

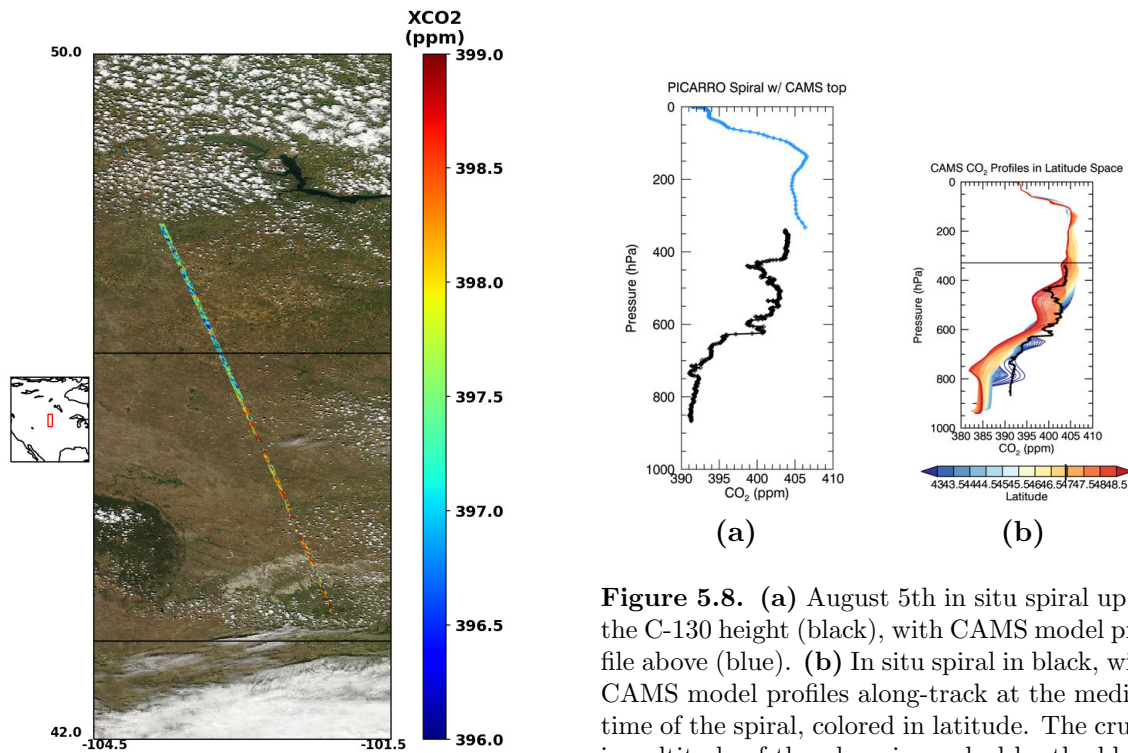


Figure 5.7. OCO-2 X_{CO_2} along the August 5, 2016 underflight track.

Figure 5.8. (a) August 5th in situ spiral up to the C-130 height (black), with CAMS model profile above (blue). (b) In situ spiral in black, with CAMS model profiles along-track at the median time of the spiral, colored in latitude. The cruising altitude of the plane is marked by the black line.

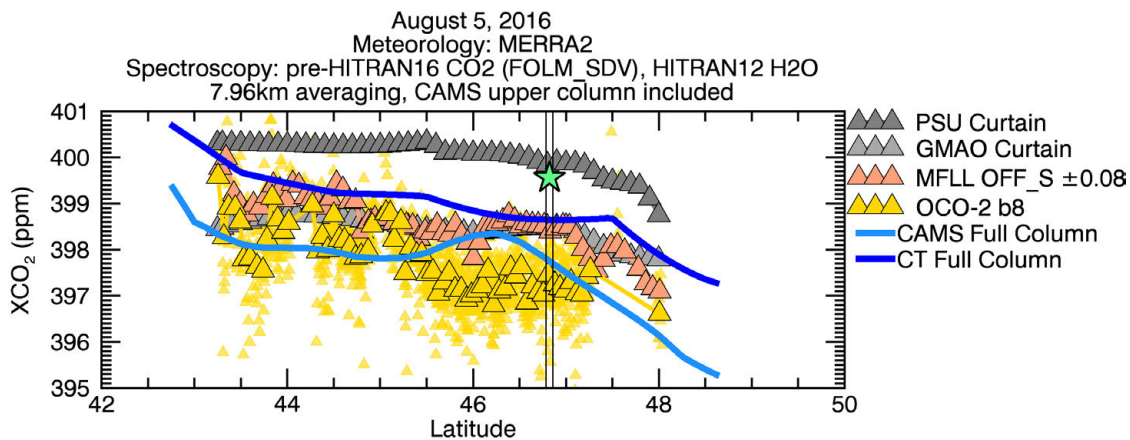


Figure 5.9. X_{CO_2} datasets from the August 5, 2016. The in situ spiral column-averaged value, with CAMS model top included, is shown as a green star. The CAMS full column values are calculated using a straight pressure weighting function.

the in situ and model data exhibit strong drawdown near the surface, and show a profile of similar shape throughout the flight track, but much of the profile appears to shift to lower concentrations in the north - once again indicating a decreasing X_{CO_2} trend in latitude.

The X_{CO_2} datasets consistently show this south-north gradient in Figure 5.9, but with varying latitudinal slopes. The OCO-2 data exhibit the strongest gradient with a slope of $-0.43 \text{ ppm}/^\circ$, as shown in Table 5.2. The MFL data have the most similar slope at $-0.36 \text{ ppm}/^\circ$, and are strongly correlated with OCO-2 with $r = 0.71$. However, both the PSU and GMAO curtains have relatively shallow slopes (-0.15 and $-0.21 \text{ ppm}/^\circ$). Note the approximately 1 ppm difference between the PSU and GMAO curtain column data along the length of the track. This is due to high CO_2 concentrations in the CAMS upper column, which fills in the PSU curtain above 10 kilometers. The same model upper column is also used to fill in the in situ spiral (star) above 10 km; when this model data is not included, both the in situ column and the PSU curtain data are in line with the magnitudes of the MFL and PSU curtain.

The CarbonTracker data have a similar slope to the MFL retrieved values, and have the strongest correlation with OCO-2 data ($r = 0.78$), notably seeing a depression in X_{CO_2} between 45.5 and 47.5N, similar to OCO-2 (though less pronounced, and an average of 1.3 ppm higher). The full-column CAMS data on this day have mean values slightly high (0.2 ppm) with respect to OCO-2, seemingly due in large part to a bump in CO_2 in that same location where OCO-2 sees a depression - their correlation is thus the lowest of all the comparisons, at 0.14. Correlations on smaller scales, when a linear regression is performed on each dataset to remove the overall latitudinal gradient, are small and sometimes negative, once again proving small-scale OCO-2 X_{CO_2} features difficult to validate.

5.3. AUGUST 27, 2016

On this flight out of Shreveport, Louisiana, almost the entirety of the OCO-2 track was obscured by popcorn cumulus clouds, as seen in Figure 5.12. Across almost 2 degrees latitude

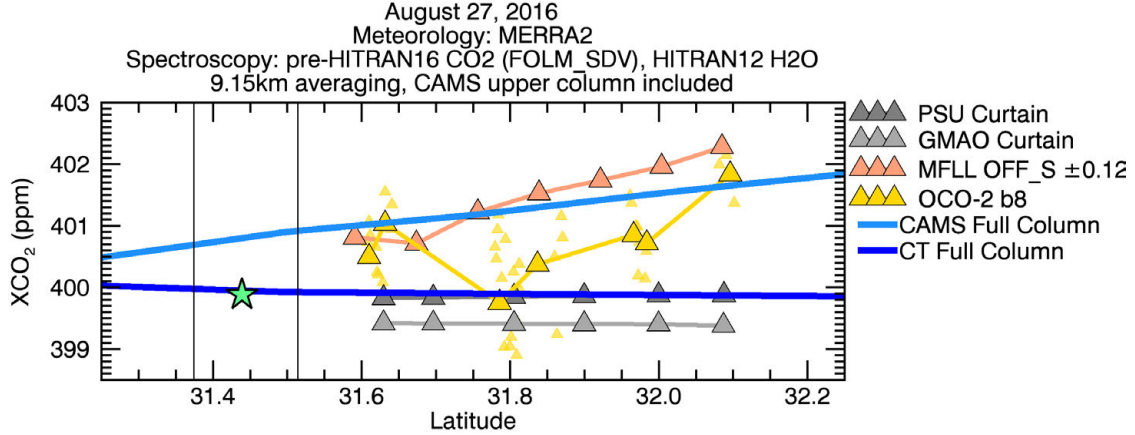


Figure 5.10. X_{CO_2} datasets from August 27, 2016. The in situ spiral column-averaged value, with CAMS model top included, is shown as a green star. The CAMS full column values are calculated using a straight pressure weighting function.

of the 9 kilometer flight track, shown in Figure 5.11, a span of only about 0.5 degrees yielded any OCO-2 data. Figure 5.10 shows the available comparison data over a few small cloud-free regions of the track. From this small dataset, it seems that both OCO-2 and the MFL_L retrieval are in relatively good agreement with both the CAMS model and the in situ spiral data; in the areas where there are data in common, OCO-2 and MFL_L are within 1 ppm of each other. It does appear as though their proximity to clouds may cause the OCO-2 data to be biased low, which affects the slope of the latitudinal gradient, seen in Table 5.3. With standard collocating of 60-second MFL bins, and the standard three OCO-2 observations required within each collocated circle, there are only four points of sufficient comparison; the correlation coefficients and ΔX_{CO_2} of those four points are listed in the table.

TABLE 5.3. August 27, 2016 Slopes and Correlations with OCO-2

	σ (ppm)	Mean $\Delta X_{\text{CO}_2} \pm$ Error (ppm)	$r_{\text{OCO-2}}$	Slope (ppm/ $^\circ$)
OCO-2	0.57	0 ± 0.24	-	1.72
MFLS	0.85	0.83 ± 0.12	0.75 (0.65)	3.23
PSU Curtain	3E-3	$-0.78 \pm 4\text{E-}4$	0.68 (-0.55)	0.12
GMAO Curtain	5E-3	$-1.23 \pm 6\text{E-}4$	-0.86 (-0.83)	-0.04
CAMS	-	0.65	0.76 (0.91)	1.31
CarbonTracker	-	-0.74	-0.73 (0.99)	-0.09

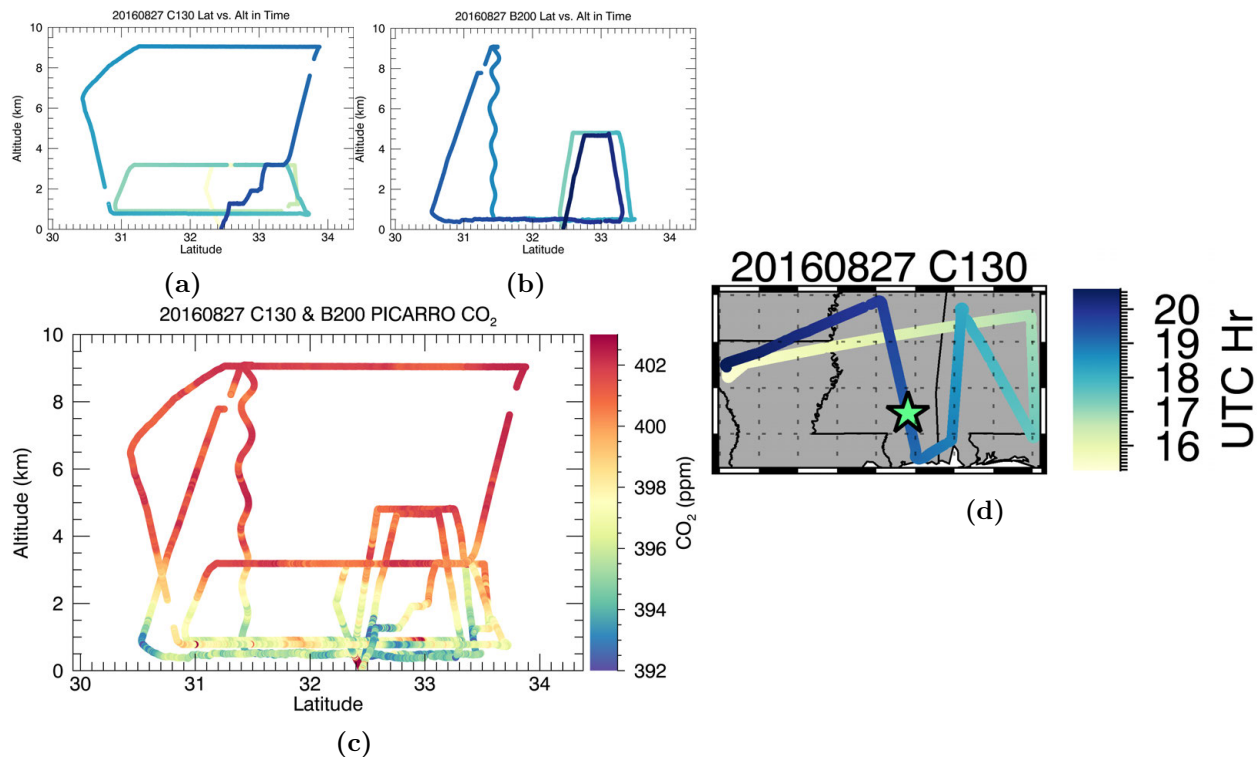


Figure 5.11. Both aircraft in latitude and altitude, colored in time (a, b and d) along with a flight map, and in situ CO₂ data (c) for August 27, 2016.

The CAMS model profiles on this day, in Figure 5.13, appear to overestimate lower tropospheric and boundary layer concentrations by at least 2 ppm at the location of the spiral, though the upper column above the C-130 altitude looks to be of appropriate magnitude.

5.4. FEBRUARY 13, 2017

The first of the winter underflights took place in the midwest, across the state of South Dakota. The B-200 executed a spiral near 43.5N spanning approximately 1.5 to 8.5 kilometers in altitude. The C-130 flew the first segment of the underflight track, south of 43.5N, at around 8.5 kilometers, but descended to 7.5 kilometers for the second portion of the track. Figure 5.14c might show a shallow, 1 ppm CO₂ gradient along the higher altitude flight tracks, and there is a small point of higher X_{CO₂} in the 7.5 kilometer track at 44.5N. There also appears to be a source at the takeoff and landing site around 41N, in Lincoln, Nebraska.

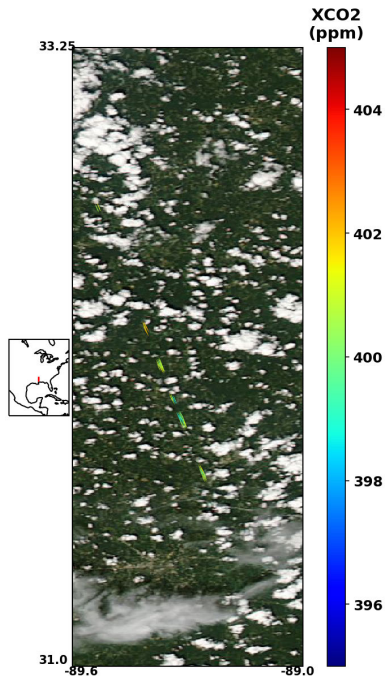


Figure 5.12. OCO-2 X_{CO_2} along the August 27, 2016 underflight track.

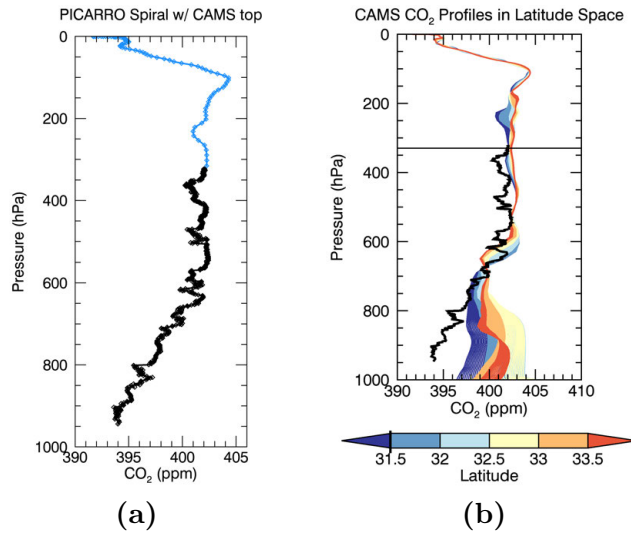


Figure 5.13. (a) August 27, 2016 in situ spiral up to the C-130 height, with CAMS model profile above. (b) In situ spiral in black, with CAMS model profiles colored in latitude.

Note that the vertical CO_2 gradient is reversed from the summer flights. This is clear in the in situ profile (Figure 5.17a), which shows higher concentrations in the boundary layer rather than the lower concentrations in summary boundary layers due to biospheric drawdown.

Much of the ground track was snow-covered, as seen in Figure 5.16 - a stretch of about 2 degrees latitude between 43 and 45N was sufficiently snow-free for OCO-2 retrievals to pass albedo filters, but the data that is available appears quite noisy.

In addition to the noisiness of the OCO-2 data, the MFL data appears particularly noisy compared to previous flights, despite flying at a lower altitude. The standard error of the mean for the MFL_S and MFL_L both average around 0.6 ppm, with values reaching as high as 0.9 ppm. In the summer campaign, this number was between 0.1 and 0.3 ppm. This noisiness can be attributed to signal loss from the degradation of the coating on the MFL viewing window.

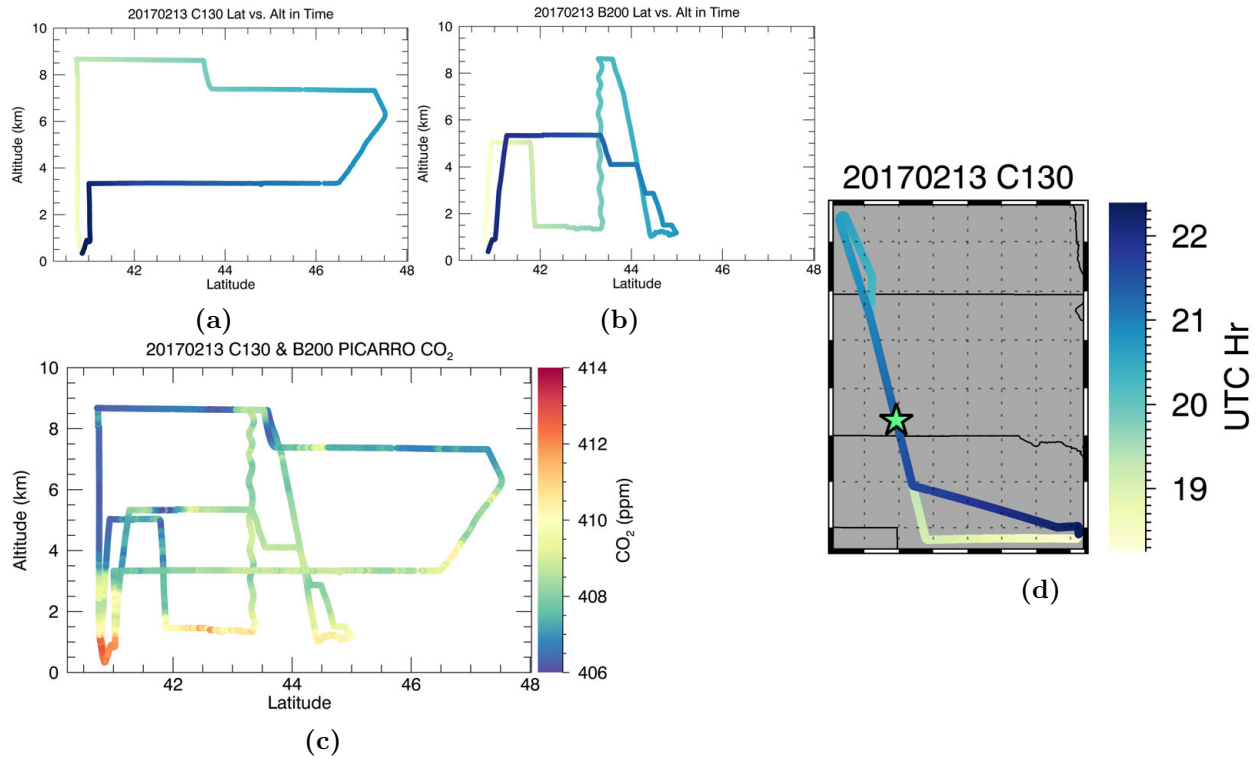


Figure 5.14. Both aircraft in latitude and altitude, colored in time (a, b and d) along with a flight map, and in situ CO₂ data (c) for February 13, 2017.

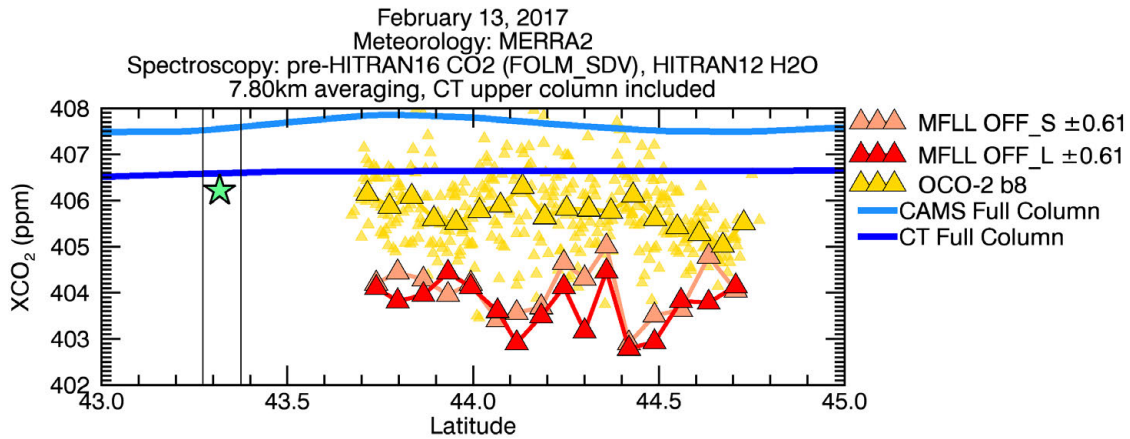


Figure 5.15. X_{CO₂} datasets from February 13, 2017. The in situ spiral column-averaged value, with CarbonTracker model top included, is shown as a green star. Both the CAMS and CarbonTracker full column values are calculated using a straight pressure weighting function.

There appears, in Figure 5.15, to be little to no agreement between the OCO-2 and MFL retrieval results, in either magnitude or spatial variability, though because of the

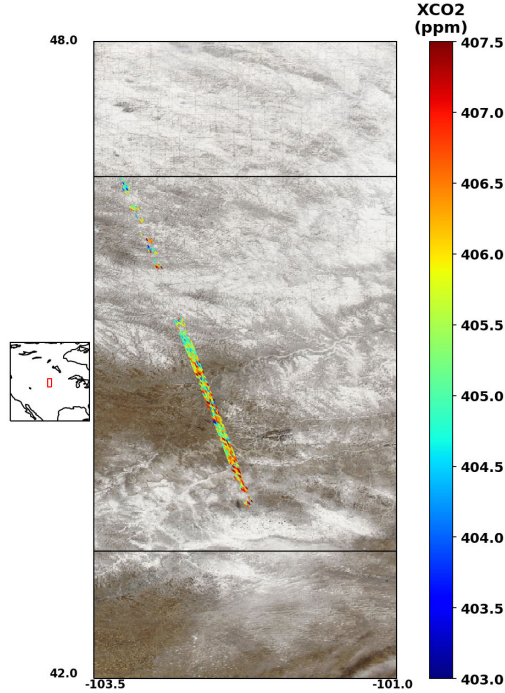


Figure 5.16. OCO-2 X_{CO_2} along the February 13, 2017 underflight track.

TABLE 5.4. February 13, 2017 Slopes and Correlations with OCO-2

	σ (ppm)	Mean $\Delta X_{CO_2} \pm$ Error (ppm)	r_{OCO-2}	Slope (ppm/ $^{\circ}$)
OCO-2	0.72	0 ± 0.16	-	-0.60
MFLLS	3.71	-1.70 ± 0.61	-0.31 (-0.41)	-0.17
MFLLL	3.74	-2.01 ± 0.61	-0.40 (-0.62)	-0.42
CAMS	-	1.93	0.41 (-0.65)	-0.45
CarbonTracker	-	0.90	-0.69 (-0.63)	5E-3

MFL viewing window issue, the MFL data (even once bias corrected) are not likely trustworthy. At its largest, around 44.4 degrees north, the magnitude difference between the two is upwards of 3 ppm. There is little latitudinal variation predicted by models, and OCO-2 likely bears this out, so we expect and see low correlation coefficients between the datasets. Magnitude differences are thus more meaningful on this day: the CAMS data exhibits is high relative to all other datasets. In Figures 5.17c and 5.17d, we see that this high bias is consistent vertically throughout the column, as well as along the full length of the flight track. This phenomenon is also consistent for all winter flights. For this reason, CarbonTracker

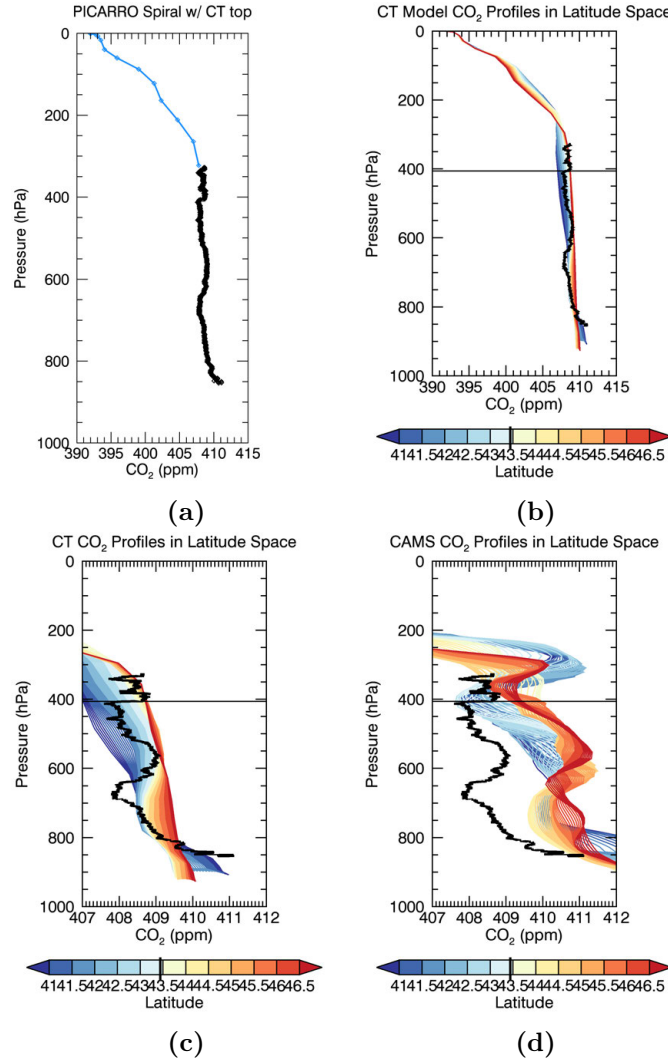


Figure 5.17. (a) February 13, 2017 in situ spiral up to the C-130 height, with CarbonTracker model profile above. (b) and (c) In situ spiral in black, with CarbonTracker model profiles colored in latitude; (c) shows this in greater detail, for comparison with the CAMS model profiles in (d).

proves the more suitable source for both upper column and weighting function corrections, and is used to make these corrections for both this flight and the rest of the winter campaign data. The CarbonTracker upper column is also included as a correction to the in situ spiral column value (green star in Figure 5.15), and when included, the X_{CO_2} at the spiral appears to agree relatively well with the magnitude of the available OCO-2 data, although there is some geographical distance between them.

5.5. FEBRUARY 15, 2017

In another midwest flight, this time south through Kansas and into Oklahoma, the C-130 under-flew OCO-2 at an altitude of about 8.7 kilometers. There were some relatively high clouds near the northern section of flight track, which can be seen in Figure 5.20. The in situ data (Figure 5.18c) show some small-scale variability at the 8.7 kilometer altitude - fluctuations on the order of 1 ppm - but no systematic gradients across the full track. The B-200 executed a spiral maneuver in the center of the underflight track just north of 38N; the spiral profile, shown in Figure 5.21 with CarbonTracker model profiles, displays a typical winter CO₂ profile shape, with concentrations peaking near the boundary layer. The CarbonTracker profiles hardly vary by 0.5 ppm anywhere in the column across the flight track, in agreement with the lack of spatial variability in the in situ data. Unfortunately, this results in little to compare between datasets, aside from magnitude.

The X_{CO₂} results in Figure 5.22 indeed show very little spatial variability. The OCO-2, CarbonTracker, and in situ data all agree in magnitude to well within 1 ppm along much of the track; both MFLR retrievals exhibit appear low by nearly 3 ppm relative to the other datasets. The MFLR data also displays enhanced noise, again, characteristic of the interference from the faulty viewing window coating.

The OCO-2 data contains one exception to the lack of spatial features, in the form of two peaks in X_{CO₂} near 39N. Upon closer inspection, it is believed that these soundings are the result of a path-lengthening effect caused by the presence of a high cloud or contrail. Figure 5.19 shows the area of interest in greater detail. It is worth noting that, while the feature remains in the data, its magnitude was significantly reduced in the OCO-2 version 8 update.

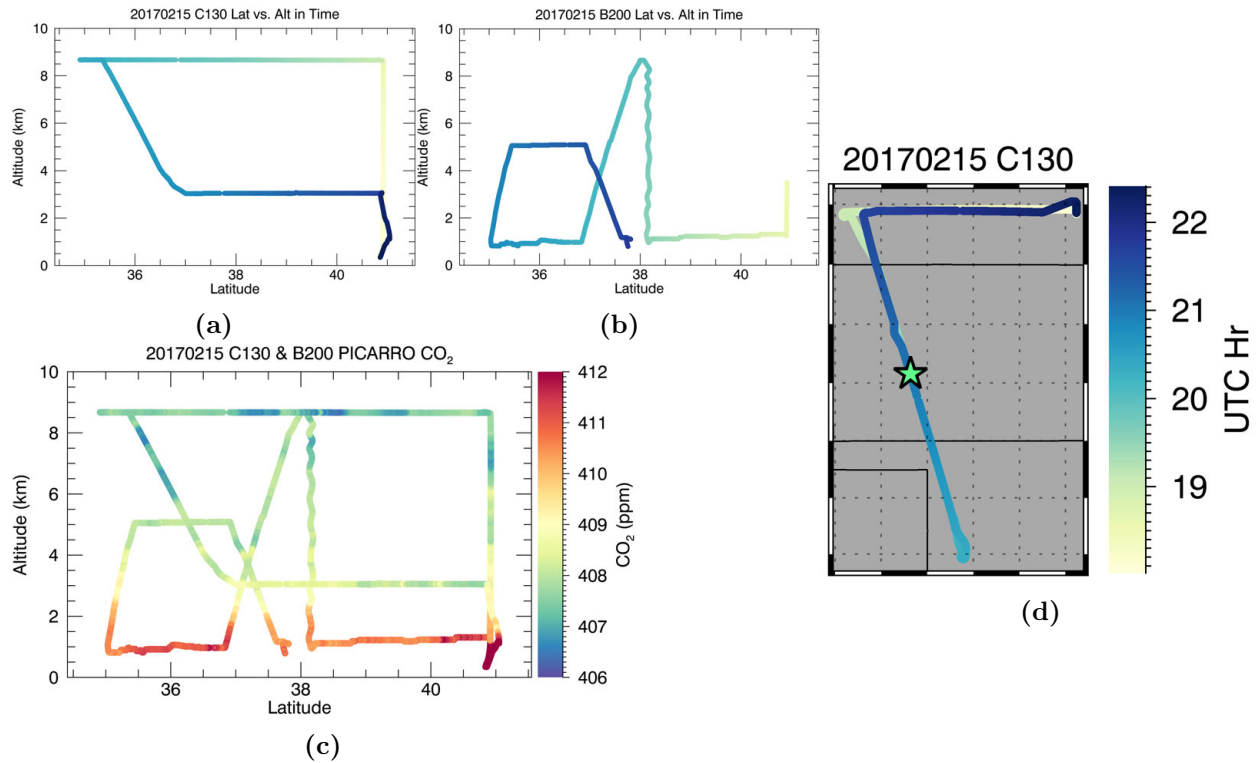


Figure 5.18. Both aircraft in latitude and altitude, colored in time (a, b and d) along with a flight map, and in situ CO₂ data (c) for February 15, 2017.

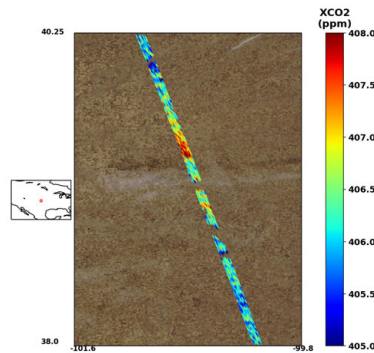


Figure 5.19. Imagery of a cloud effect on the OCO-2 X_{CO₂} measurement on February 15, 2017.

TABLE 5.5. February 15, 2017 Slopes and Correlations with OCO-2

	σ (ppm)	Mean $\Delta X_{CO_2} \pm$ Error (ppm)	r_{OCO-2}	Slope (ppm/°)
OCO-2	0.41	0 ± 0.09	-	-0.02
MFLLS	3.76	-3.82 ± 0.53	0.02 (0.01)	-0.10
MFL_L	3.85	-2.98 ± 0.55	0.14 (0.12)	-0.32
CAMS	-	1.66	-0.34 (-0.45)	-0.009
CarbonTracker	-	0.32	0.05 (-0.14)	-0.04

5.6. MARCH 8, 2017

The final flight of the winter campaign flew up the east coast. By this time, the team was aware of the reduced SNR caused by the viewing window coating, so the C-130 flew at a lower altitude on this day - around 6 kilometers rather than the usual 9 kilometers

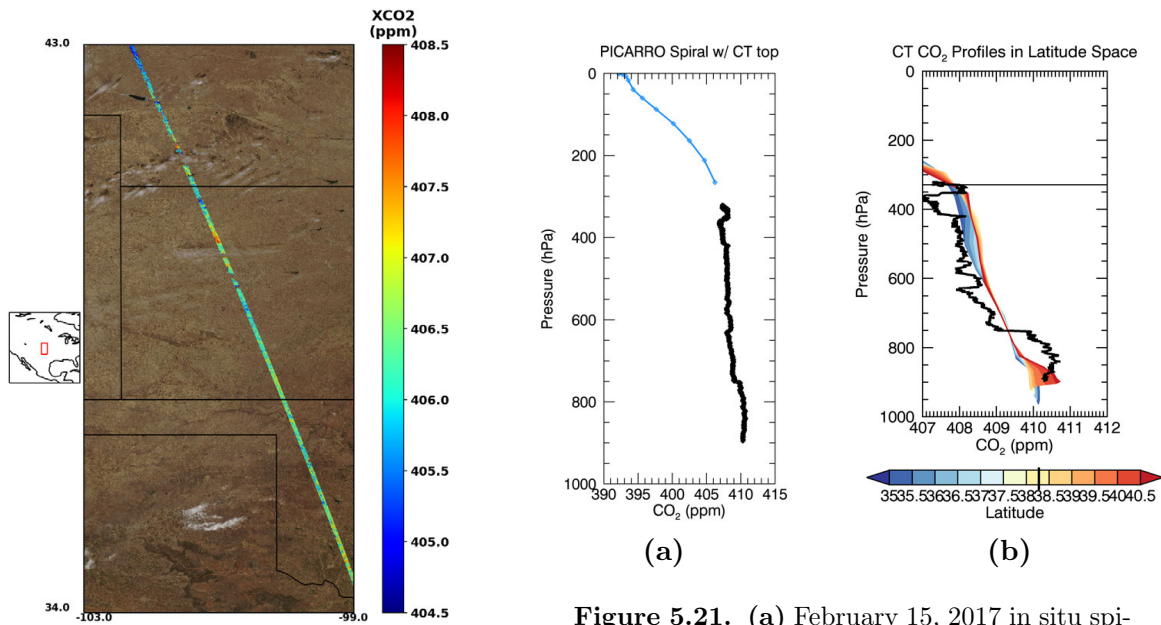


Figure 5.20. OCO-2 XCO₂ along the February 15, 2017 underflight track.

Figure 5.21. (a) February 15, 2017 in situ spiral up to the C-130 height, with CarbonTracker model profile above. (b) In situ spiral in black, with CarbonTracker model profiles in latitude.

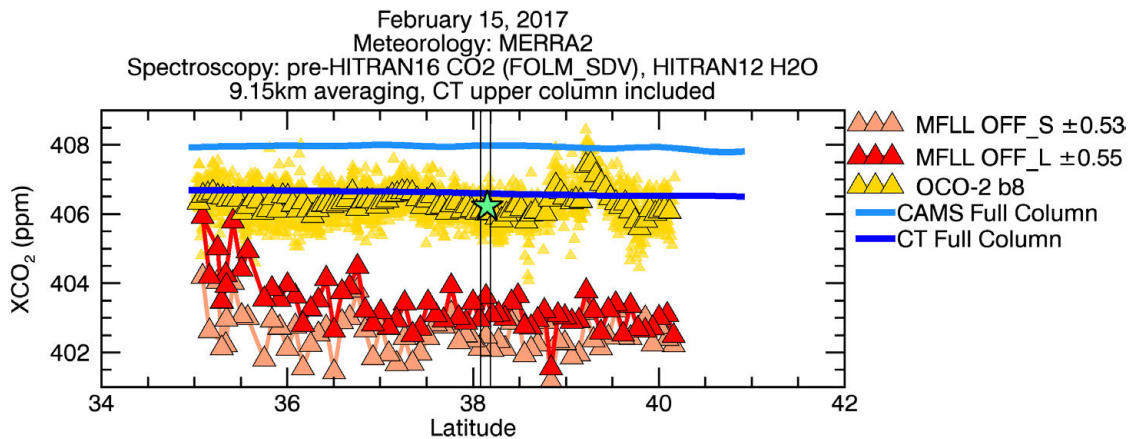


Figure 5.22. XCO₂ datasets from February 15, 2017. The in situ spiral column-averaged value, with CarbonTracker model top included, is shown as a green star. CarbonTracker full column values are calculated using a straight pressure weighting function.

- in order to improve the measurement noise. One spiral maneuver was completed by the B-200 at 38N in the east of Virginia, indicated by the star in Figure 5.23d. The in situ CO₂ data shows some variability along the 6 km flight track on the order of 1 ppm; in particular, a low of about 407.5 ppm at 40N. There appears to be a slight north-south gradient as well at this altitude, also on the order of 1 ppm, between 408 and 410 ppm, with concentrations higher in the north. A slightly stronger gradient of the same sign appears to exist in the data below 4 kilometers, which indicates the possibility of an increasing south-north gradient in the column data; however, a strong surface source between 36 and 37N may dampen this latitudinal effect. The B-200 spiral data unfortunately only reaches the C-130 cruising altitude of 6 kilometers. The CO₂ profile is shown in Figure 5.25 along with the CarbonTracker profile used to complete the upper column and the full CarbonTracker profiles colored in latitude. The in situ column appears relatively well-mixed, and CarbonTracker predicts the CO₂ concentrations accurately throughout the column at the spiral location, apart from overestimating near-surface values by a few parts per million. The upper column profile is of consistent magnitude where it meets the in situ profile at 400 hPa.

The northern and southernmost ends of the OCO-2 track were partly obscured by scattered clouds, and some high clouds interrupt the center of the track as well, as seen in Figure 5.24. The OCO-2 data, from Figures 5.24 and 5.26, show values fairly steady around 407

TABLE 5.6. March 8, 2017 Slopes and Correlations with OCO-2

	σ (ppm)	Mean $\Delta X_{\text{CO}_2} \pm$ Error (ppm)	$r_{\text{OCO-2}}$	Slope (ppm/°)
OCO-2	0.72	0 ± 0.19	-	-0.11
MFLLS	2.79	-0.68 ± 0.43	-0.08 (-0.07)	-0.12
MFLLS	2.99	-0.38 ± 0.46	-0.10 (-0.07)	-0.26
CAMS	-	1.74	-0.01 (-0.05)	0.09
CarbonTracker	-	0.46	0.49 (0.52)	-0.02

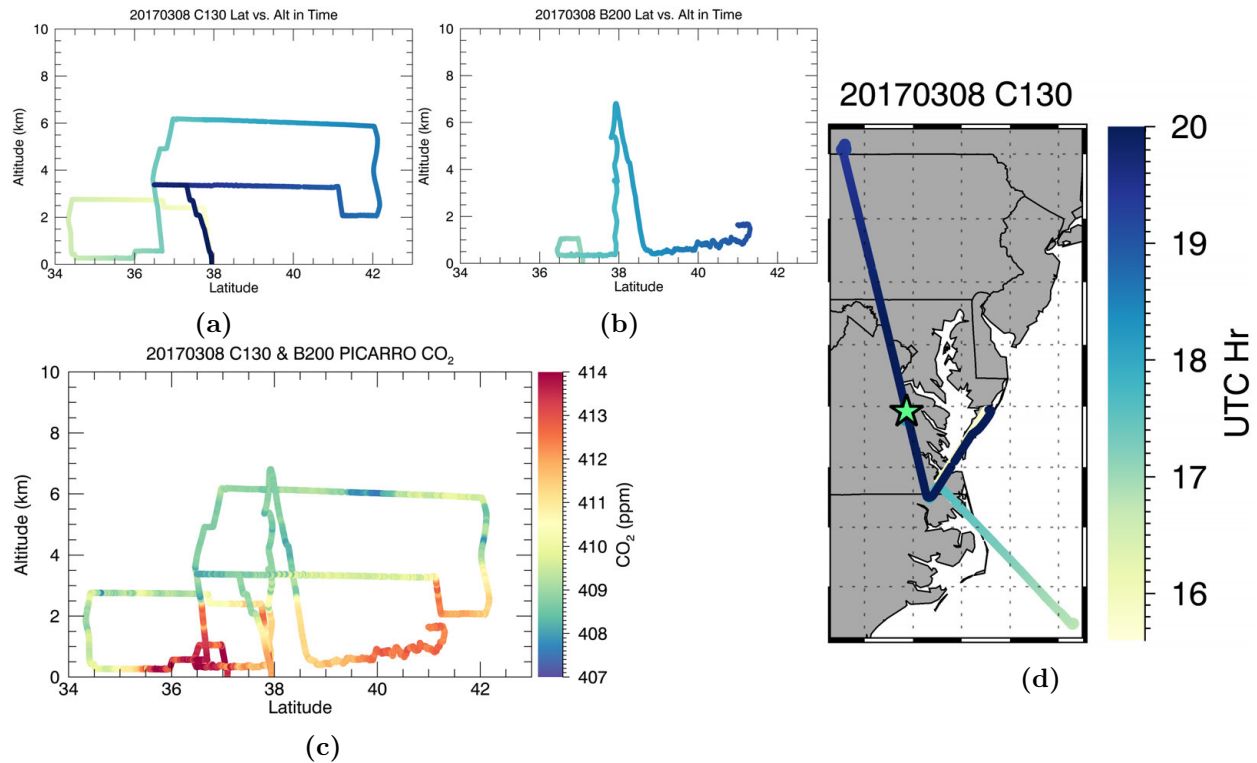


Figure 5.23. Both aircraft in latitude and altitude, colored in time (a, b and d) along with a flight map, and in situ CO_2 data (c) for March 8, 2017.

ppm along the full track, apart from a feature at 38N which appears similar to the high cloud feature observed in the February 13th flight.

The MFL data show X_{CO_2} values in line with those of OCO-2, low by less than 1 ppm in the ON/OFF_S and less than 0.5 ppm in the ON/OFF_S, and SNR is clearly improved from the previous two flights by flying at lower altitude: the standard error of the two MFL datasets are 0.43 and 0.46, as opposed to 0.53 and up to 0.61 in the other winter flights. The spiral X_{CO_2} , shown as a green star in Figure 5.26, is in agreement with the MFL data at that location, and though in a cloudy area with spurious OCO-2 values, appears to agree with OCO-2 as well. CarbonTracker X_{CO_2} estimates are slightly higher than any of the other datasets, perhaps due to high values near the surface.

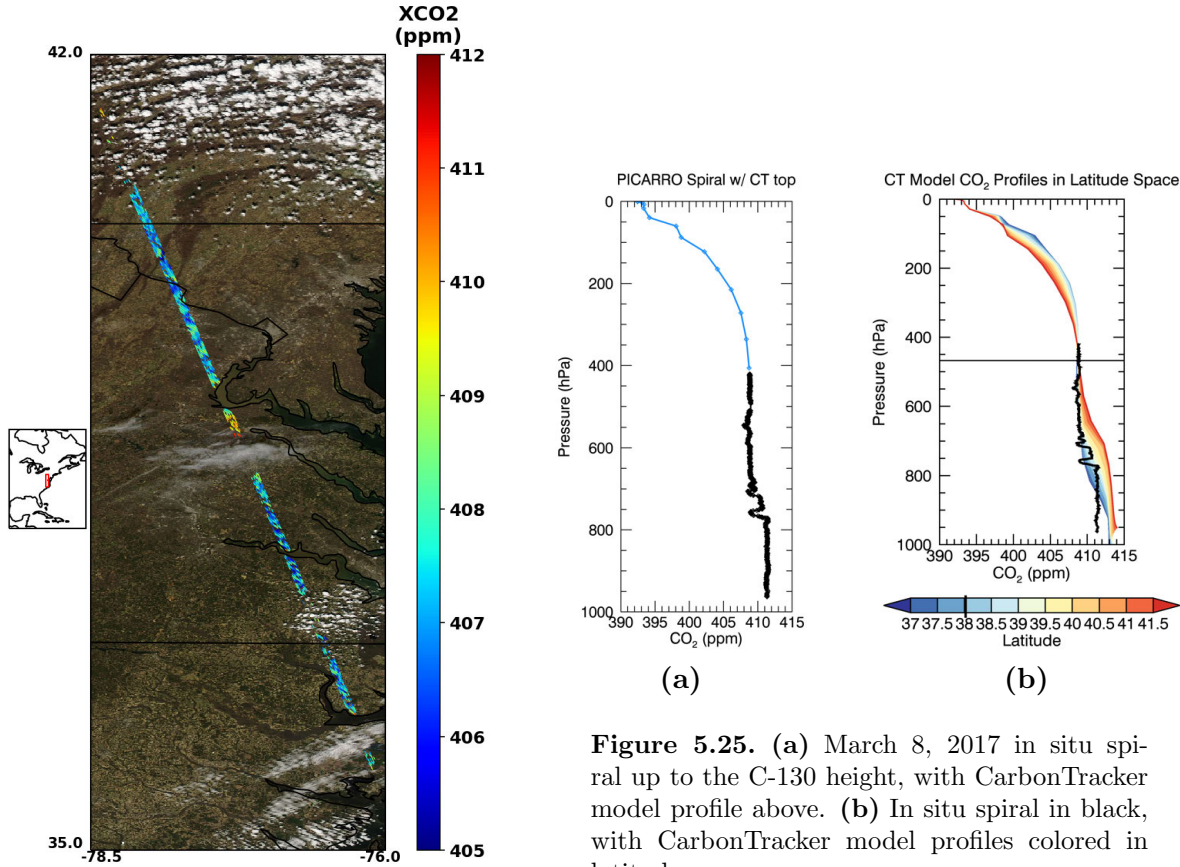


Figure 5.24. OCO-2 X_{CO_2} along the March 8, 2017 underflight track.

Figure 5.25. (a) March 8, 2017 in situ spiral up to the C-130 height, with CarbonTracker model profile above. (b) In situ spiral in black, with CarbonTracker model profiles colored in latitude.

5.7. OCTOBER 22, 2017

The first fall underflight saw completely clear skies over Kansas in the midwest, with little X_{CO_2} variability along the flight track. The MFL viewing window received a proper coating treatment between the winter and fall campaigns, so underflights in the fall resumed

TABLE 5.7. October 22, 2017 Slopes and Correlations with OCO-2

	σ (ppm)	Mean $\Delta X_{CO_2} \pm$ Error (ppm)	r_{OCO-2}	Slope (ppm/ $^{\circ}$)
OCO-2	0.48	0 ± 0.11	-	0.07
MFLLS	1.63	-2.99 ± 0.24	0.19 (0.05)	0.15
MFLLL	1.67	-3.31 ± 0.25	-0.09 (-0.21)	0.10
CAMS	-	0.96	0.46 (0.56)	0.15
CarbonTracker	-	-	-	-

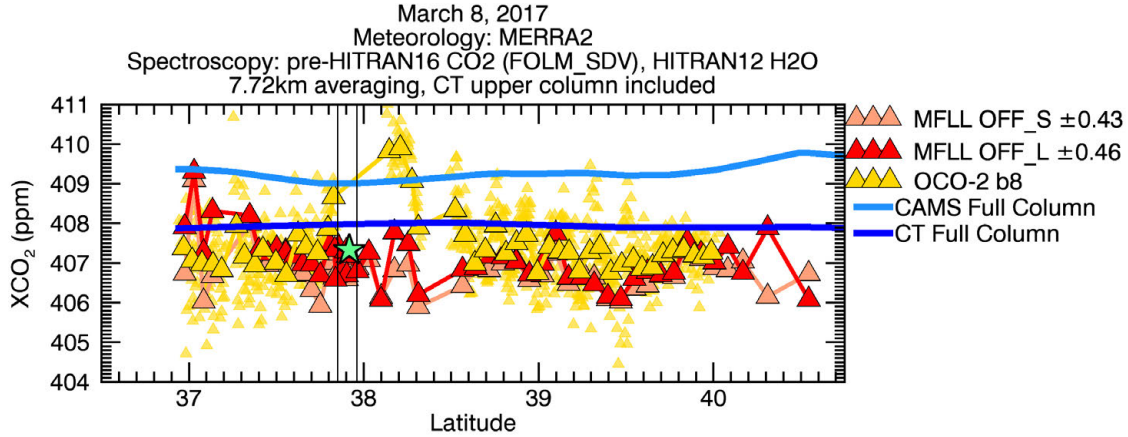


Figure 5.26. X_{CO_2} datasets from March 8, 2017. The in situ spiral column-averaged value, with CarbonTracker model top included, is shown as a green star. CarbonTracker full column values are calculated using a straight pressure weighting function.

at an altitude of 9 kilometers. In a renewed pursuit of in situ column data, the B-200 flew a spiral maneuver in the center of the underflight track, just north of 38N, and the C-130 also flew two spirals: one at the southernmost end of the track, and one just north of the B-200 spiral.

The in situ data in Figure 5.27c shows slightly enhanced CO_2 , from what appear to be surface sources, at the northern- and southernmost ends of the flight track, with concentrations in those areas around 407.5 ppm as opposed to 406 - 406.5 ppm along the rest of the 1 km altitude track. The 9 kilometer data does not show much variability aside from an increasing latitudinal gradient of 0.5 ppm maximum from south to north.

The OCO-2 data does show a slight latitudinal gradient as well, in Figure 5.28, though X_{CO_2} only varies by less than 1 part per million for the most part. Note that the color bar for this figure only spans a range of 2 ppm. The scene is almost completely cloud-free, though in the north there are some high clouds visible to the east of the track; it appears as though there is no cloud interference along the track itself.

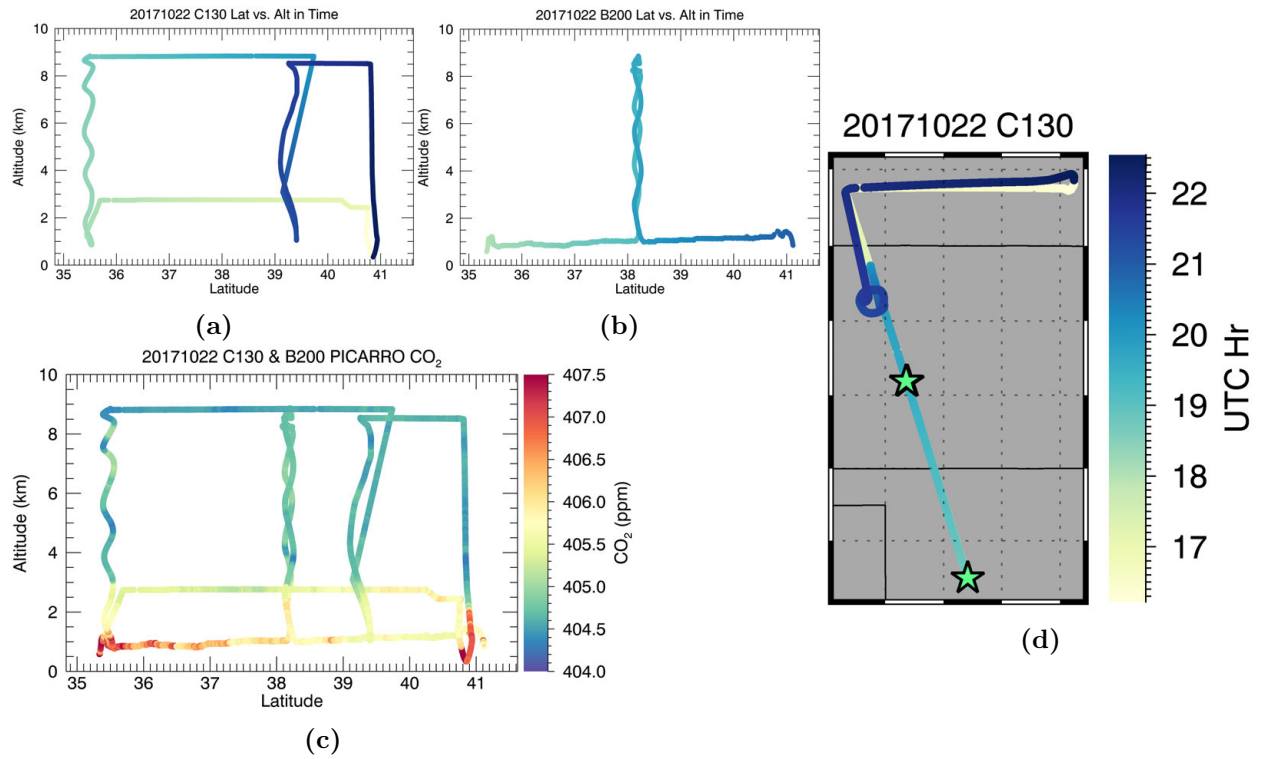


Figure 5.27. Both aircraft in latitude and altitude, colored in time (a, b and d) along with a flight map, and in situ CO₂ data (c) for October 22, 2017.

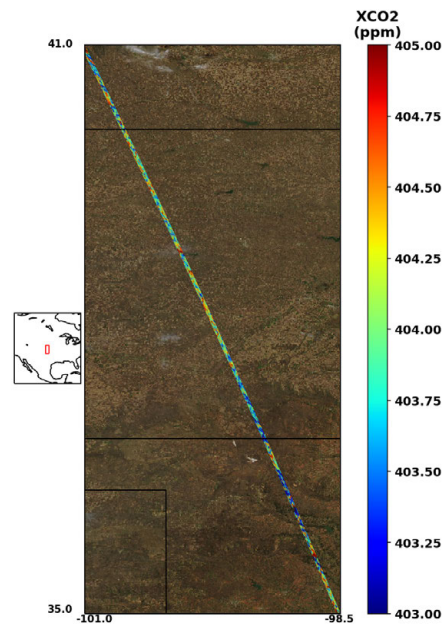


Figure 5.28. OCO-2 XCO₂ along the October 22, 2017 underflight track.

CarbonTracker data is not yet available for the fall campaign dates, so CAMS data is used for X_{CO_2} comparison and for weighting function and upper column corrections, with the footnote in mind that CAMS is often biased high in the cold seasons, as discussed in Section 5.4. This does indeed appear to be the case: in Figures 5.30, the model values at 300-350 hPa are higher than the in situ values by about 0.5 ppm. Although the model values across the flight track in 5.30 do look approximately correct in magnitude when compared to the upward spiral profile, the X_{CO_2} values appear 1 ppm high compared to the OCO-2 data in Figure 5.29. The in situ values appear slightly high as well, and though they include the CAMS upper column in the figure shown here, their partial column values are nearly 0.5 ppm higher.

In this flight we see a typical MFLL low bias - both the MFLL_S and MFLL_L retrievals yield a result about 3 ppm lower than OCO-2 and the in situ spirals. Do note, however, that the MFLL SNR returns to target levels in this dataset, with standard errors around 0.25 ppm rather than the 0.5 or 0.6 seen in winter from the window coating degradation. There is once again not much of a latitudinal gradient and no particularly notable X_{CO_2} features, apart from a depression of about 1 ppm in the OCO-2 data between 36 and 37N which is not present in either the MFLL or CAMS data, nor the PICARRO data in Figure 5.27c.

5.8. OCTOBER 27, 2017

TABLE 5.8. October 27, 2017 Slopes and Correlations with OCO-2

	σ (ppm)	Mean $\Delta X_{\text{CO}_2} \pm$ Error (ppm)	$r_{\text{OCO-2}}$	Slope (ppm/°)
OCO-2	0.54	0 ± 0.14	-	-0.18
MFLL_S	1.01	-2.71 ± 0.14	0.10 (0.27)	0.02
MFLL_L	1.07	-2.81 ± 0.15	0.03 (0.05)	-0.006
CAMS	-	1.91	0.64 (0.10)	-0.09
CarbonTracker	-	-	-	-

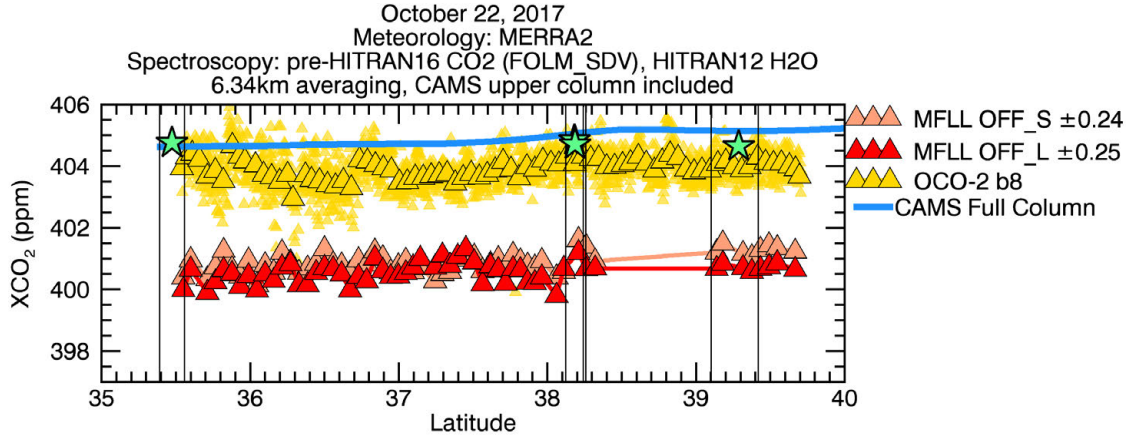


Figure 5.29. X_{CO_2} datasets October 22, 2017. The in situ spiral column-averaged value, with CAMS model top included, is shown as a green star. CAMS full column values are calculated using a straight pressure weighting function.

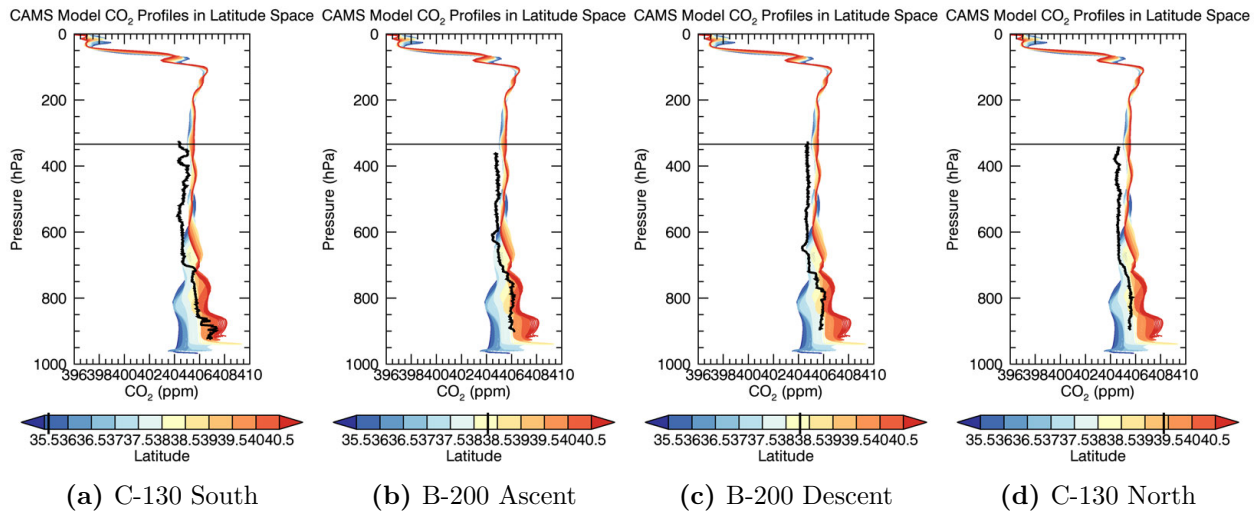


Figure 5.30. October 22, 2017 in situ spiral profiles in black, from south on the left (a) to north on the right (d), with CAMS profiles colored in latitude. The location of each spiral is marked by a tick on the color bar.

The October 27 underflight also took place over Kansas in the midwest. The C-130 completed two spirals, one at either end of the underflight track, though the spiral at the northern end only extends down to three kilometers. The underflight track spans nearly 5 degrees latitude, was flown just above 8.5 kilometers altitude, and is completely cloud-free as shown in Figure 5.32. The in situ data in Figure 5.31c shows some spatial variability in CO₂ at 8.5 kilometers, with concentrations increasing by up to 2 ppm from south to north

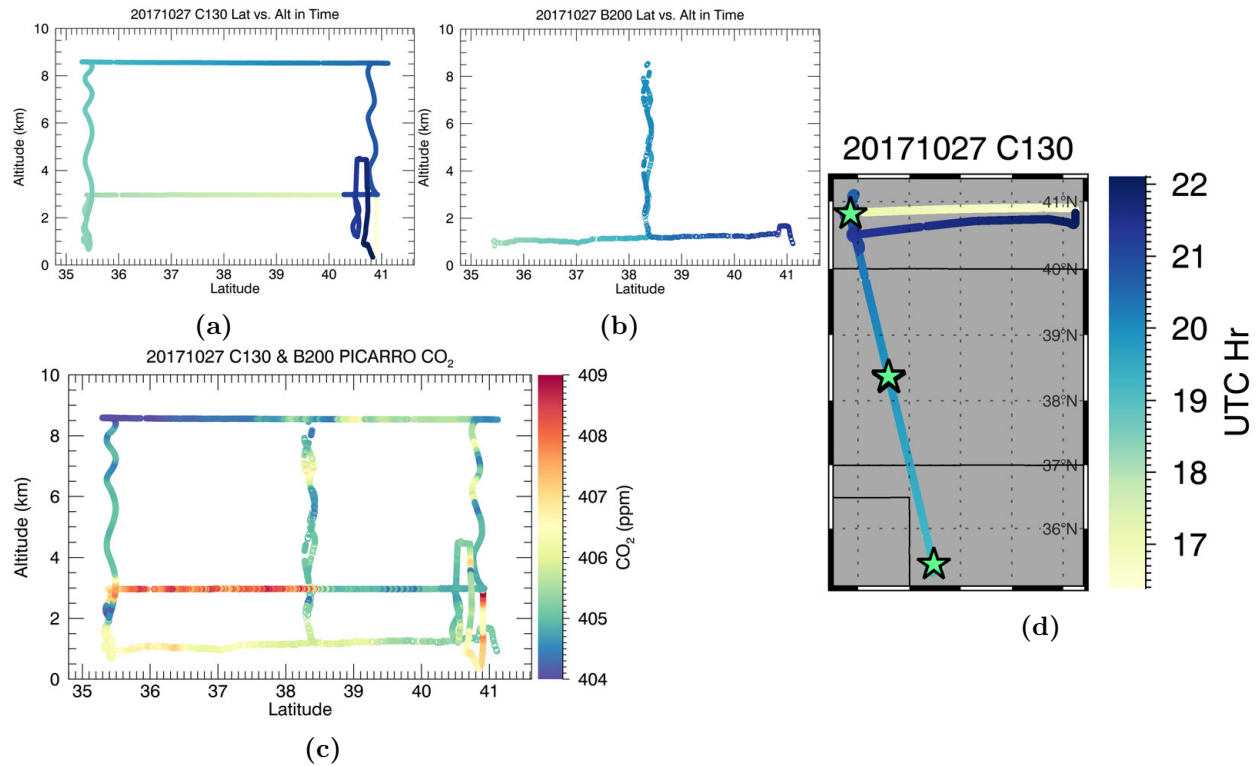


Figure 5.31. Both aircraft in latitude and altitude, colored in time (a, b and d) along with a flight map, and in situ CO₂ data (c) for October 27, 2017.

across the flight track, with a local maximum of about 406.5 ppm at 39N. However, the 3 kilometer data reveals a stronger gradient in the opposite direction, with maximum CO₂ of nearly 409 ppm throughout the southern half of the track and concentrations between 404 and 405 throughout the northern half. The combination of these opposing gradients might lead to little observable gradient in the column-averaged values.

Four sets of in situ spiral data were taken: two by the C130 at the northern and southern ends of the underflight track, and two by the B-200 in the middle of the track (one ascending, one descending). The northernmost spiral and the B-200 spirals both show some significant vertical variability between 6 and 8 kilometers in altitude, concentrations jumping by 2 to 2.5 ppm around 7 km in the B-200 profiles. Note that the northern C-130 spiral only spans

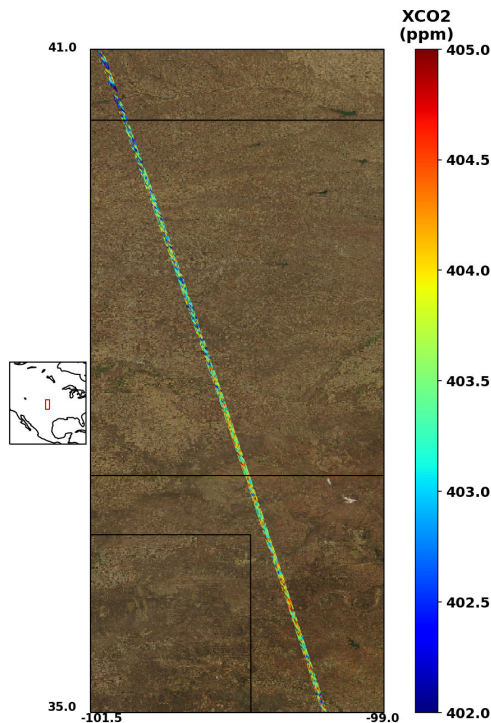


Figure 5.32. OCO-2 X_{CO_2} along the October 27, 2017 underflight track.

an altitude of 3 to 8 kilometers. Also note that there is some data loss from the B-200 throughout the flight track.

Two of the four spirals are shown in Figure 5.33 with upper column CAMS profiles and with CAMS profiles in latitude. Both profiles reveal the high bias in CAMS, particularly in the mid-troposphere above 600 hPa. The southern C-130 spiral is plotted in the left-hand panels, and shows elevated CO_2 just above the boundary layer near 700 hPa, which CAMS does not accurately predict. Below that level, the CAMS profile (dark blue) matches the spiral quite well, to within 0.5 ppm. The right-hand panels of Figure 5.33 show the descending B-200 spiral. The variability in the free troposphere just below the plane is evident between 350 and 500 hPa and not predicted by CAMS at that latitude (yellow). There is also variability at the top of the boundary layer, at 700 hPa, that is not captured well in the CAMS profiles, but the magnitude of the concentrations below 650 hPa do seem

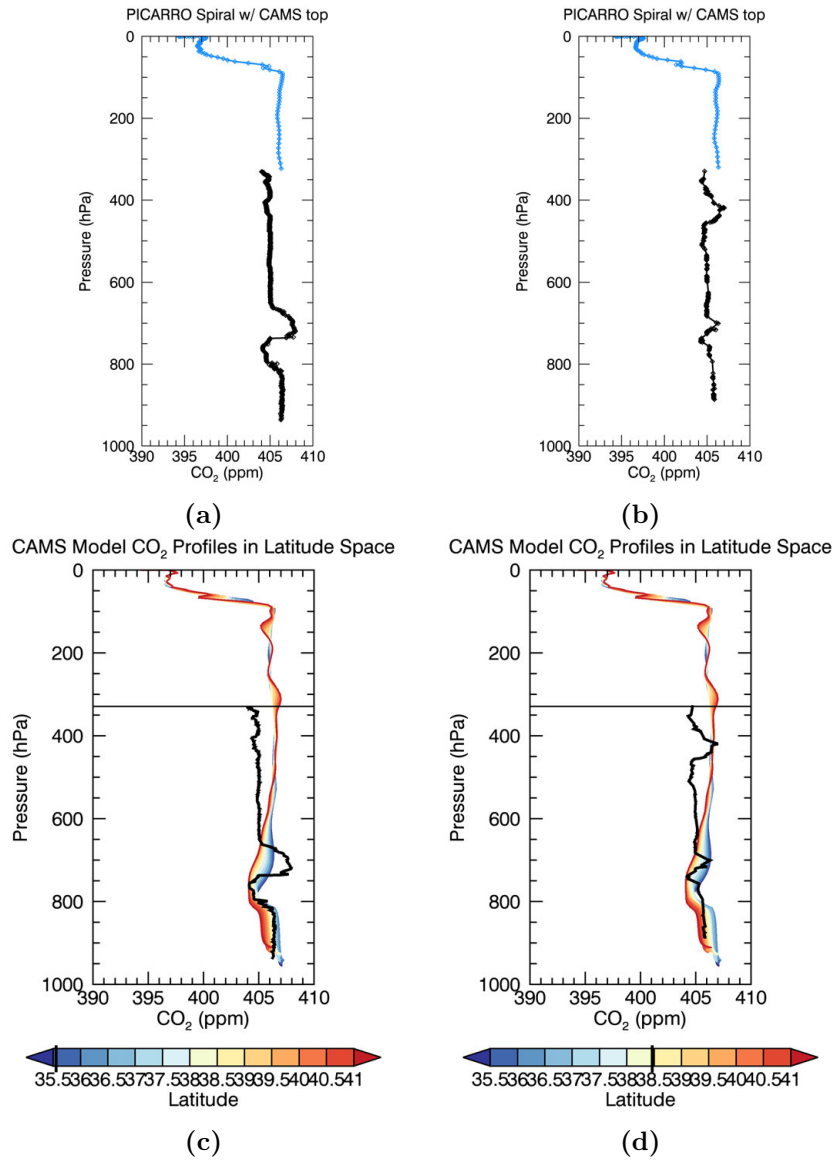


Figure 5.33. (a, b) October 27, 2017 in situ spirals up to the C-130 height, with CAMS model profiles above. (c, d) In situ spiral in black, with CAMS model profiles colored in latitude.

accurate to within 1 ppm. The high bias of the model values above 600 hPa extends into the upper troposphere above the plane; there is an offset of 1-2 parts per million between the in situ profiles and the model data at the point where they meet, clearly visible in all four panels of Figure 5.33.

The OCO-2 data in Figure 5.35 shows a decrease in X_{CO_2} , of approximately 1 ppm in magnitude, from south to north across the length of the underflight track, indicating that it

may see some of the 3-kilometer variability shown by in situ. Figure 5.35 shows that, when the OCO-2 data is averaged, the total latitudinal change across the underflight track is just under 1 part per million. In addition, there is a dramatic X_{CO_2} minimum just north of 40N, which may be due to some albedo effect; Figure 5.34 shows this feature more closely, and that some data are filtered out completely - closer inspection of warn level variables might reveal the cause.

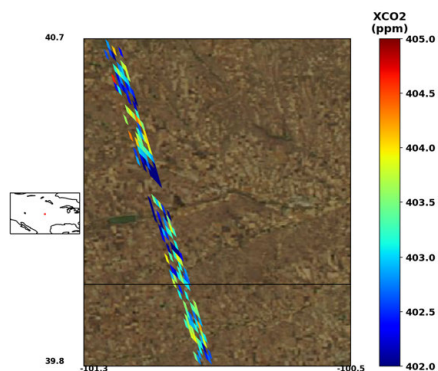


Figure 5.34. Unusual feature in the OCO-2 X_{CO_2} data on October 27, 2017.

X_{CO_2} comparisons in Figure 5.35 indeed show that the CAMS data is once more biased high compared to OCO-2, in this case by about 1.5 ppm consistently along the flight track. The in situ spiral data are similarly high compared to OCO-2, both as shown (with CAMS upper column included) and without model top included. The MFL data are low compared to OCO-2 by 2-3 ppm along the full length of the track, but show high SNR, with standard error of 0.14 and 0.15 ppm for MFL_S and MFL_L. The MFL data show significant along-track variability even with weighting function and upper column corrections included, both of which have a tendency to smooth the data in space. The source of this pattern in the column data is not yet known; the correlation coefficient between either MFL dataset and the PICARRO CO_2 data at 3km, where concentrations are quite variable, is -0.3. There

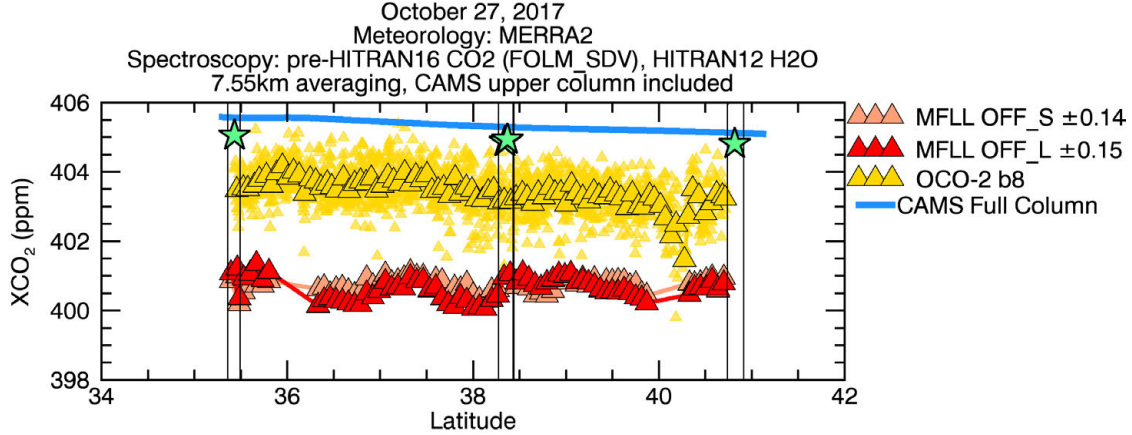


Figure 5.35. X_{CO_2} datasets from October 27, 2017. The in situ spiral column-averaged value, with CAMS model top included, is shown as a green star. CAMS full column values are calculated using a straight pressure weighting function.

are some odd gaps in the MFL data, due to some data sparseness which does not meet the minimum 20 observation requirement when 60-second averaging is performed.

The OCO-2 data does show some subtle smaller-scale variability of the spatial magnitude as the MFL features, but the two are entirely uncorrelated. OCO-2 observes the steepest latitudinal gradient, with a slope -0.18 ppm per degree latitude, and the MFL and CAMS datasets have slopes close to zero - which, given the shallowness of the gradient, is probably within the margin of error.

5.9. NOVEMBER 9, 2017

TABLE 5.9. November 9, 2017 Slopes and Correlations with OCO-2

	σ (ppm)	Mean $\Delta X_{CO_2} \pm$ Error (ppm)	r_{OCO-2}	Slope (ppm/ $^{\circ}$)
OCO-2	0.88	0 ± 0.27	-	-0.14
MFL_S	1.06	-1.15 ± 0.28	0.18 (0.18)	0.09
MFL_L	1.11	-1.33 ± 0.29	0.13 (0.19)	0.45
CAMS	-	2.01	0.47 (0.58)	-0.20
CarbonTracker	-	-	-	-

The final fall underflight began in the northwest corner of Texas and crossed western Oklahoma into Kansas. Four spirals were flown in total between the B-200 and C-130: the

C-130 completed one at each end of the 8-kilometer underflight track, and the B-200 recorded PICARRO data in both an ascending and descending spiral close to the time of the OCO-2 overpass, in the mid-northern section of the underflight track (see Figure 5.36d for spiral locations as green stars). The C-130 flew a secondary leg at an altitude of 2.5 kilometers,

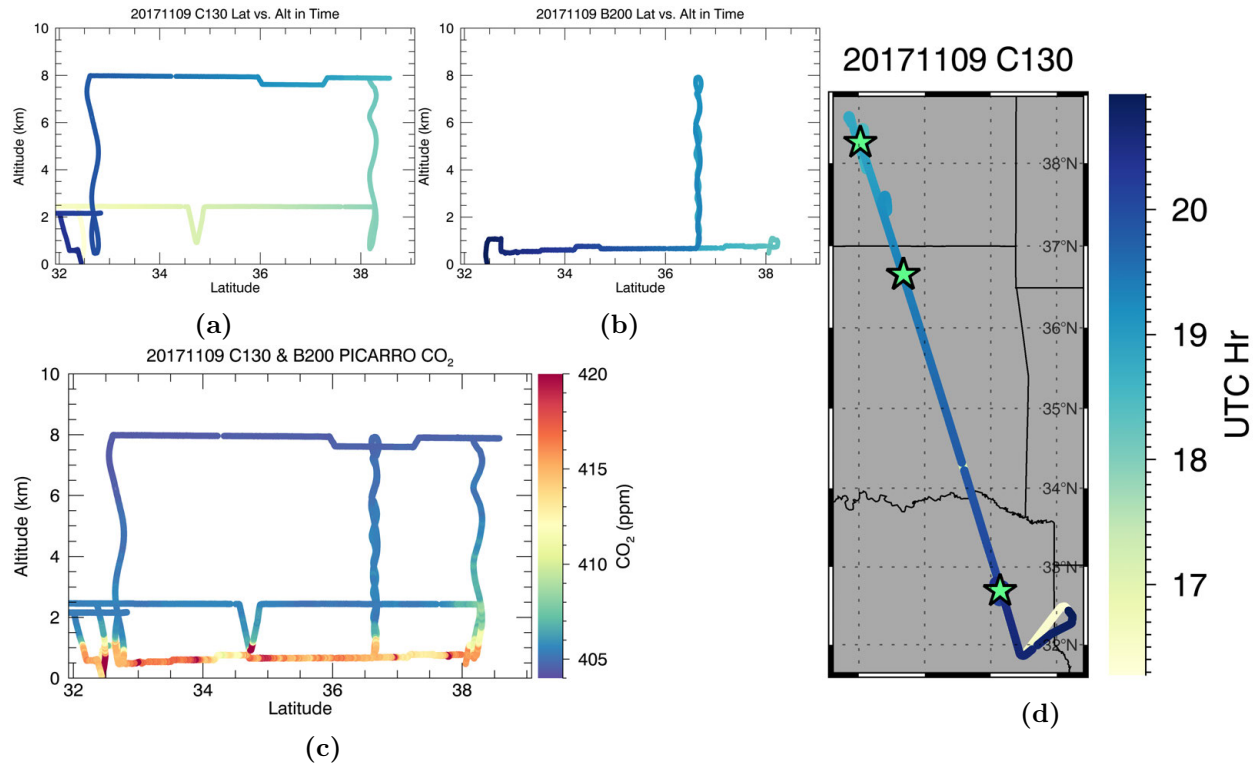


Figure 5.36. Both aircraft in latitude and altitude, colored in time (a, b and d) along with a flight map, and in situ CO₂ data (c) for November 9, 2017.

while the B-200 stayed in the boundary layer, at half a kilometer. Figure 5.36c shows the in situ CO₂ data from both aircraft: the boundary layer appears shallow (about 1km) and well-defined, with concentrations consistently within the range of 412 to 420 ppm. Above 1 kilometer, CO₂ values drop to 408 or less and the column appears well-mixed along the length of the flight track. There is little to no variability visible in the 8 kilometer data, with concentrations between 404 and 405 ppm across nearly 5 degrees latitude.

Unfortunately, much of the flight track, which spans from 32.5 to 38.5N, is obscured by clouds, as shown in Figure 5.37a. Only a short section of track between 33 and 34N contains enough clear-sky OCO-2 data for comparison to MFL; this section is enlarged in Figure 5.37b. The clear-sky data, however, has fairly significant scatter and there are some spatial gaps which may be due to surface features. There are thus no coherent X_{CO_2} features visible in the OCO-2 data.

Two of the four in situ profiles are shown in Figure 5.38, with the CAMS upper tropospheric profile (interpolated to the proper location and time) in the top panels and with the CAMS profiles in latitude at the time of the OCO-2 overpass in the bottom panels. The left column shows the southernmost C-130 spiral data, taken about 1 hour after the OCO-2 overpass, and the right column shows the northernmost C-130 spiral, taken around 1.5 hours prior to the overpass time. The location of the in situ spiral relative to the model profiles is indicated by a tick mark on the color bar. In both cases, CAMS CO_2 model values are higher than in situ observations by at least 1 ppm throughout much of the sampled column, particularly in the lower troposphere of the southern spiral between 800 and 900 hPa, where the model does not capture the sharp boundary layer transition. The B-200 ascending and descending spiral data, not pictured here, show a similar relation to the CAMS data.

The X_{CO_2} data in Figure 5.39 show little agreement between CAMS, OCO-2, and MFL datasets. It should be noted that due to clouds, the MFL data on this day is spatially sparse, and looser restrictions were placed on data density when averaging: only ten MFL measurements are required per 60-second bin, rather than the usual twenty. The MFL once again displays a low bias relative to OCO-2, and shows some relatively coherent spatial features which do not appear in the OCO-2 data. OCO-2 is higher than the MFL by 1

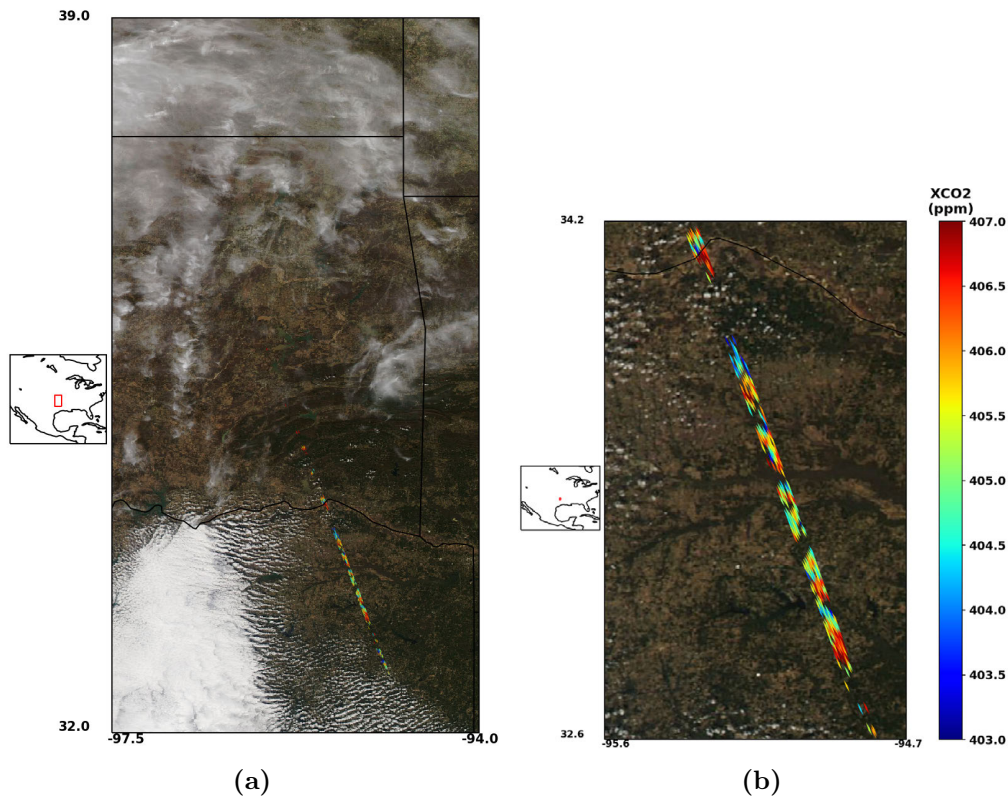


Figure 5.37. OCO-2 XCO₂ along the November 9, 2017 underflight track.

ppm or more along most of the track, and CAMS shows its typical seasonal high bias. The in situ column-averaged value, including the CAMS upper tropospheric column, appears to best match the magnitude of the OCO-2 data, but was taken in the cloudy region just south of the area of comparison. The other three spirals were also taken in locations where there is no OCO-2 data available for comparison.

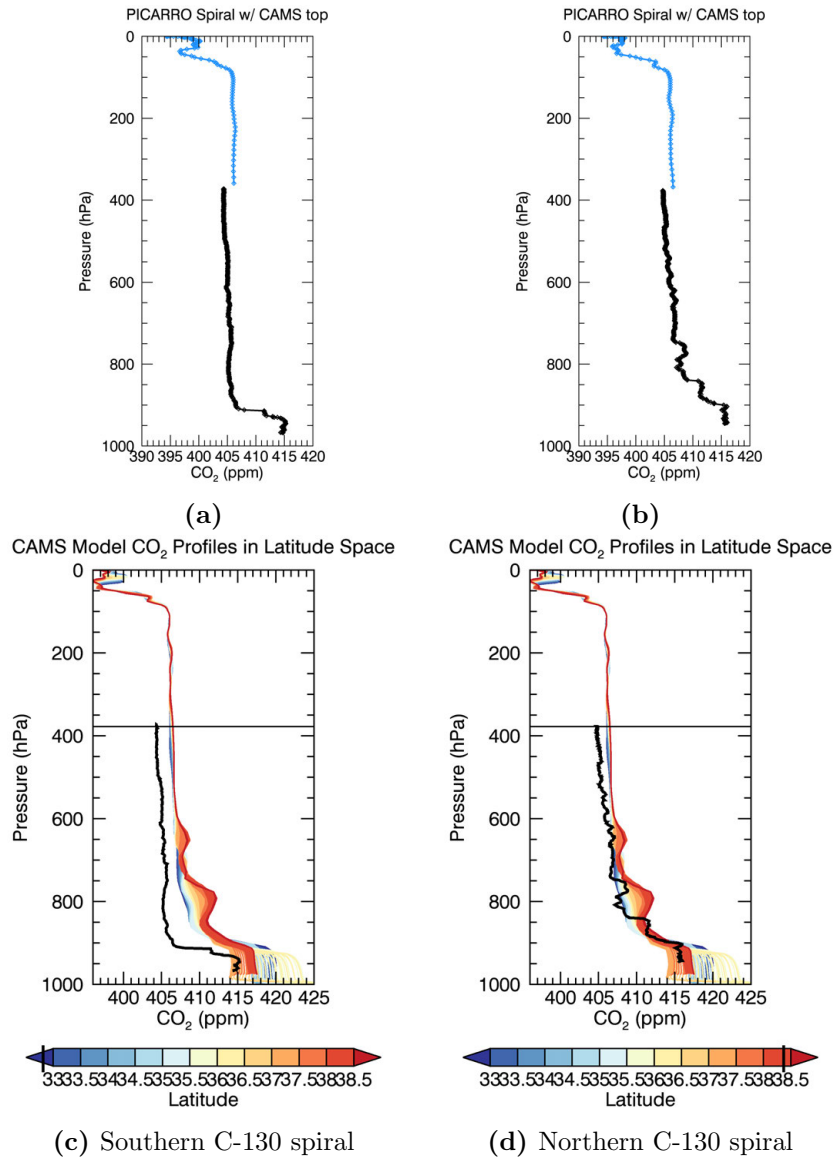


Figure 5.38. (a, b) November 9, 2017 in situ spirals up to the C-130 height, with CAMS model profiles above. (c, d) In situ spiral in black, with CAMS model profiles colored in latitude.

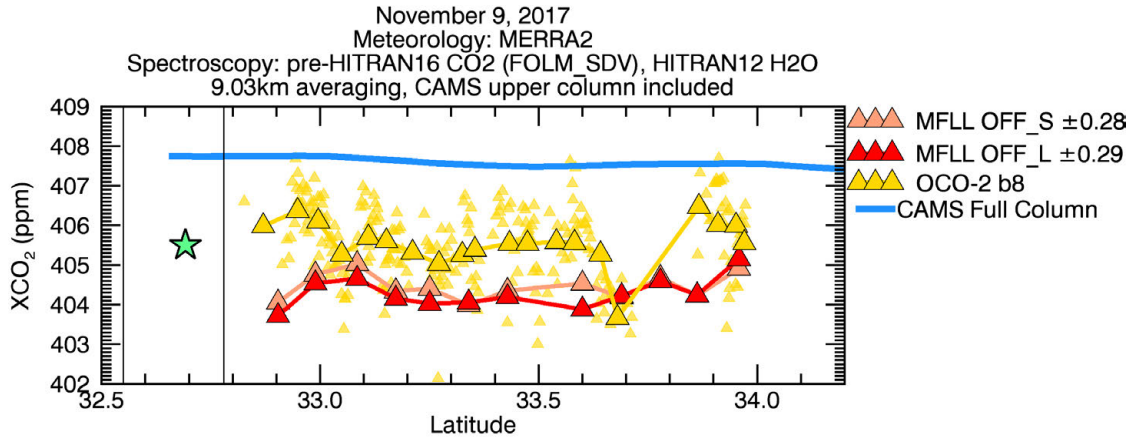


Figure 5.39. X_{CO₂} datasets from November 9, 2017. The in situ spiral column-averaged value, with CAMS model top included, is shown as a green star. CAMS full column values are calculated using a straight pressure weighting function.

COMPARISONS AND DISCUSSION

This chapter includes key comparison results and figures which primarily address the first two hypotheses laid out in Chapter 1. All three campaigns are included in this discussion, though some flights did not yield useful comparisons. For in-depth detail on each of the nine flights, including in situ profiles, flight tracks, model evaluation, and tables of statistics, please refer to Chapter 5.

We turn to the first question of the study from Chapter 1 to frame the discussion of our comparisons: Is the majority of the OCO-2 observed gradient at scales of ten to hundreds of kilometers primarily real or spurious, and does the answer to this question depend on the scale chosen? Can the causes of apparently spurious features be individually attributed to surface or scattering features?

After three campaigns, nine underflights of OCO-2 were completed by the MFLL and ACT-America teams in pursuit of validation for lower tropospheric X_{CO_2} - three flights from each season: summer, fall, and winter. Summer flights yield the most successful comparisons between OCO-2 and the MFLL, and though the winter campaign was plagued by high MFLL measurement noise, winter and fall data both hold some interesting observations, particularly regarding OCO-2.

The first summer flight holds the most successful comparisons to date. On July 27, 2016 the ACT-America team underflew OCO-2 along the east coast through the state of Pennsylvania, with an in situ spiral flown over State College. The MFLL level 1 optical depth product, which includes ON/OFF_S values with crosstalk and bias corrections, was used in our X_{CO_2} retrievals. Results along the track are shown in Figure 6.1. All datasets compared

aside from the CarbonTracker NRT model show a similar decreasing gradient in X_{CO_2} values from south to north along the track; OCO-2 observations have a -0.75 ppm/ $^\circ$ slope in latitude, while the MFLL results are steeper at -0.98 ppm/ $^\circ$. The MFLL data are higher than OCO-2 by an average of 0.58 ppm along the length of the flight track, which spans about 3.5 degrees in latitude, and curtain-derived X_{CO_2} values from PSU and GMAO are different from OCO-2 by only 0.4 and 0.38 ppm, respectively. CarbonTracker matches OCO-2 best in slope, though final spatial features disagree, with an r value of only 0.24 between the datasets. The two curtains are next closest to OCO-2 in slope, OCO-2 at -0.7 ppm/ $^\circ$ and curtains near -0.8 ppm/ $^\circ$. The curtains also have the highest correlation with OCO-2, PSU with $r = 0.72$ and GMAO with $r = 0.75$. The curtains look remarkably similar to one another despite notable differences in the methods of their construction, and both have a small mean ΔX_{CO_2} of ≤ 0.4 ppm compared to OCO-2. The CAMS model data slightly overestimate the strength of the gradient with a slope of -1.20 ppm/ $^\circ$, and CarbonTracker displays what we've observed as a typical growing season low bias, with $X_{\text{CO}_2} \geq 2$ ppm lower than the curtain values. Overall, the MFLL, curtain, and model data demonstrate the fidelity of the OCO-2 observed gradient over the nearly 400-kilometer track. When this larger latitudinal gradient is removed via linear regression, however, no correlation to OCO-2 remains: r values actually dip negative for all data but CAMS, with $r = 0.07$, indicating that OCO-2 variability on smaller scales is not seen by any of the other datasets. A majority of the variability remaining after the overall gradient is regressed out is quite small, a few tenths of a ppm, and though a few ppm-sized features remain in the OCO-2 data, the MFLL and curtains, even with their fine spatial resolution, do not see those features. This says that on scales of tens of kilometers, OCO-2 data may be too contaminated by cloud and surface effects to show realistic features.

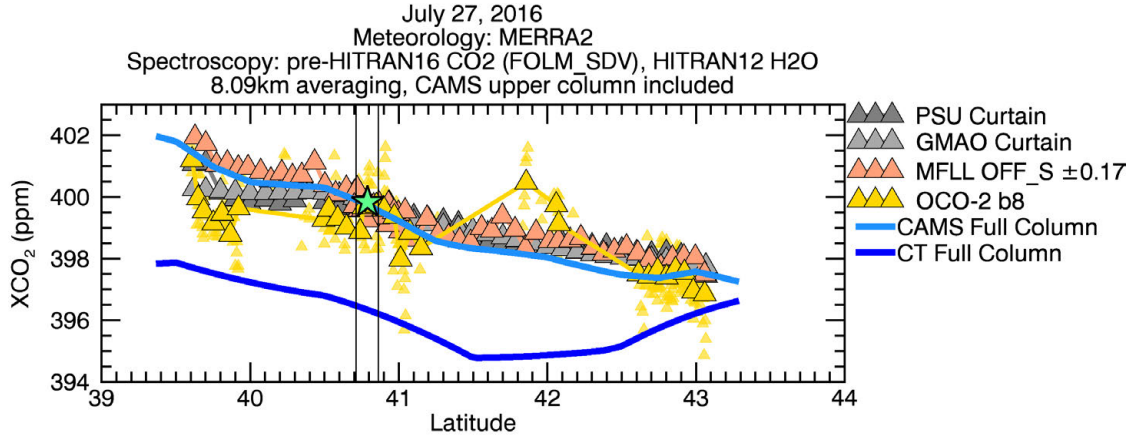


Figure 6.1. Comparing various X_{CO_2} datasets from the July 27 underflight. The in situ spiral column-averaged value, with CAMS model top included, is shown as a green star. The CAMS full column values are calculated using a straight pressure weighting function.

Inefficiency in OCO-2 cloud screening algorithms may be one such contributor to OCO-2 small-scale variability in this case: X_{CO_2} values around 42°N appear to be spurious, at least 1 ppm higher than the observed latitudinal gradient predicts. These are retrieved from within a field of popcorn cumulus clouds, seen in Figure 6.2a. In cases like this, current work by the OCO-2 science team seeks to develop either an improved cloud screening algorithm or a correction factor based on predicted and observed three-dimensional cloud effects (Schmidt et al. (2016), Massie et al. (2017)). This is our first example of attributing a particular spurious feature to its cause.

In addition, there is a slight bias related to topography over the hills of Pennsylvania. Figure 6.2b shows this section of the track, between 40 and 41N, in greater detail. The higher X_{CO_2} on the northern (trailing) sides of the hills in this area could be due to a pointing error within the OCO-2 instrument, a correction for which is currently being developed by the OCO-2 science team. Individual-track features like this may exist in areas with similar topography throughout the dataset, contributing to unnecessary sparsity in local datasets,

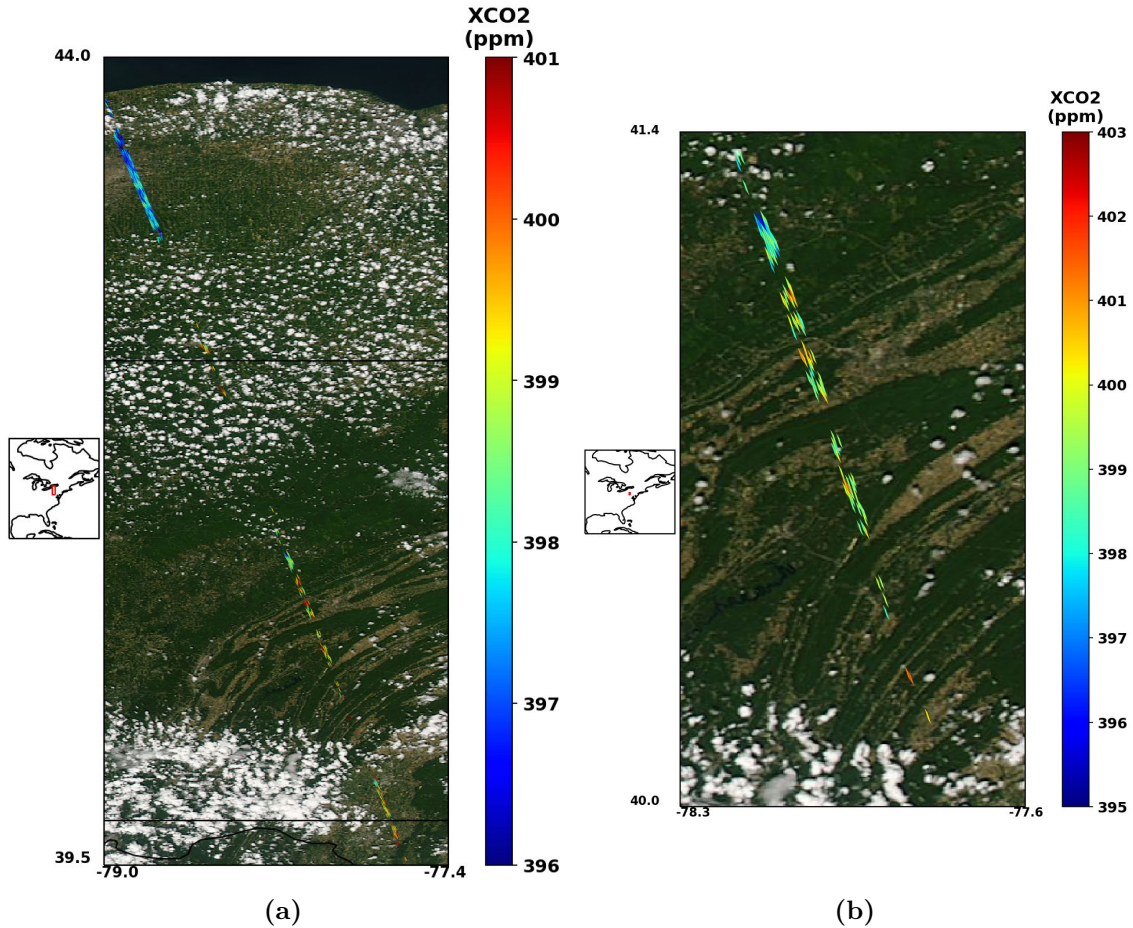


Figure 6.2. OCO-2 X_{CO_2} along the MFL underflight track on July 27th, showing all eight footprints atop MODIS visible imagery. Figure (a) shows the full underflight track, and Figure (b) shows a potential filtering issue related to topography between 40 and 41N.

and also resulting in some spurious X_{CO_2} values. We thus identify a potential cause of one spurious feature.

The second summer flight, on August 5, 2016, also provides an interesting comparison study, and some insight into certain differences stemming from their construction methods. As shown in Figure 6.3, a latitudinal gradient similar to that of July 27th, decreasing to the north, is present. However, a few other features are notably different. Firstly, all datasets show a decrease in X_{CO_2} at the northern end of the track between 47 and 48N. Secondly, CarbonTracker agrees fairly well in magnitude with the MFL and curtain data, though slightly high.

The OCO-2 data have a slope of $-0.43 \text{ ppm}/^\circ$, which is steeper than the rest of the datasets - the MFL data is closest at $-0.36 \text{ ppm}/^\circ$. The CAMS and curtain data all have slopes between -0.15 and $-0.26 \text{ ppm}/^\circ$, and CarbonTracker has a slope of $-0.31 \text{ ppm}/^\circ$. It appears that the higher X_{CO_2} values from OCO-2 at the southern end of the track may be spurious, as these data were taken between cloud fields (see Figure 6.4). Interestingly, CarbonTracker has the highest correlation with OCO-2 in space ($r = 0.78$), notably due to a similar, though smaller, depression in X_{CO_2} between 45.5 and 47.5N , which the other datasets do not see. The MFL data has the next best correlation with OCO-2 at $r = 0.71$. Once again, when the larger latitudinal gradient is removed, there is no apparent validation agreement of OCO-2's smaller-scale features - the GMAO curtain has the highest correlation at 0.24 . We see the the second case the MFL data and in situ data being unable to replicate the OCO-2 features on sub-degree-latitude scales, addressing part of our first question of the study - data on this scale may not be representative of real gradients. It is worth noting that there appears to be some significant small-scale variability in the MFL data, on the order of 1 ppm , but that neither in situ nor curtains are able to replicate those features. Remote sensing instruments in general appear to struggle at such scales.

In addition, there is a difference ranging 1.2 to 1.9 ppm between the PSU and GMAO curtains. Closer examination has shown that this is due to the inclusion of the CAMS model above 9 km in the PSU curtain calculations. The CAMS data above 9 km are consistently several ppm higher than the PSU curtain values; when CAMS data is not included in the PSU X_{CO_2} calculation, the results below 9 km agree with the full-column GMAO results, with an average difference of only 0.25 ppm , though highly variable along-track. When compared to partial-column GMAO results (below 9 km), the two have a similar difference to that

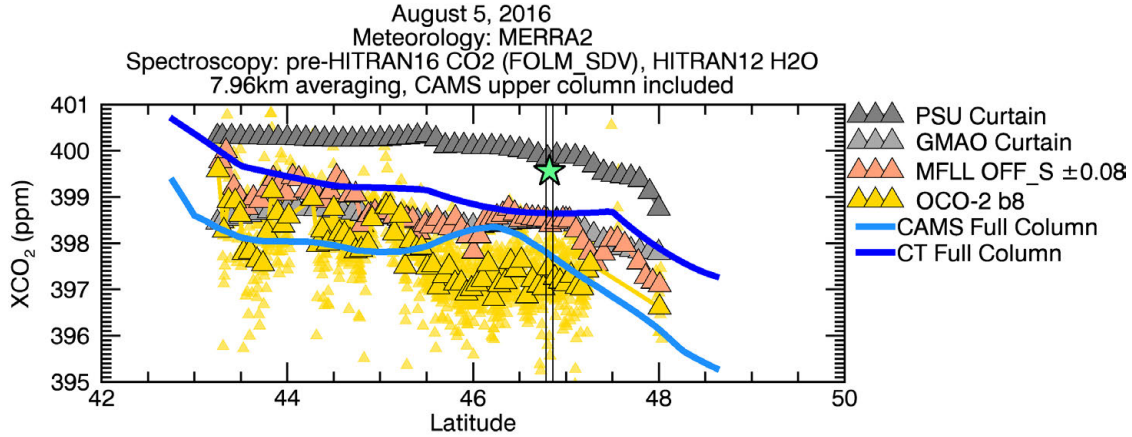


Figure 6.3. X_{CO₂} datasets from the August 5, 2016. The in situ spiral column-averaged value, with CAMS model top included, is shown as a green star. The CAMS and Carbon-tracker full column values are calculated using a straight pressure weighting function.

shown in the Figure 6.3 - the GMAO curtain shows much lower CO₂ values throughout the troposphere, although in situ features are clearly visible, and X_{CO₂} is nearly 1.5 ppm lower than PSU along much of the track. The PSU curtain also washes out features within the boundary layer, showing constant CO₂ concentrations below 750 mb. These differences may be due to a variety of factors: the GMAO curtain takes temporal variations into account, whereas the PSU curtain does not; the GMAO curtain uses all in situ data with the aid of spatial decorrelation lengths to account for longitudinal variations, whereas the PSU does not use any data beyond a certain distance away from the underflight track. Fine-tuning of the curtain construction and comparison processes is thus an important factor in future when interpreting curtain, and thus in situ, data.

The third summer underflight, August 27, 2016, is one of three underflights with relatively little comparison data. With only four points of comparison after cloud and data density screening, CAMS, MFL, and OCO-2 have steeper slopes, while both curtains and CarbonTracker predict a nearly flat latitudinal trend. Both CAMS and the MFL have correlations of 0.75 with OCO-2, but given the limited data availability, the numbers don't

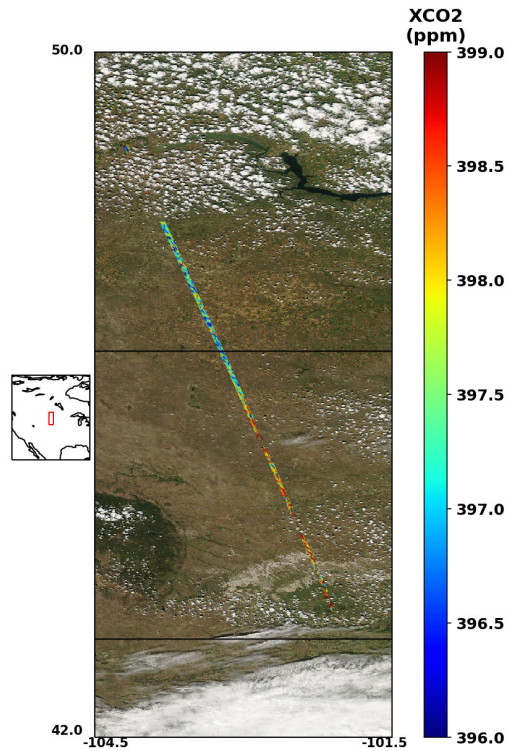


Figure 6.4. OCO-2 X_{CO_2} along the August 5, 2016 underflight track.

carry much weight. The February 13, 2017 flight has similarly little OCO-2 data available along-track due to snow cover, and the November 9, 2017 underflight track is mostly obscured by clouds as well.

Three OCO-2 underflights were completed in the winter 2017 campaign, in February and March. All three show decreased MFLL SNR, due to a coating degradation on the MFLL viewing window, which could not be fixed until after the campaign's conclusion. The C-130 flew lower than 9 kilometers throughout the campaign in an attempt to improve the SNR, but the results remain noisy: MFLL errors in the winter campaign were about 3.5 times higher than those of the summer campaign, with typical 60-sec average errors of 0.5-0.6 ppm, large enough to make interpretation of any MFLL small-scale variability nearly impossible. The February 13th flight was also largely snow-covered, such that an underflight spanning nearly 41 to 47N only yielded OCO-2 data between 43.7 and 44.7N. The other two flights, February

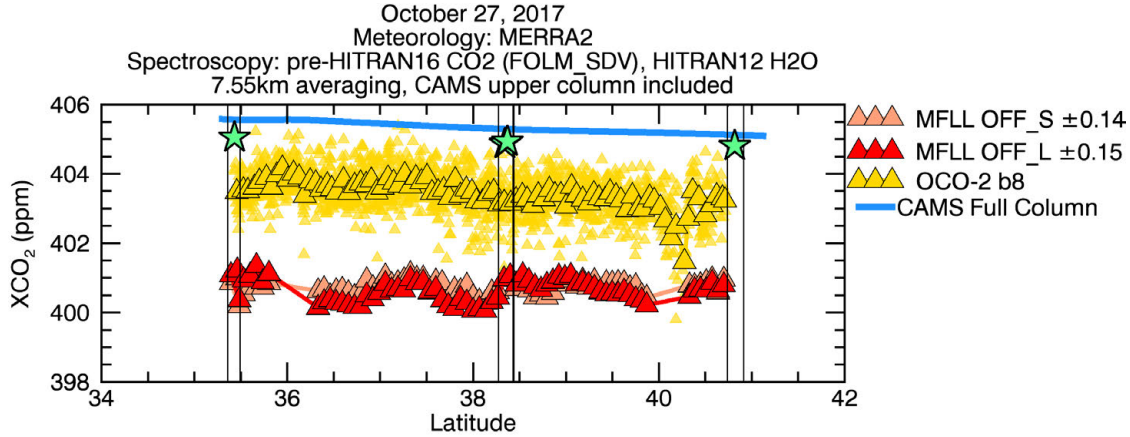


Figure 6.5. XCO₂ datasets from October 27, 2017. The in situ spiral column-averaged value, with CAMS model top included, is shown as a green star. CAMS full column values are calculated using a straight pressure weighting function.

15th and March 8th, held clear skies, but both flights showed fairly flat XCO₂ fields along the track. There is consistently little to no correlation between OCO-2 and any of the other datasets - the highest is with CarbonTracker on March 8th, at $r = 0.49$. It is thus difficult to use these flights to comment on the validation of spatial gradients, because the gradients are nearly nonexistent.

The most interesting results from the winter campaign do not concern large-scale spatial trends, but rather high cloud signals. In both the February 15th and March 8th flights, there are coherent peaks in XCO₂ at the location of what appear to be high clouds, via a cursory look at MODIS cloud top heights in the regions. See Figures 6.6 and 6.7 at 39.25 and 38.2N, respectively. Figures 6.8a and 6.8b show the MODIS visible imagery for these two OCO-2 tracks. These recurring scenes are further evidence of our ability to identify the sources of spurious OCO-2 small-scale features. While the elimination of such features may not affect the global dataset, they do affect the interpretation of local data and potentially affect the biases of small scenes such as those assimilated into regional flux inversions.

The fall data are similar to the winter in that there are no strong spatial gradients present in the three flights, and the MFLl demonstrates a persistent low bias, though its SNR returns to target levels, matching that of OCO-2 with the installation of a new viewing window on the C-130. The October 27th flight shows some interesting spatial variability in both the MFLl and OCO-2 datasets (see Figure 6.5), but they show some of the lowest correlations of the project thus far at 0.10 and 0.03 between OCO-2 and MFLl_S and MFLl_L, respectively. In an effort to understand the small-scale MFLl variability, which is on the order of 1 ppm, we also look at the in situ data, which shows variable CO₂ concentrations particularly along the 3 km track, but the correlation between the two is -0.3. This is an example of a flight for which an in situ curtain might prove particularly enlightening, and help us to draw some conclusions related to our question of the scale of OCO-2 validation, as well as MFLl biases. The CAMS model is actually the dataset most highly correlated with OCO-2 on this day, with $r = 0.64$, due to the agreement of the larger gradient across the track.

We see another mysterious feature in the OCO-2 X_{CO₂} on this day which is potentially related to some surface feature. There is a notable drop in X_{CO₂} near 40N which is co-located

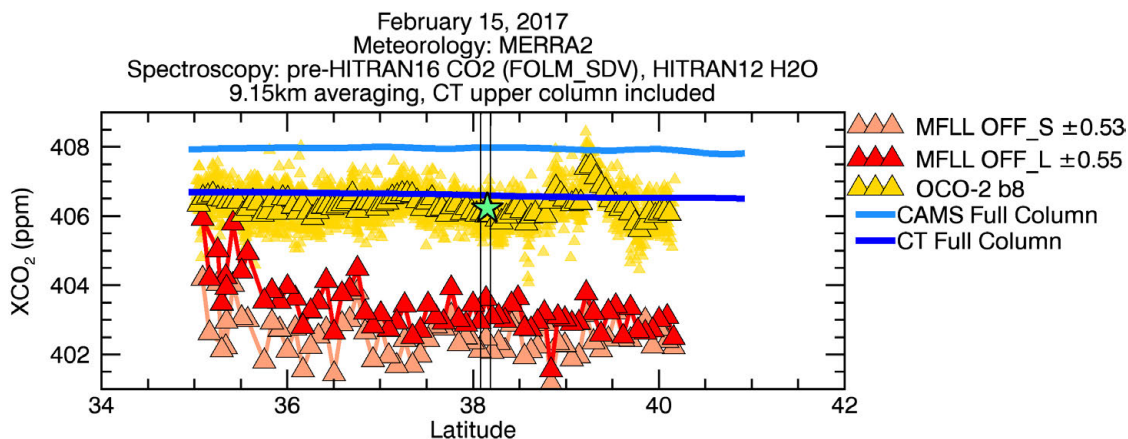


Figure 6.6. X_{CO₂} datasets from February 15, 2017. The in situ spiral column-averaged value, with CarbonTracker model top included, is shown as a green star. CarbonTracker full column values are calculated using a straight pressure weighting function.

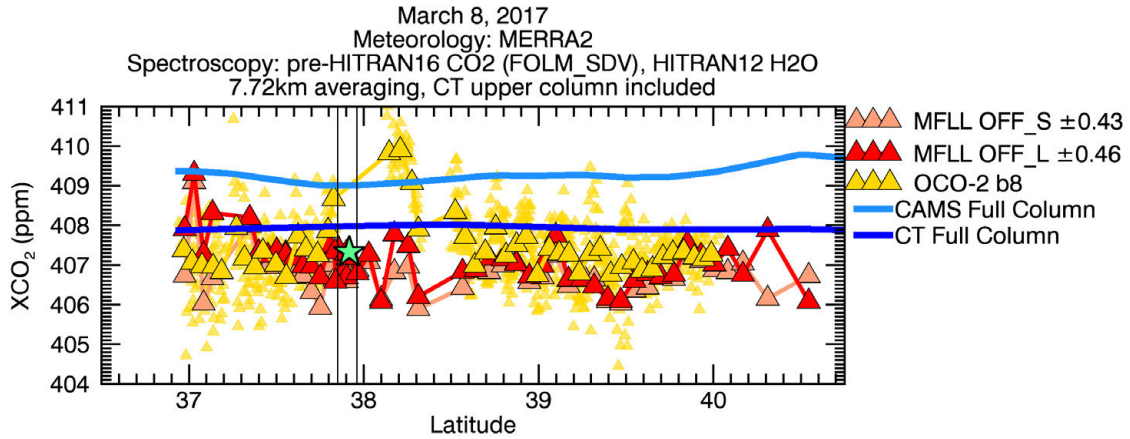


Figure 6.7. X_{CO_2} datasets from March 8, 2017. The in situ spiral column-averaged value, with CarbonTracker model top included, is shown as a green star. CarbonTracker full column values are calculated using a straight pressure weighting function.

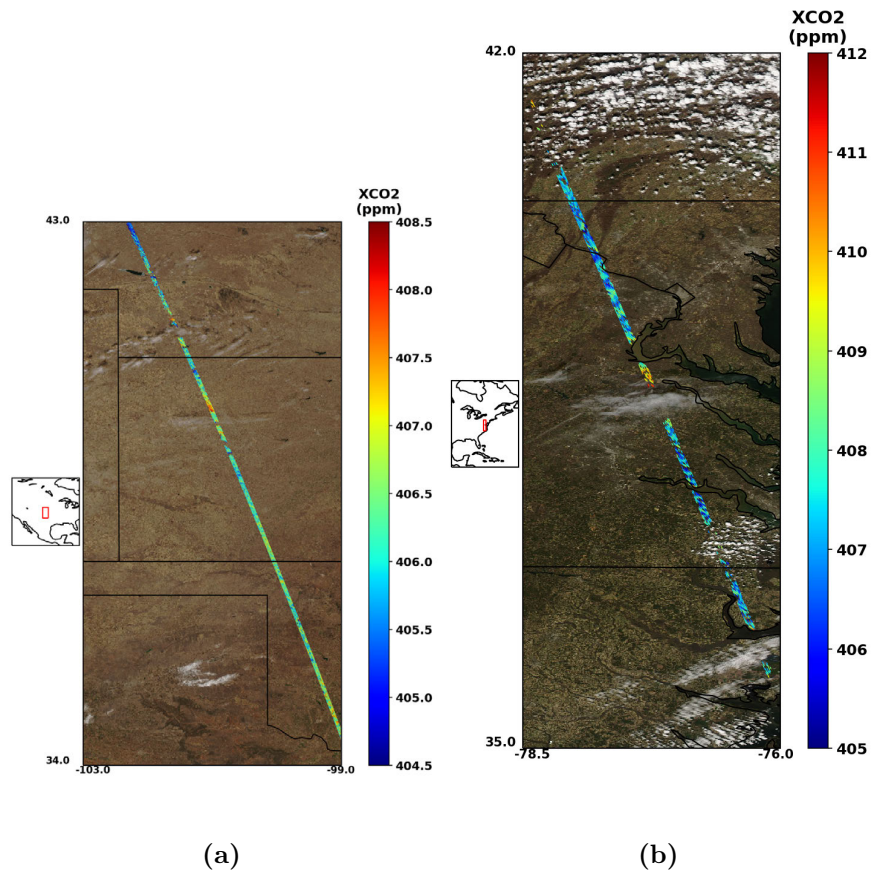


Figure 6.8. OCO-2 X_{CO_2} data for (a) February 15th and (b) March 8th, 2017. Note that the peaks in X_{CO_2} are co-located with visible high cloud features.

with a gap in the data, shown in Figure 6.9. The cause of this feature is yet unknown, but may be another example of a feature caused by atmospheric scattering or surface features.

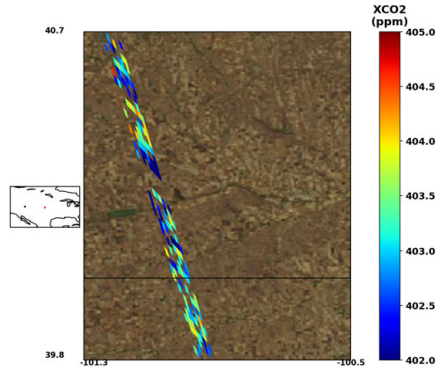


Figure 6.9. Unusual feature in the OCO-2 X_{CO_2} data on October 27, 2017.

Both the winter and fall data display a persistent low bias in the MFLR retrievals prior to bias correction, on the order of 2-4 ppm depending on the day. This may be due in part to an observed range-dependent bias which is currently under investigation by the MFLR team. A single average bias correction is applied to all flights in a campaign - but the slope of the range-dependent bias varies from flight to flight, for reasons as yet unknown. The summer data shown in this work prove that the bias correction largely results in a realistic, useful dataset. Further bias corrections are currently in development.

CONCLUSIONS AND FUTURE WORK

NASA’s ACT-America mission seeks in part to provide a validation source for the Orbiting Carbon Observatory, whose millions of global X_{CO_2} measurements each day represent a major step forward in global monitoring of greenhouse gases. Its success at measuring CO_2 on smaller spatial scales (tens to hundreds of kilometers) is difficult to measure because ground-based measurements are so sparse and mostly at fixed geographic locations; the Langley C-130 underflies OCO-2 overpass tracks with a CO_2 lidar in tow as part of the ACT-America campaign in order to provide a meaningful validation source. The Multifunctional Fiber Laser Lidar has flown nine OCO-2 underflights across three seasons. In this study we compare the MFLL and OCO-2 data for all nine underflights, as well as in situ spiral and “curtain” data.

In our comparisons between the OCO-2 and ACT-America data, as well as that of two models, we set out hoping to address the following questions:

- (1) How well can the MFLL validate OCO-2?
- (2) Is the majority of the OCO-2 observed gradient at scales of hundreds of kilometers primarily real or spurious?
- (3) Is the majority of the OCO-2 observed gradient at scales of tens of kilometers primarily real or spurious?
- (4) Can we identify spurious variability and its causes in the OCO-2 X_{CO_2} data?

To test the first question, we run MFLL X_{CO_2} retrievals using three different sets of meteorology, several different sets of H_2O and CO_2 spectroscopy, and various wavelength offsets. We show that the ON/OFF_L retrievals are more sensitive than the ON/OFF_S to

changes in most input variables, except for CO₂ spectroscopy, which has the largest effect on the X_{CO₂} results - up to nearly 10 ppm in some cases. Different water vapor tables can cause similar, if slightly smaller, differences in X_{CO₂}, but meteorology differences only change results by a few tenths of a ppm. Differences in water vapor vary the most in space, whereas changes due to CO₂ spectroscopy manifest in the form of a nearly-constant offset. When the ON wavelength is changed by a constant amount, we also see near-constant offsets in the X_{CO₂} values across the track - larger offsets in the ON/OFF_L than in the ON/OFF_S. At a $\Delta\lambda$ of 0.4 pm, ON/OFF_L X_{CO₂} changes exceed 1 ppm. All of these results combined tells us that the relative immaturity of the MFLL retrieval can lead to significant uncertainty in the X_{CO₂} product.

We show that additional uncertainties are introduced based on the different vertical sampling of the MFLL and OCO-2. Contrary to the original intentions of the ACT-America proposal, MFLL retrievals are shown to have systematic differences from OCO-2 retrievals due to differences in both the sampled column extent and weighting function. In Chapter 4, we show that both magnitude and spatial variability of the resulting along-track X_{CO₂} change when the same model profiles are sampled in the style of the two instruments. The OCO-2 results more closely resemble (within a few tenths of a ppm, consistently) the shape and size of straight pressure-weighted X_{CO₂}, while MFLL retrievals of the same CO₂ profiles consistently show larger magnitude differences and which vary in space. We conclude that some correction must be made for both the upper column and the weighting function shape to account for these trends; we show that these corrections can indeed improve the retrieved results. However, we acknowledge that such corrections as we apply them here rely necessarily on model data, which is not always representative of the true atmospheric state. Two CO₂

models, the ECMWF CAMS model and the CarbonTracker near-real-time model, have been tested for 6 of the 9 flights. In general, from comparisons to in situ profiles, OCO-2, and MFL data, the CAMS model is shown to be several ppm too high in the cold seasons, while CarbonTracker (in winter) is on par; in the growing season, CAMS is consistently in relatively good agreement with OCO-2 and MFL in terms of both magnitude and spatial gradient, but CarbonTracker is quite variable, sometimes several ppm too low, and sometimes within 1.5 ppm of the OCO-2 data with a similar latitudinal slope.

The corrections which we develop from these models can reflect this kind of unsuitable model variability, and we must be consistently careful moving forward not to attribute those features of the model-derived correction to the MFL retrieval itself. In the results shown, this kind of misinterpretation is most easily seen in the August 5th case, in which the in situ spiral column (star) appears nearly 1 ppm higher than the MFL data. In that particular case, this is due to the inclusion of the CAMS upper column, which is anomalously high above 9 km. When the CAMS upper column is not included, the in situ spiral aligns with the MFL results at that location. To prevent some of this potential misinterpretation, future work involves using the in situ curtains as the source of the correction below the plane. Unfortunately, model data above the plane in both curtains remains unaffected by in situ observations, which only exist up to 9 kilometers in the best cases. While the upper tropospheric data can be quite different between models, as discussed in Chapter 4, we see the largest difference in magnitude rather than spatial variability. When the upper column is included, its weight (by fraction of total column dry air molecules) is nearly 30% of the total, so these effects on the full column result are subtle, but present, and should be noted with care. The high values of the in situ spirals in the fall 2017 flights, for example, include

the CAMS upper column. We show the CAMS profiles in the cold seasons to be too high throughout the column; once CarbonTracker data is used for the upper column correction, agreement between the in situ profile and both OCO-2 and MFLl should improve.

Based on these uncertainties in the both MFLl retrieval and the corrections we apply, we conclude that the ability of the MFLl to validate OCO-2 observations is relatively limited. We thus turn to the in situ data as another potential source of validation. In situ “curtains” are constructed, using two different methods, from 2-dimensional CO₂ fields along the flight track sampled by PICARRO instruments aboard both the C-130 and B-200 aircraft. By using both a simple nearest-neighbor approach and a more advanced method of data assimilation, we are able to replicate the magnitude and spatial gradients observed by the MFLl and OCO-2 with relative success.

We can now move on to our second research question: Is the majority of the OCO-2 observed gradient at scales of hundreds of kilometers primarily real or spurious? Our MFLl - OCO-2 comparisons show that the ACT-America underflights have observed features primarily on the scale of hundreds of kilometers; the slopes of the two datasets on these scales appear largely in agreement. In addition to the MFLl data, we show in Chapter 6 that in situ profiles, often providing multiple high-precision X_{CO₂} estimates along the flight track, agree with OCO-2 data to within 1 ppm in 8 of 9 cases when a model upper column is included in the profile. On the two days when strong spatial gradients are present, the MFLl ON/OFF_S level 1 optical depths produce retrieved X_{CO₂} results with fairly strong correlations to OCO-2, up to $r = 0.75$, though their slopes differ slightly across the length of the underflight track. Curtain data successfully reaffirm the observed gradients from the first two summer flights, with similarly strong correlations to OCO-2 across the track and, in

the July 27th case, slopes more consistent with that of OCO-2. On August 5th, the curtains also appear to confirm the slightly higher values of the MFLL retrieval. From these two days, we conclude that both the MFLL and in situ measurements are successfully able to validate OCO-2 gradients on the scale of a few hundred kilometers. Unfortunately, winter and fall flights were devoid of strong spatial gradients. On days with decent data density, comparisons show MFLL slopes within 0.3 ppm per degree latitude of OCO-2 slopes, but no correlation ($r = 0.14$ at best) due to noise and lack of strong signal. The slopes of these datasets, however, still seem to be in agreement within the uncertainties of the data. Further work will seek to quantify the uncertainties in these slopes and compare for the statistical significance of their differences.

These nine underflights have provided abundant opportunity to look for regional features in OCO-2 data, in an attempt to answer our third research question: Is the majority of the OCO-2 observed gradient at scales of tens of kilometers primarily real or spurious? When linear regression is performed to remove the larger latitudinal gradients of each dataset, none of the flights are able to replicate OCO-2 smaller-scale features, with r values persistently near (and below) zero. Smaller-scale features do present themselves in the OCO-2 data, but thus far can be largely attributed to surface and cloud effects. On two occasions (February 15 and March 8), we see coherent peaks in the OCO-2 X_{CO_2} data due to path-lengthening effects of visible, co-located high clouds. In one summer case, July 27th, we see both insufficient cloud filtering resulting in spurious high values, and topography-related biases over hilly regions. While these various cloud and topography effects may have small impacts when scaled up to the global dataset, they may yet affect the biases of local datasets which regional flux inversions seek to assimilate, and may sometimes be mistaken for real sources and

sinks. The identification of such features in this work has strengthened the motivation of the OCO-2 science team to develop improvements for each of these effects - high cloud features, insufficient filtering of lower cloud-contaminated scenes, and bias issues related to topography, due to an instrument pointing error.

Curtain data has proven useful, in our work, for invalidating some of these features in the OCO-2 dataset, and for invalidating some small-scale features of the MFL as well. This utilization of in situ data may prove especially enlightening in other cases where the MFL sees smaller-scale patterns which are not present in the OCO-2 observations, such as in the October 27 case. Overall, both statistically and from individual attribution, we conclude thus far that OCO-2 features on the scale of tens of kilometers are not representative of real X_{CO_2} patterns. We also conclude with regards to our fourth research question (Can we identify spurious variability and its causes in the OCO-2 X_{CO_2} data?) that the MFL and in situ data make the identification of spurious OCO-2 features possible, and that in most cases, we can successfully identify the causes of such features. Once corrections are developed for these types of features, the smoother OCO-2 datasets can be compared to the MFL data afresh to statistically re-evaluate their agreement.

The MFL results have faced a few challenges over the course of the three flight campaigns, including excessive SNR from a viewing window coating degradation (winter flights only) and a mysterious range-dependent bias which varies in magnitude from flight to flight. A campaign-wide bias correction has been developed for the summer 2016 flights, which eliminates the low bias often seen in the MFL X_{CO_2} results. Similar bias corrections are in development for the winter and fall campaigns and will presumably have similar effects on the magnitude X_{CO_2} retrievals, in addition to some smaller effect on their slopes. The

cause of this range-dependent bias is under investigation, and until it is resolved, the team must rely on bias corrections to address it. Once the bias-corrected, calibrated level 1 optical depths are available for the winter and fall campaigns, X_{CO_2} should be recalculated, and the agreement between the MFLL and OCO-2 should be re-evaluated.

OCO-2 represents a major step forward in our observation of the global carbon cycle, with measurements at fine enough spatial scales to observe emissions from individual cities and power plants. Such data has the potential to significantly improve regional flux models, but at such scales has always been difficult to validate using stationary ground-based techniques. We have shown in this work that even with directly collocated remote sensing data at high spatial resolution, instrument differences and retrieval sensitivities make the validation of small-scale OCO-2 X_{CO_2} patterns challenging. However, though variations at tens of kilometers remain difficult to both observe and validate, we are generally able to reproduce patterns on synoptic scales and directly attribute several local OCO-2 features to surface and cloud effects. Further development of the OCO-2 data product, MFLL retrieval algorithm, and in situ curtain construction methods may yet shed light on smaller-scale patterns: the state of greenhouse gas monitoring science continues to advance, and both OCO-2 and the ACT-America mission are strong evidence of its progress.

REFERENCES

- Browell, E., Dobbs, M., Dobler, J., Kooi, S., Choi, Y., Harrison, F., Moore III, B., and Zaccheo, T.: Airborne demonstration of 1.57-micron laser absorption spectrometer for atmospheric CO₂ measurements, presented at the 24th International Laser Radar Conference in Boulder, Colorado, 2008.
- Browell, E. V., Wilkerson, T. D., and McIlrath, T. J.: Water vapor differential absorption lidar development and evaluation, *Applied Optics*, 18, 3474–3483, doi:10.1364/AO.18.003474, 1979.
- Browell, E. V., Dobler, J., Kooi, S. A., Choi, Y., Harrison, F. W., Moore, III, B., and Zaccheo, T. S.: Airborne Validation of Laser Remote Measurements of Atmospheric Carbon Dioxide, in: EGU General Assembly Conference Abstracts, vol. 12 of *EGU General Assembly Conference Abstracts*, p. 3721, 2010.
- Crowell, S., Rayner, P., Zaccheo, S., and Moore, B.: Impacts of atmospheric state uncertainty on O₂ measurement requirements for the ASCENDS mission, *Atmospheric Measurement Techniques*, 8, 2685–2697, doi:10.5194/amt-8-2685-2015, 2015.
- Davis, K., Baier, B., Baker, D., Barkley, Z., Bell, E., Bowman, K., Browell, E., Campbell, J., Chen, H., Choi, Y., DiGangi, J., Dobler, J., Erxleben, W., Fan, T., Feng, S., Fried, A., Gaudet, B., Jacobson, A., Keller, K., Kooi, S., Lauvaux, T., Lin, B., McGill, M., McGregor, D., Michalak, A., Obland, M., O’Dell, C., Pal, S., Parazoo, N., Pauly, R., Randazzo, N., Samaddar, A., Schuh, A., Sweeney, C., Wesloh, D., Williams, C., Zhang, F., and Zhou, Y.: Progress toward improving regional atmospheric inversions using airborne measurements: Results from ACT-America, presented at American Geophysical Union

Fall Meeting 2017, 2017.

Dobbs, M., Krabill, W., Cisewski, M., Harrison, F. W., Shum, C. K., McGregor, D., Neal, M., and Stokes, S.: A Multi-Functional Fiber Laser Lidar for Earth Science and Exploration, in: IGARSS 2008 - 2008 IEEE International Geoscience and Remote Sensing Symposium, vol. 3, pp. III – 350–III – 353, doi:10.1109/IGARSS.2008.4779355, 2008.

Dobler, J. T., Harrison, F. W., Browell, E. V., Lin, B., McGregor, D., Kooi, S., Choi, Y., and Ismail, S.: Atmospheric CO₂ column measurements with an airborne intensity-modulated continuous wave 157 μm fiber laser lidar, *Applied Optics*, 52, 2874, doi:10.1364/AO.52.002874, 2013.

Eldering, A., O'Dell, C. W., Wennberg, P. O., Crisp, D., Gunson, M. R., Viatte, C., Avis, C., Braverman, A., Castano, R., Chang, A., Chapsky, L., Cheng, C., Connor, B., Dang, L., Doran, G., Fisher, B., Frankenberg, C., Fu, D., Granat, R., Hobbs, J., Lee, R. A. M., Mandrake, L., McDuffie, J., Miller, C. E., Myers, V., Natraj, V., O'Brien, D., Osterman, G. B., Oyafuso, F., Payne, V. H., Pollock, H. R., Polonsky, I., Roehl, C. M., Rosenberg, R., Schwandner, F., Smyth, M., Tang, V., Taylor, T. E., To, C., Wunch, D., and Yoshimizu, J.: The Orbiting Carbon Observatory-2: first 18 months of science data products, *Atmospheric Measurement Techniques*, 10, 549–563, doi:10.5194/amt-10-549-2017, 2017.

Gelaro, R., McCarty, W., Suárez, M. J., Todling, R., Molod, A., Takacs, L., Randles, C. A., Darmenov, A., Bosilovich, M. G., Reichle, R., Wargan, K., Coy, L., Cullather, R., Draper, C., Akella, S., Buchard, V., Conaty, A., da Silva, A. M., Gu, W., Kim, G.-K., Koster, R., Lucchesi, R., Merkova, D., Nielsen, J. E., Partyka, G., Pawson, S., Putman, W., Rienecker, M., Schubert, S. D., Sienkiewicz, M., and Zhao, B.: The Modern-Era

Retrospective Analysis for Research and Applications, Version 2 (MERRA-2), *Journal of Climate*, 30, 5419–5454, doi:10.1175/JCLI-D-16-0758.1, 2017.

Gordon, I. E., Rothman, L. S., Hill, C., Kochanov, R. V., Tan, Y., Bernath, P. F., Birk, M., Boudon, V., Campargue, A., Change, K. V., Drouin, B., Flaud, J. M., Gamache, R., Hodges, J., Jacquemart, D., Perevalov, V., Perrin, A., Shine, K., Smith, M. A., Tennyson, J., Toon, G., Tran, H., Tyuterev, V., Barbe, A., Császár, A., Devi, V. M., Furtenbacher, T., Harrison, J., Hartmann, J. M., Jolly, A., Johnson, T., Karman, T. and Kleiner, I., Kyuberis, A., Loos, J., Lyulin, O., Massie, S., Mikhailenko, S., Moazzen-Ahmed, N., Muller, H., Naumenko, O., Nikitin, A., Polyansky, O., Rey, M., Rotger, M., Sharpe, S., Sung, K., Starikova, E., Tashkun, S., Vander Auwere, J., Wagner, G., Wilzewski, J., Wcislo, P., Yu, S., and Zak, E.: The HITRAN2016 molecular spectroscopic database, *Journal of Quantitative Spectroscopy and Radiative Transfer*, 203, 3–69, doi:10.1016/j.jqsrt.2017.06.038, 2017.

Heymann, J., Reuter, M., Hilker, M., Buchwitz, M., Schneising, O., Bovensmann, H., Burrows, J. P., Kuze, A., Suto, H., Deutscher, N. M., Dubey, M. K., Griffith, D. W. T., Hase, F., Kawakami, S., Kivi, R., Morino, I., Petri, C., Roehl, C., Schneider, M., Sherlock, V., Sussmann, R., Velasco, V. A., Warneke, T., and Wunch, D.: Consistent satellite XCO₂ retrievals from SCIAMACHY and GOSAT using the BESD algorithm, *Atmospheric Measurement Techniques*, 8, 2961–2980, doi:10.5194/amt-8-2961-2015, 2015.

Kalnay, E., Kanamitsu, M., Kistler, R., Collins, W., Deaven, D., Gandin, L., Iredell, M., Saha, S., White, G., Woollen, J., Zhu, Y., Leetmaa, A., Reynolds, B., Cheliah, M., Ebisuzaki, W., Higgins, W., Janowiak, J., Mo, K. C., Ropelewski, C., Wang, J., Jenne, R., and Joseph, D.: The NCEP/NCAR 40-Year Reanalysis

- Project., *Bulletin of the American Meteorological Society*, 77, 437–472, doi:10.1175/1520-0477(1996)077<0437:TNYRP>2.0.CO;2, 1996.
- Keppel-Aleks, G., Wennberg, P. O., Washenfelder, R. A., Wunch, D., Schneider, T., Toon, G. C., Andres, R. J., Blavier, J.-F., Connor, B., Davis, K. J., Desai, A. R., Messerschmidt, J., Notholt, J., Roehl, C. M., Sherlock, V., Stephens, B. B., Vay, S. A., and Wofsy, S. C.: The imprint of surface fluxes and transport on variations in total column carbon dioxide, *Biogeosciences Discussions*, 8, 7475–7524, doi:10.5194/bgd-8-7475-2011, 2011.
- Lin, B., Ismail, S., Wallace Harrison, F., Browell, E. V., Nehrir, A. R., Dobler, J., Moore, B., Refaat, T., and Kooi, S. A.: Modeling of intensity-modulated continuous-wave laser absorption spectrometer systems for atmospheric CO₂ column measurements, *Applied Optics*, 52, 7062, doi:10.1364/AO.52.007062, 2013.
- Liu, J., Bowman, K., Schimel, D., Parazoo, N., Jiang, Z., Lee, M., Bloom, A., Wunch, D., Frankenberg, C., Sun, Y., O’Dell, C., Gurney, K., Menemenlis, D., Gierach, M., Crisp, D., and Eldering, A.: Contrasting carbon cycle responses of the tropical continents to the 2015-2016 El Niño, *Science*, 358, doi:10.1126/science.aam5690, 2017.
- Massart, S., Agustí-Panareda, A., Heymann, J., Buchwitz, M., Chevallier, F., Reuter, M., Hilker, M., Burrows, J. P., Deutscher, N. M., Feist, D. G., Hase, F., Sussmann, R., Desmet, F., Dubey, M. K., Griffith, D. W. T., Kivi, R., Petri, C., Schneider, M., and Velasco, V. A.: Ability of the 4-D-Var analysis of the GOSAT BESD XCO₂ retrievals to characterize atmospheric CO₂ at large and synoptic scales, *Atmospheric Chemistry and Physics*, 16, 1653–1671, doi:10.5194/acp-16-1653-2016, URL <https://www.atmos-chem-phys.net/16/1653/2016/>, 2016.

- Massie, S. T., Schmidt, K. S., Eldering, A., and Crisp, D.: Observational evidence of 3-D cloud effects in OCO-2 CO₂ retrievals, *Journal of Geophysical Research: Atmospheres*, 122, 7064–7085, doi:10.1002/2016JD026111, URL <https://agupubs.onlinelibrary.wiley.com/doi/abs/10.1002/2016JD026111>, 2017.
- Nassar, R., Hill, T. G., McLinden, C. A., Wunch, D., Jones, D. B. A., and Crisp, D.: Quantifying CO₂ Emissions From Individual Power Plants From Space, *Geophysical Research Letters*, 44, 10, doi:10.1002/2017GL074702, 2017.
- O’Dell, C. W., Connor, B., Bösch, H., O’Brien, D., Frankenberg, C., Castano, R., Christi, M., Eldering, D., Fisher, B., Gunson, M., McDuffie, J., Miller, C. E., Natraj, V., Oyafuso, F., Polonsky, I., Smyth, M., Taylor, T., Toon, G. C., Wennberg, P. O., and Wunch, D.: The ACOS CO₂ retrieval algorithm - Part 1: Description and validation against synthetic observations, *Atmospheric Measurement Techniques*, 5, 99–121, doi:10.5194/amt-5-99-2012, 2012.
- Osterman, G., Eldering, A., Mandrake, L., O’Dell, C., Wunch, D., Wennberg, P., Fisher, B., and Marchetti, Y.: Warn Level, Bias Correction, and Lite File Product Description, Tech. rep., NASA Jet Propulsion Laboratory and California Institute of Technology, version 2, Data Releases 8 and 8R, Lite File Version 8xxxAr, 2017.
- Peters, W., Jacobson, A. R., Sweeney, C., Andrews, A. E., Conway, T. J., Masarie, K., Miller, J. B., Bruhwiler, L. M. P., Pétron, G., Hirsch, A. I., Worthy, D. E. J., van der Werf, G. R., Randerson, J. T., Wennberg, P. O., Krol, M. C., and Tans, P. P.: An atmospheric perspective on North American carbon dioxide exchange: CarbonTracker, *Proceedings of the National Academy of Sciences*, 104, 18 925–18 930, doi:10.1073/pnas.0708986104, URL <http://www.pnas.org/content/104/48/18925>, 2007.

Rothman, L. S., Gordon, I. E., Babikov, Y., Barbe, A., Chris Benner, D., Bernath, P. F., Birk, M., Bizzocchi, L., Boudon, V., Brown, L. R., Campargue, A., Chance, K., Cohen, E. A., Coudert, L. H., Devi, V. M., Drouin, B. J., Fayt, A., Flaud, J.-M., Gamache, R. R., Harrison, J. J., Hartmann, J.-M., Hill, C., Hodges, J. T., Jacquemart, D., Jolly, A., Lamouroux, J., Le Roy, R. J., Li, G., Long, D. A., Lyulin, O. M., Mackie, C. J., Massie, S. T., Mikhailenko, S., Müller, H. S. P., Naumenko, O. V., Nikitin, A. V., Orphal, J., Perevalov, V., Perrin, A., Polovtseva, E. R., Richard, C., Smith, M. A. H., Starikova, E., Sung, K., Tashkun, S., Tennyson, J., Toon, G. C., Tyuterev, V. G., and Wagner, G.: The HITRAN2012 molecular spectroscopic database, *Journal of Quantitative Spectroscopy and Radiative Transfer*, 130, 4–50, doi:10.1016/j.jqsrt.2013.07.002, 2013.

Schmidt, S., Massie, S., Iwabuchi, H., Okamura, R., and Crisp, D.: 3D Cloud Effects in OCO-2 Observations - Evidence and Mitigation, in: *EGU General Assembly Conference Abstracts*, vol. 18 of *EGU General Assembly Conference Abstracts*, pp. EPSC2016–3644, 2016.

Taylor, T. E., O'Dell, C. W., Frankenberg, C., Partain, P., Cronk, H. Q., Savtchenko, A., Nelson, R. R., Rosenthal, E. J., Chang, A. Y., Fisher, B., Osterman, G., Pollock, R. H., Crisp, D., Eldering, A., and Gunson, M. R.: Orbiting Carbon Observatory-2 (OCO-2) cloud screening algorithms; validation against collocated MODIS and CALIOP data, *Atmospheric Measurement Techniques Discussions*, 8, 12 663–12 707, doi:10.5194/amtd-8-12663-2015, 2015.

- Thompson, D. R., Chris Benner, D., Brown, L. R., Crisp, D., Malathy Devi, V., Jiang, Y., Natraj, V., Oyafuso, F., Sung, K., Wunch, D., Castaño, R., and Miller, C. E.: Atmospheric validation of high accuracy CO₂ absorption coefficients for the OCO-2 mission, *Journal of Quantitative Spectroscopy and Radiative Transfer*, 113, 2265–2276, doi:10.1016/j.jqsrt.2012.05.021, 2012.
- Worden, J. R., Doran, G., Kulawik, S., Eldering, A., Crisp, D., Frankenberg, C., O’Dell, C., and Bowman, K.: Evaluation and attribution of OCO-2 XCO₂ uncertainties, *Atmospheric Measurement Techniques*, 10, 2759–2771, doi:10.5194/amt-10-2759-2017, 2017.
- Wunch, D., Wennberg, P. O., Osterman, G., Fisher, B., Naylor, B., Roehl, C. M., O’Dell, C., Mandrake, L., Viatte, C., Kiel, M., Griffith, D. W. T., Deutscher, N. M., Velazco, V. A., Notholt, J., Warneke, T., Petri, C., De Maziere, M., Sha, M. K., Sussmann, R., Rettinger, M., Pollard, D., Robinson, J., Morino, I., Uchino, O., Hase, F., Blumenstock, T., Feist, D. G., Arnold, S. G., Strong, K., Mendonca, J., Kivi, R., Heikkinen, P., Iraci, L., Podolske, J., Hillyard, P. W., Kawakami, S., Dubey, M. K., Parker, H. A., Sepulveda, E., García, O. E., Te, Y., Jeseck, P., Gunson, M. R., Crisp, D., and Eldering, A.: Comparisons of the Orbiting Carbon Observatory-2 (OCO-2) XCO₂ measurements with TCCON, *Atmospheric Measurement Techniques*, 10, 2209–2238, doi:10.5194/amt-10-2209-2017, URL <https://www.atmos-meas-tech.net/10/2209/2017/>, 2017.
- Zaccheo, T., Pernini, T., Snell, H., and Browell, E.: Impact of atmospheric state uncertainties on retrieved XCO₂ columns from laser differential absorption spectroscopy measurements, *Journal of Applied Remote Sensing*, 8, 083575, doi:10.1117/1.JRS.8.083575, 2014.